THE ANTENNA LABORATORY

UNPUBLISHED PRELIMINARY DATA

RESEARCH ACTIVITIES AT

by

R. A. Williams

Grant Number NsG-574-63

Department of ELECTRICAL ENGINEERING

THE OHIO STATE UNIVERSITY

NOTICES

When Government drawings, specifications, or other data are used for any purpose other than in connection with a definitely related Government procurement operation, the United States Government thereby incurs no responsibility nor any obligation whatsoever, and the fact that the Government may have formulated, furnished, or in any way supplied the said drawings, specifications, or other data, is not to be regarded by implication or otherwise as in any manner licensing the holder or any other person or corporation, or conveying any rights or permission to manufacture, use, or sell any patented invention that may in any way be related thereto.

The Government has the right to reproduce, use, and distribute this report for governmental purposes in accordance with the contract under which the report was produced. To protect the proprietary interests of the contractor and to avoid jeopardy of its obligations to the Government, the report may not be released for non-governmental use such as might constitute general publication without the express prior consent of The Ohio State University Research Foundation.

Qualified requesters may obtain copies of this report from the Defense Documentation Center, Cameron Station, Alexandria, Virginia. Department of Defense contractors must be established for DDC services, or have their "need-to-know" certified by the cognizant military agency of their project or contract.

REPORT 1093-25

REPORT

by

THE OHIO STATE UNIVERSITY RESEARCH FOUNDATION
COLUMBUS, OHIO 43212

Sponsor	National Aeronautics and Space Administration Office of Grants and Research Contracts Washington, D.C. 20546
Grant Number	NsG-74-60
Investigation of	Receiver Techniques and Detectors for Use at Millimeter and Submillimeter Wave Lengths
Subject of Report	An Interferometric Receiver for Submillimeter Radiometry
Submitted by	R. A. Williams Antenna Laboratory Department of Electrical Engineering
Date	1 February 1965

The material contained in this report is also used as a dissertation submitted to the Department of Electrical Engineering, The Ohio State University as partial fulfillment for the degree Doctor of Philosophy.

ACKNOWLEDGMENTS

The research work described in this dissertation was financed in part by Grant-in-Aid funds from the Department of Electrical Engineering of The Ohio State University.

The author wishes to acknowledge the valuable comments and suggestions of Dr. William S.C. Chang of the Department of Electrical Engineering and those of Drs. Ely E. Bell and Richard B. Sanderson and Mr. Ed Russell of the Department of Physics.

ABSTRACT

10882

Radiometry in the submillimeter wavelength region differs from centimeter-wavelength radiometry in three basic aspects: (1) for low-temperature sources the Rayleigh-Jean approximation to Planck's radiation law no longer applies and the complete Planck expression must be used, (2) due to the large size of the radiation detector the radiometer beamwidth is determined by geometrical optical effects rather than by diffraction effects due to the size of the antenna aperture, and (3) since the superheterodyne principle used at lower frequencies has not yet been developed for use in the submillimeter-wavelength region the selection of the wavelength region which it is desired to measure must be accomplished by quasi-optical means. The first two aspects of the submillimeter radiometry problem are discussed and summarized in graphical and tabular form. The third aspect of the problem is the major subject matter of the dissertation. author

One of the quasi-optical means of wavelength selection in the submillimeter region is the Michelson-type of interferometer adapted for the submillimeter region by the use of wire-mesh beam splitters and front-surfaced mirrors. Such an interferometer may be used in one of two modes of operation: either an interferogram function is obtained as one mirror is moved slowly

and the Fourier transform of the interferogram taken by means of digital computation techniques to obtain the power spectral density; or else the power spectral density may be obtained directly by means of a process commonly known as periodic interferometric modulation. These two methods are discussed theoretically and are compared to each other and to the use of a grating monochromator with respect to signal-to-noise ratio, measurement efficiency, and ease of operation. Methods of improving the shape of the interferometer response function and of trading signal-to-noise ratio for higher instrument resolution are discussed.

An interferometric instrument suitable for operation in either the aperiodic or periodic modes has been built and tested. Measurements made in both modes of the atmospheric water-vapor absorption over a two-meter path length show good agreement with measurements made by other experimenters using grating-type instruments. Data is also given on experimental tests of the methods for improving the instrument response function and for trading signal-to-noise ratio for higher resolution. It is concluded that such an instrument would be satisfactory for making submillimeter-wavelength radio-astronomy measurements.

CONTENTS (Continued)

CONTENTS

CHAPTER I
INTRODUCTION

A. Centimeter vs Submillimeter Radiometry

A radiometer - whether at centimeter, millimeter, submillimeter, or optical wavelengths - consists of a sensitive receiver or detector connected to a directional energy collector, or antenna, which is pointed towards the radiation source. In this dissertation the basic difference between making observations at longer (centimeter) wavelengths, or shorter (near-infrared or visible) wavelengths will be considered, and the different methods of making submillimeter-wavelength radiation measurements will be discussed and analyzed. For convenience, the submillimeter region will here be considered as from 50 to 1000 microns wavelength.

One of the differences between submillimeter-wavelength and centimeter-wavelength radiometry is the difference in the form of the radiative power law. At centimeter wavelengths the Rayleigh-Jean approximation to Planck's radiation law is valid for most sources of interest ($\lambda T_s \geq 77$ cm - degrees Kelvin) and permits a simple linear relation between the source temperature and the total

radiated-power spectral density per wavenumber (frequency) unit:

$$(1) \qquad E_{(\nu)} \propto \nu^2 k T_s \qquad \text{(watt-cm)},$$

and

$$(2) \qquad \Delta E_{(\nu)} \propto \nu^2 k(\Delta T_s) \qquad \text{(watt-cm)} .$$

At visible and near-infrared wavelengths (where $\lambda T_s < 0.3$ cm-deg K) the Wien approximation can often be used to obtain a degree of simplification:

$$(3) \qquad E_{(\nu)} \propto \nu^3 \epsilon^{-ch/\lambda k T_s} \qquad \text{(watt-cm)}.$$

However, in the submillimeter-wavelength region neither of these approximations usually apply and one must go directly to the complete Planck expression to obtain a relationship between the source temperature and the radiated-power spectral density.

B. Detector Detectivity

In the submillimeter region the sensitive low-noise superheterodyne receivers of the microwave region and the efficient low-noise quantum detectors or photographic plates of the optical region are not operable. Thus, one must, at the present time, at least,

resort to the use of thermal-type detectors such as bolometers, thermocouples, and pneumatic detectors (Golay cells). In general the detectivity of these detectors is several orders of magnitude less than that of the detectors or receivers available at other wavelengths.

C. Limitations Imposed by Geometrical Optics

In the case of a radiometer where the detector size or receiver input size is comparable to or smaller than the radiation wavelength and the antenna aperture diameter is several wavelengths or larger the beamwidth or spatial resolution is determined primarily by the size of the antenna aperture. This is true both in the case of a microwave dish antenna and an optical telescope, where in the former the detector input is a waveguide or a coaxial line and in the second the detector size corresponds to a single grain on the photographic plate and the aperture of the objective lens or main mirror corresponds to the antenna aperture. In both cases the diffraction spot size is larger than the detector input. Therefore the spatial resolution is determined by diffraction effects controlled by the size of the antenna aperture. In contrast to these, the spatial resolution of a submillimeter radiometer using a thermal detector is limited by geometrical optics. This occurs because the

detector size is large compared to the diffraction spot size for any receiving dish diameter of practical interest. The result is that the radiometer resolution is dependent upon the detector area and the focal length of the collecting mirror system rather than upon the diffraction limitations imposed by the mirror system aperture.

D. Minimum Detectable Temperature Change

Consider the minimum variation in the equivalent black-body temperature, T_s, of a source which can be detected by a radiometer equipped with a receiver which can detect a minimum change in its input power of $[\Delta P_{min}]$ watts. It can be shown[1, 2] that[1]

$$[\Delta T_s \min] = \frac{\eta \Gamma}{ck[\Delta \nu]} \; [\Delta P_{min}] \quad (^\circ K) \tag{4}$$

The equations for the factors η and Γ are (from Appendix I)

$$\eta = \left[\frac{\lambda k T_s}{ch}\right]^2 \frac{[\epsilon^{ch/\lambda k T_s} - 1]^2}{\epsilon^{ch/\lambda k T_s}} \; , \tag{5}$$

---

[1] See the List of Symbols for the definitions and units of the various symbols, and see Appendix I for a derivation of equations (4), (5), and (6).

and

$$(6)\quad \Gamma \begin{cases} = \dfrac{\lambda^2 \delta_1^2}{2a A_m} = \dfrac{2\lambda^2 F_o^2}{\pi a} & \text{for } [\Delta\Omega]_s > \text{beamwidth at submillimeter wavelengths} \\ = 1 \text{ (unity)} & \text{for } [\Delta\Omega]_s > \text{beamwidth at centimeter wavelengths} \\ = \dfrac{\lambda^2}{2A_m[\Delta\Omega]_s} & \text{for } [\Delta\Omega]_s < \text{beamwidth at submillimeter wavelengths} \\ = \dfrac{\lambda^2}{A_e[\Delta\Omega]_s} & \text{for } [\Delta\Omega]_s < \text{beamwidth at centimeter wavelengths} \end{cases}$$ [2]

The value of η vs λ and T_s is plotted in Fig. 1. We can also relate $[\Delta T_{s_{min}}]$ to the minimum detectable change in the input power spectral density, $[\Delta E_{i_{(\nu)_{min}}}]$, of the collected incoming radiation by letting $[E_{i_{(\nu)_{min}}}] = [\Delta P_{min}]/[\Delta\nu]$ in Eq. (4).

Note that in the case of the centimeter radiometer looking at a source whose solid angle $[\Delta\Omega]_s$ is larger than the beamwidth $[\Delta T_{s_{min}}]$ is not a function of the antenna area so long as the antenna is not made so small that the beamwidth becomes larger than the source. In the case of the submillimeter radiometer the beamwidth is not determined by the antenna area, and the temperature sensitivity

---

[2] The instrument f-number, F_o, is equal to the f-number of either the collection mirror system or that of the radiation receiver whichever is numerically larger.

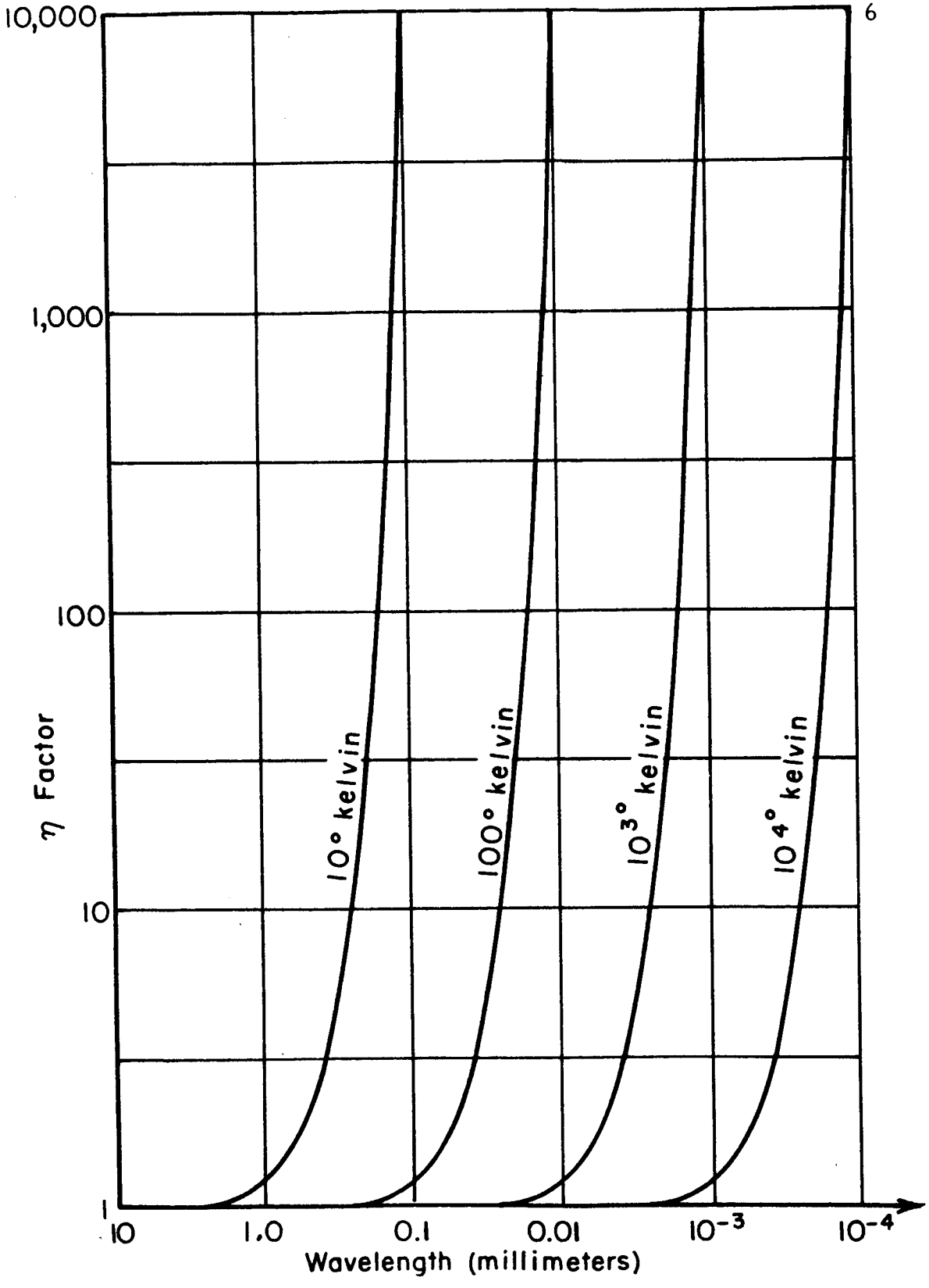

Fig. 1--η factor vs temperature and wavelengths.

can be increased (theoretically) by making F_o smaller (by making the antenna area larger and by using larger mirrors within the submillimeter receiver). The beamwidth of the submillimeter radiometer is given by $\sqrt{4a/\pi}/\delta_1$ as compared with $1.22\lambda/\sqrt{4A_e/\pi}$ for the centimeter radiometer.

E. Water Vapor Absorption

Another problem with which one must contendwhen working in the submillimeter-wavelength region is the heavy absorption of the radiation by atmospheric water vapor. This absorption occurs throughout the entire region except for a small number of partial atmospheric "windows," and is moderately severe even over short path lengths at a relatively low humidity index.

F. Wavelength Selection

Since the highly selective superheterodynes of the microwave region are not presently available throughout the submillimeter region, and since fundamental-mode cavities cannot be constructed at these wavelengths, one must resort to some type of quasi-optical means of wavelength selection, such as diffraction gratings or interference techniques. The instrument which has been constructed and which will be described in this dissertation uses the interference

technique found in the Michelson interferometer to enable one to obtain a measurement of the power spectral density either directly from the instrument using a technique commonly called "periodic interferometric modulation" or indirectly by obtaining an interferogram function as the instrument output which is then processed in a digital computer to obtain the measured power spectral density, a process sometimes referred to as "aperiodic interferometric modulation."

G. The Submillimeter Radiometer

The submillimeter radiometer which will be described here uses a thermal radiation detector and an interferometric means of wavelength selection, and has a spatial resolution which is determined by the detector size and the collecting mirror focal length. The instrument has been built to be operated in either the periodic or aperiodic mode of interferometric modulation. In the following chapter the theory of its operation will be discussed, and its use compared to the use of a diffraction grating monochromator as a means of wavelength selection. An estimate is made of its sensitivity in terms of the minimum temperature change which it can detect in an equivalent black-body source. Later chapters will discuss the construction of the instrument and the experimental results obtained.

CHAPTER II
THE THEORY OF THE INTERFEROMETRIC SUBMILLIMETER RADIOMETER RECEIVER

A. Historical Background

The idea of using interference phenomenon to determine the power spectral density of radiation by taking the Fourier transform of the interference pattern was proposed in the latter part of the nineteenth century by Michelson[3], who performed his experiments in the visible region. Because of the difficulty of performing the Fourier transform and the advent of prism and grating spectrometers for use in the visible region, the interferometric method fell into disuse until the early 1950's. At that time Peter Fellgett of Cambridge University, England applied the interferometric method to the measurement of stellar spectra and revived interest in the method[4, 5, 6]. The new interest was based primarily on three factors: the greater efficiency of this method as compared to a slit (grating or prism) spectrometer, the availability of modern digital methods for computing the Fourier transform, and the easy applicability of the method to the far-infrared region. Much of this early renascence work was reported at the

"Colloque International sur les Progre's Re'cents en Spectroscopie Interférentielle"[7]. Since this period considerable research and analysis has taken place concerning the interferometric method, most of this being in the far infrared utilizing both the Michelson type of interferometer[8, 9, 10] and the variable-groove-depth-lamellar-grating interferometer[11, 12]. The technique has also been applied to the millimeter-wavelength region using waveguide components[13, 14]. Both the aperiodic[6, 9, 10, 15] and the periodic[7, 16, 17, 18] modes of operation have been discussed, and in some cases compared theoretically[19].

The present dissertation briefly summarizes and unifies the theory of both the aperiodic and the periodic modes of operation and discusses the fundamental resolution of the interferometric receiver by analyzing its response-function integral equation, and also presents a simple method by which the shape of the instrument response function can be improved[20, 21]. This method is applicable to both the aperiodic and periodic modes, and gives a better response function thanthe appodization method suggested earlier[8, 12]. A description is given of an instrument, which was constructed along

the Michelson design using a wire-mesh beam splitter,[1] which is operable in either the aperiodic or the periodic mode (in the latter case using an improved signal-processing method which helps to eliminate backlash and turn-around problems). Data is presented on the results of tests in both modes of operation which shows the beam-splitter characteristics and the effects of the response-function improvement, and which permits a comparison between the two modes of operation.

B. The Aperiodic Method

1. Theory: The purpose of any radio receiver is the selection of a desired wavelength or band of wavelengths from the total of all of the radiation entering the receiver and the conversion of this radiation into a form which can be perceived by the operator of the equipment. In the receiver to be discussed herein, a quasi-optical interference method is used as the means of wavelength selection and a bolometric or thermal radiation detector is used to convert the radiation into an electrical signal which can be

---

[1] The decision to use a wire mesh as the beam splitter was made after discussions with E.E. Bell, R.F. Rowntree, M.E. Vance and P.B. Burnside concerning measurements made on the transmission and reflection of various beam-splitter materials. These data were obtained in part at The Ohio State University (Dept. of Physics)[22], and in part at The University of Freiburg (Germany) Inst. of Physics (the latter by E.E. Bell and L. Genzel)[33].

electronically processed and displayed or recorded on an indicating instrument. The basic wavelength-selection mechanism which is employed is that of the optical Michelson interferometer, which is here adapted for use in the submillimeter-wavelength region. Its operating principles shall be reviewed briefly.

Let the radiation incident upon the receiver input area have a total power spectral density $E_{i(\nu)}$ watt-cm, where ν is the radiation wavenumber in cm^{-1} units, and let it be divided into two paths, one of which is γ centimeters longer than the other, before being recombined. Upon recombination an interference phenomenon will take place and the power spectral density of the recombined radiation will be

$$(7) \qquad E_{o(\nu,\gamma)} = \frac{E_{i(\nu)}}{2} (1 + \cos 2\pi\nu\gamma) \quad \text{(watt-cm)}.$$

If $E_{o(\nu,\gamma)}$ is integrated over the wavenumber range of the radiation entering the receiver, the total power of the recombined radiation is

$$(8) \qquad I_{o(\gamma)} = \int_o^\infty E_{o(\nu,\gamma)} d\nu = \frac{1}{2} \int_o^\infty E_{i(\nu)} d\nu + \frac{1}{2} \int_o^\infty E_{i(\nu)} \cos 2\pi\nu\gamma \, d\nu \quad \text{(watts)}.$$

$I_{o(\gamma)}$ is composed of one term which is independent of γ and a second which is dependent upon γ and which is one-half the cosine Fourier

transform of $E_{i(\nu)}$. Thus, if the variable portion of $I_{o(\gamma)}$ is recorded as γ is varied from $-\infty$ to $+\infty$ (or from zero to $+\infty$, since $I_{o(\gamma)}$ should be an even function of γ) it should be possible to obtain the function $E_{i(\nu)}$ by taking the inverse cosine Fourier transform of $I_{o(\gamma)}$. Only the varying portion of $I_{o(\gamma)}$ will contribute, since the Fourier transform of a constant is zero at all frequencies other than $\nu = 0$ (where it is an impulse function), and thus, for the frequencies of interest here, one has

$$(9) \quad E_{i(\nu)} = 4 \int_{-\infty}^{\infty} I_{o(\gamma)} \cos 2\pi\nu\gamma \, d\gamma = 8 \int_{o}^{\infty} I_{o(\gamma)} \cos 2\pi\nu\gamma \, d\gamma \quad \text{(watt-cm)}.$$

Since it is not practical to let γ go to infinity, one must take into consideration the effects of truncating $I_{o(\gamma)}$ at some finite value where $\gamma = \gamma_{max}$. In effect this truncation can be thought of as resulting from multiplying the true $I_{o(\gamma)}$ by a window function which extends from $-\gamma_{max}$ to $+\gamma_{max}$:

$$(10) \quad I'_{o(\gamma)} = I_{o(\gamma)} \cdot W_{(\gamma)} \quad \text{(watts)},$$

where

$$(11) \quad \begin{aligned} W_{(\gamma)} &= 1 && -\gamma_{max} \leq \gamma \leq +\gamma_{max} \\ &= 0 && \begin{cases} \gamma < -\gamma_{max} \\ \gamma > +\gamma_{max} \end{cases} . \end{aligned}$$

It will be remembered that the effect of multiplying together the transforms of two functions is equivalent to convolving the actual functions themselves[23]. Since $W_{(\gamma)}$ is the transform of the function $(\sin 2\pi\nu\gamma_{max}/\pi\nu)$, the inverse transform of $I'_{o(\gamma)}$, which here shall be called the measured power spectral density, $E_{m_{I(\nu)}}$, is given by

$$(12) \qquad E_{m_{I(\nu)}} = \int_o^\infty E_{i(\nu')} \frac{\sin 2\pi\gamma_{max}(\nu-\nu')}{\pi(\nu-\nu')} \, d\nu'$$

$$= \int_o^\infty E_{i(\nu')} R_{I(\nu,\nu')} \, d\nu' \qquad \text{(watt-cm)}.$$

$R_{I(\nu,\nu')}$ - which is convolved with the actual spectral density $E_{i_{(\nu)}}$ to give the measured spectral density $E_{m_{I(\nu)}}$ - will be called the instrument response function, and can be thought of as being very similar to the passband response function of a conventional radio or microwave receiver.

The constant-value component of $I_{o(\gamma)}$ causes some problems when $I_{o(\gamma)}$ is truncated at γ_{max}, since the contribution of this term to the inverse transform will be zero only if the inverse transform is calculated at wavenumber values where $\nu = \nu_n = n/2\gamma_{max}$. Therefore, one way of determining $E_{m_{I(\nu)}}$ with validity is to calculate it only where $\nu = \nu_n$:

$$(13) \qquad Em_{I(\nu_n)} = 8 \int_0^{\gamma_{max}} I_{o(\gamma)} \cos \frac{n\pi\gamma}{\gamma_{max}} \, d\gamma \quad \text{(watt-cm)}.$$

A second method of calculating a valid $Em_{I(\nu)}$ would be to subtract the constant term in $I_{o(\gamma)}$ from $I_{o(\gamma)}$ before taking the inverse transform. However, there may be some difficulty in determining the value of this constant component from the data taken, especially if the radiation spectrum contains sharp absorption or transmission lines and if γ_{max} is rather small, since in this case $I_{o(\gamma)}$ will still be varying rather greatly as a function of γ for γ greater than γ_{max}. But under these conditions the passband of the instrument - which can be defined as the distance between the first zeros on either side of the instrument response function peak, $\Delta\nu = 1/\gamma_{max}$ - would be wider than the lines appearing in the radiation spectrum, and hence $Em_{I(\nu)}$, the measured power spectral density, would not, at any rate, be a good representation of the actual spectral density, $E_{i(\nu)}$. This is discussed further at the end of this chapter.

The actual calculation of the inverse transform can be most conveniently carried out by using a digital computer and digitizing the interferogram function $I_{o(\gamma)}$. One precaution which must be observed here is to make the increment between digital points, $\Delta\gamma$, small enough that the resulting digitized function is a good representation of $I_{o(\gamma)}$, and to select its value so that γ_{max} (which must be an integer multiple of $\Delta\gamma$)is some mathematically convenient value.

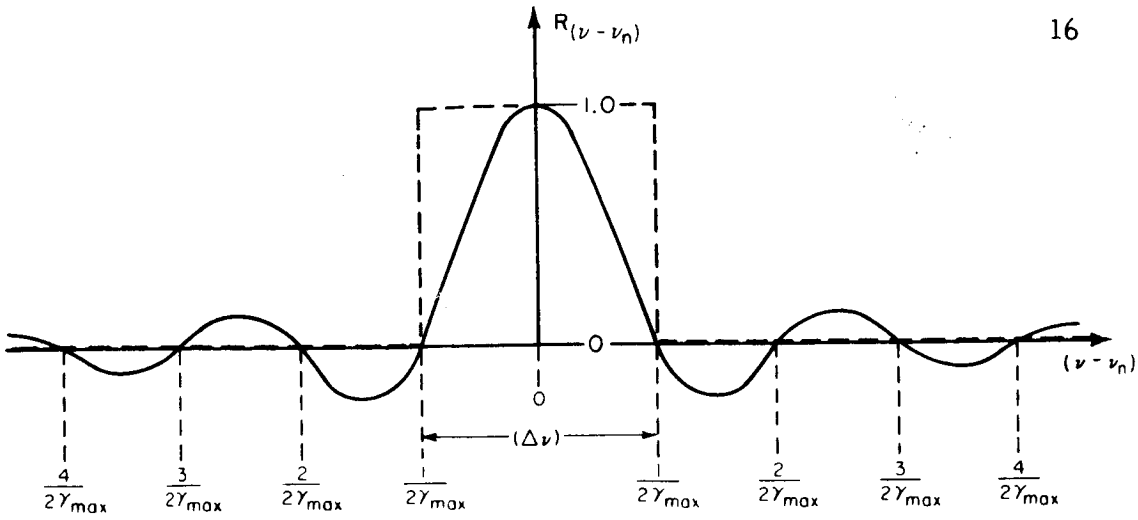

Fig. 2--The basic instrument response function.

As may be seen in Fig. 2, the interferometric instrument response function (solid line) has less central-peak area than the ideal rectangular response function which is usually desired for receiver passbands (dotted line). Other defects are the sloping sides of the main peak and the large side responses. Quite a bit of improvement in the overall receiver response function can be made by adding together several of the basic sin x/x type of response functions which peak at values of ν which differ from each other by $1/2\ \gamma_{max}$. Figure 3 shows how three such basic response functions were combined to give a new function whose main peak is more rectangular and whose side responses are smaller. In order to maintain the same overall bandwidth, $\Delta\nu$, it was necessary (for the case of three added functions) to make $\gamma'_{max} = 2\gamma_{max}$ so that the width of the individual peaks is decreased. The formula for calculating $E'_{m(\nu)}$ is written by combining three of

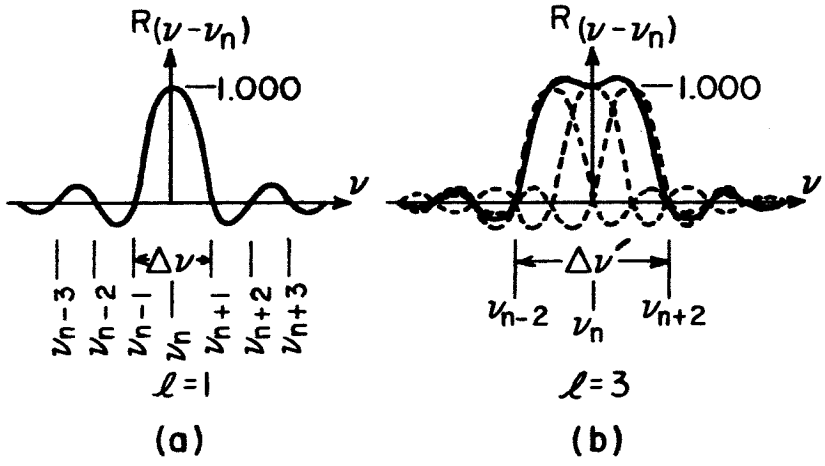

Fig. 3--Improved instrument response function (b) obtained by adding three of the basic response functions (a).

the basic transform equations:

$$(14)\quad E'_{m_{I(\nu)}} = 8\int_o^{\gamma'_{max}} I_{o(\gamma)}[\cos 2\pi\nu\gamma]\,d\gamma + 8\int_o^{\gamma'_{max}} I_{o(\gamma)}\left[\cos 2\pi\left(\nu - \frac{1}{2\gamma'_{max}}\right)\gamma\right]d\gamma$$

$$+ 8\int_o^{\gamma'_{max}} I_{o(\gamma)}\left[\cos 2\pi\left(\nu + \frac{1}{2\gamma'_{max}}\right)\gamma\right]d\gamma \quad \text{(watt-cm)},$$

or, if $E'_{m(\nu)}$ is calculated at the permitted values of $\nu_n = n/2\gamma'_{max}$, then

$$(15)\quad E'_{mI(\nu_n)} = 8 \int_o^{\gamma'_{max}} I_{o(\gamma)} \left[\cos \frac{n\pi\gamma}{\gamma'_{max}} + \cos \frac{(n-1)\pi\gamma}{\gamma'_{max}} + \cos \frac{(n+1)\pi\gamma}{\gamma'_{max}} \right] d\gamma \quad \text{(watt-cm)}.$$

Since each of the terms in (15) represents adjoining points on $E_{mI(\nu)}$ as determined using the basic instrument response function, the value of $E'_{mI(\nu)}$ may be calculated very easily from $E_{mI(\nu)}$ by simply adding $E_{mI(\nu_n)}$, $E_{mI(\nu_{n+1})}$, and $E_{mI(\nu_{n-1})}$ to form $E'_{mI(\nu_n)}$. Thus it is not necessary to repeat the entire transform-taking procedure a second time to determine $E'_{mI(\nu)}$ if $E_{mI(\nu)}$ is already available. Table I tabulates the effects of combining various numbers, ℓ, of basic response functions to obtain an improved response function. It shows that the most improvement for the amount of calculation needed is obtained by using three, five, or seven as the value of ℓ. In each case, $\gamma'_{max} = (\ell+1)\gamma_{max}/2$.

TABLE I
VARIATION OF RESPONSE FUNCTION WITH ℓ

ℓ	d-c output due to radiation at wavenumbers in main peak (A)	d-c output due to radiation at wavenumbers in side lobes (B)	percentage side lobes are of main peak (100 × B/A)	ratio of main peak output for k reference signals to main peak output for ℓ = 1 (A/3.7038)
1	3.7038	-0.5622	15.18%	1.0000
3	4.9449	-0.2325	4.70	1.3351
5	5.3807	-0.1447	2.69	1.4528
7	5.6026	-0.1048	1.87	1.5127
9	5.7370	-0.0821	1.43	1.5489
11	5.8270	-0.0674	1.16	1.5732
13	5.8916	-0.0572	0.97	1.5907
15	5.9429	-0.0524	0.88	1.6045
17	5.9804	-0.0463	0.77	1.6147
19	6.0105	-0.0415	0.69	1.6228
21	6.0351	-0.0375	0.62	1.6294
23	6.0557	-0.0343	0.56	1.6350
25	6.0731	-0.0316	0.52	1.6396

2. Noise analysis. It is interesting to compare the theoretical noise level of the interferometric receiver with that of a grating-type monochromator wherein the radiation is admitted through a narrow slit and dispersed by a diffraction grating. A second narrow slit positioned at a selected point in the grating diffraction pattern allows radiation in a narrow wavenumber region, $(\Delta\nu)_G$, to pass on through to a radiation detector. By increasing the slit widths in the instrument and also the grating dispersion factor it is possible to make the size of the grating instrument input aperture equal to that of the interferometric instrument and still

maintain the desired spectral resolution, although this will not be the maximum resolution of which the grating instrument would be capable with smaller slit widths[24]. Some fraction, K, of the power spectral density entering the grating instrument is dispersed into the first grating order, which is the order in which the output slit is usually located. The dispersion factor of the grating and the widths of the input and the output slits determine the effective passband, $(\Delta\nu)_G$, of the grating receiver. The power delivered to the detector is therefore given by

$$(16) \qquad P_D = \frac{1}{2} E_{i_{(\nu)}} K (\Delta\nu)_G \qquad \text{(watts)},$$

where the factor of one-half occurs because of the fact that the radiation must be chopped in order to obtain a signal from the detector, thereby eliminating one-half of the average input power. If the radiation detector has a noise equivalent power (NEP) for one cycle of bandwidth centered at the audio frequency at which the radiation is chopped, and if the integration time following the synchronous detector or rectifier is τ_D, then the effective signal-to-noise ratio, $(S/N)_G$, of the grating receiver will be

---

[2] Here it is assumed that (NEP) is determined by means of a correlator-amplifier with an effective bandwidth of 1 cps due to the time constant of its integrator. This (NEP) will be one-half of the (NEP) measured with a 1-cps-bandwidth tuned amplifier.

$$(17)\quad (S/N)_G = \frac{P_D\sqrt{2\tau_D}}{(NEP)} = \frac{K\sqrt{(2\tau_D)(\Delta\nu)_G}}{2} \cdot \frac{E_{i(\nu)}}{(NEP)} ,$$

where the effective noise-power audio bandwidth has been taken to be equal to $1/2\tau_D$. Since K and $(\Delta\nu)_G$ are more or less fixed by the application and the inherent properties of the instrument, the only way in which the S/N ratio of the grating receiver can be improved is by increasing the integration time, τ_D, thereby decreasing the rate at which the spectrum can be scanned.

In determining the S/N ratio of the interferometric instrument it is convenient to consider the interferogram as a voltage time function existing from time t = 0 to time t = T_t, where T_t is the total length of time required to record the interferogram data. T_t is equal to γ_{max}/s, where $s = d\gamma/dt$ is the time rate of change of the path-length difference. As $I_{o(t)}$, where $t = \gamma/s$, is recorded there will also be recorded along with it a noise voltage, $N_{(t)}$, where the power density spectrum of this voltage is given by

$$(18)\quad N_{(f)} = \frac{[(NEP)\Omega]^2}{1 + (2\pi f \tau_D)^2} \quad \frac{(volts)^2}{CPS} ,$$

where (NEP) is the noise equivalent power of the radiation-detector system[3] (in watts per $\sqrt{cps}$) and Ω and τ_D are the response factor

---

[3] The radiation-detection system is taken to include the radiation chopper, the bolometer, the amplifier, the synchronous rectifier, and the R-C low-pass filter following the rectifier.

(in volts per watt) and the rectifier time constant (in seconds) respectively of this system. The time constant, τ_D, must be small enough so as to not introduce any appreciable attenuation and/or phase shift of the signal at the frequency $f = \nu s$, where ν is the wavenumber of the radiation being measured. The attenuation will be less than 3 db and the phase shift less than forty-five degrees if $\tau_D < 1/2\pi\nu s$. Usually τ_D should be made somewhat smaller than this, and therefore the factor $(1 + (2\pi\tau_D\nu s)^2)$ will be approximately unity at the audio frequencies of interest.

If one takes the final output signal (expressed as a voltage) to be

$$(19) \quad S_{I(f)} = 8 \int_o^{T_t} \left(\frac{\Omega I_{o(t)}}{2} \right) (\cos 2\pi ft)dt \qquad \text{(volt-sec)},$$

it is easily seen that $S_{I(f)} = \Omega E_{mI(\nu)}/2s$, which, if an input having a smooth spectral density, $E_{i(\nu)}$, is being measured, gives $S_{I(f)} = \Omega E_{i(\nu)}/2s$, where the factor of two results from the fact that the radiation must be chopped in order to activate the detector system.

The noise voltage density on the output signal (where the signal itself is proportional to the measured power spectral density) will then be given by

$$(20) \qquad N_{I(f)} = 8 \int_{o}^{T_t} N_{(t)} (\cos 2\pi ft)\, dt \qquad \text{(volt-sec)}.$$

In the limit as T_t goes to infinity this is just four times the cross-correlation coefficient of the function $(N_{(t)} \times T_t)$ with the function $(\cos 2\pi ft)$. At finite values of T_t is it equivalent to passing $4(N_{(t)} \times T_t)$ through a bandpass filter of noise-power bandwidth $1/2T_t$ centered at the frequency $f = \nu s$. Thus, the mean-square value of the noise density on the output is given by

$$(21) \qquad \frac{[4(NEP)\Omega\, T_t]^2 \times (1/2\,T_t)}{2} \qquad \text{(volt-sec)}^2,$$

and the rms noise voltage density by

$$(22) \qquad N_{I(f)} = 2(NEP)\Omega \sqrt{T_t} \qquad \text{(volt-sec)},$$

where the $1/2$ factor in Eq. (21) enters because only the cosine function is employed in the correlation integral rather than both the cosine and sine functions. Thus, the S/N ratio for the interferometric receiver becomes

$$(23) \qquad \left(\frac{S}{N}\right)_I = \frac{E_{i(\nu)}}{4\,s(NEP)\sqrt{T_t}} = \frac{E_{i(\nu)}\,(\Delta\nu)_I \sqrt{T_t}}{4(NEP)} .$$

Since the sensitivity of both the grating-and the Michelson-interferometer-type receivers can be increased by increasing the length of time used to take a complete set of measurements (time, T_t, required to measure from ν_1 to ν_2 in wavenumber) under similar conditions of input power and instrument bandwidth, it is interesting to consider a quantitative figure of merit, Q, for each case, where

$$(24) \qquad Q = (S/N) \cdot \frac{(\nu_2 - \nu_1)}{T_t} \cdot \frac{1}{\overline{E_{i(\nu)}} (\Delta\nu)^2} \qquad (1/\text{watt-sec}),$$

or, alternatively as

$$(25) \qquad Q = \frac{\int_{\nu_1}^{\nu_2} (S/N) \frac{d\nu}{\overline{E_{i(\nu)}} (\Delta\nu)^2}}{\int_{\nu_1}^{\nu_2} \frac{\partial t}{\partial \nu} \, d\nu} \qquad (1/\text{watt-second}).$$

For the grating receiver it can be shown that for a fixed slit width and constant rate of slit motion along the diffraction pattern (see Appendix II), the above becomes

$$(26) \qquad Q_G = \frac{\int_{\nu_1}^{\nu_2} \frac{K \sqrt{2\tau_D} (\Delta\nu)_G E_{i(\nu)}}{2 (NEP)} \cdot \frac{d\nu}{E_{i_{(\nu)}} (\Delta\nu)_G^2}}{\int_{\nu_1}^{\nu_2} \frac{2\tau_D \, m \, d\nu}{\nu^2 \, d(\cos \psi) \, |\Delta\psi|}}$$

(26) (cont)
$$= \frac{K\sqrt{2\tau_D}}{2(NEP)} \cdot \frac{\int_{\nu_1}^{\nu_2} \frac{m\ d\nu}{d(\cos\psi)\ |\Delta\psi|\ \nu^2}}{2\tau_D \int_{\nu_1}^{\nu_2} \frac{m\ d\nu}{\nu^2\ d(\cos\psi)\ |\Delta\psi|}}$$

$$= \frac{K}{4(NEP)} \sqrt{\frac{2}{\tau_D}} = \sqrt{\frac{2}{\tau_D}} \cdot \frac{1}{4(NEP)} \qquad (1/\text{watt-sec}),$$

where m is the grating order used (m usually equals one), d is the spacing between grating lines, and ψ is the angle of diffraction; and where it has now been assumed that the order of magnitude of K is unity.

For the case of the interferometric receiver (since $\gamma_{max}=1/(\Delta\nu)_I$, $T_t = \gamma_{max}/s = 1/s(\Delta\nu)_I$, and $s_{max} = 1/2\pi\tau_D\nu_2$),

(27)
$$\tau_D = 1/2\ \pi s\nu_2 = (\Delta\nu)_I\, T_t/2\pi\nu_2 \qquad \text{(seconds)},$$

or

(28)
$$T_t = \frac{2\pi\nu_2\tau_D}{(\Delta\nu)_I} \qquad \text{(seconds)}.$$

Therefore

(29)
$$Q_I = \frac{E_{i_{(\nu)}}\,(\Delta\nu)_I\sqrt{T_t}\,(\nu_2-\nu_1)}{4(NEP)\,T_t\,E_{i_{(\nu)}}(\Delta\nu)_I^2}$$

$$= \frac{(\nu_2-\nu_1)}{(4\sqrt{2\pi})(NEP)\sqrt{(\Delta\nu)_I\,\nu_2\tau_D}} \qquad (1/\text{watt-seconds}).$$

From a comparison of Eqs. (29) and (26) one sees that Q_I is about $0.3\ (\nu_2-\nu_1)/\sqrt{\nu_2(\Delta\nu)_I}$ larger than Q_G, or since $(\nu_2-\nu_1)$ and ν_2 are about the same order of magnitude, Q_I is almost $\frac{1}{3}\sqrt{\frac{(\nu_2-\nu_1)}{(\Delta\nu)_I}}$ times Q_G. Since $(\nu_2-\nu_1)$ can be as large as desired, this in effect says that if the signal-to-noise ratios and the instrument bandwidths of the two instruments can be made equal, the interferometric receiver can acquire the necessary data needed to calculate the entire spectrum (consisting of $M = (\nu_2-\nu_1)/(\Delta\nu)$ measurements between ν_1 and ν_2) while the grating instrument is acquiring the data necessary to determine the power spectral density at slightly more than $3\sqrt{M}$ points in the spectrum; or one can say that the interferometric receiver is about $\sqrt{M}/3$ times more efficient than is the grating receiver[5]. All of this of course does not take into account the beam splitter efficiency, grating efficiency, and other problems of a more practical nature which will affect the S/N ratio and the figure of merit of the two types of receivers. These matters will be discussed in detail in the next chapter.

C. The Periodic Method

Consider the case where a complete scan from $-\gamma_{max}$ to $+\gamma_{max}$ is performed rather rapidly in $2\tau_p$ seconds (τ_p is the time required to scan from $-\gamma_{max}$ to zero, from zero to $+\gamma_{max}$, etc.) and let this scan, or its equivalent from $+\gamma_{max}$ to $-\gamma_{max}$, be repeated once every T_p seconds (see Fig. 4). The audio components of the

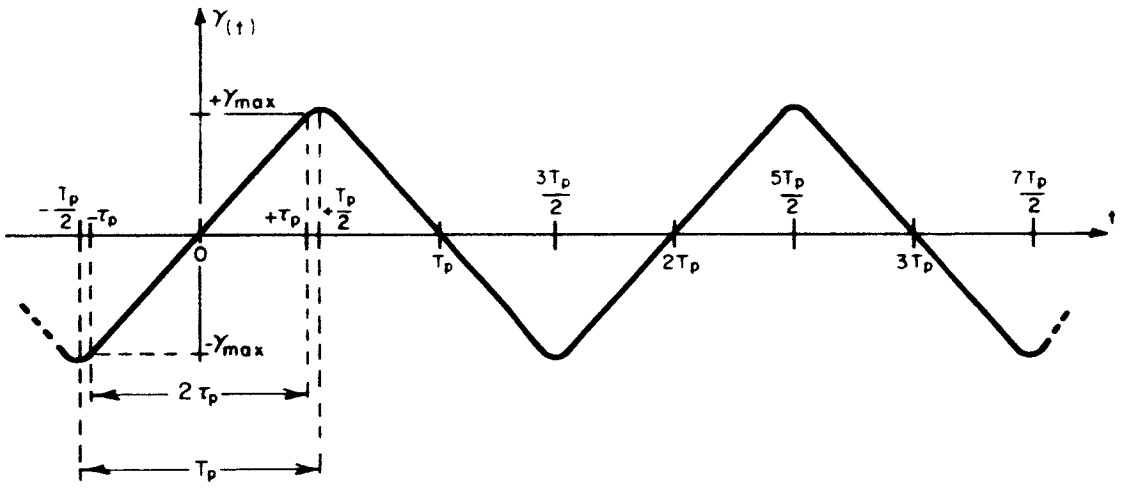

Fig. 4--Path-length difference function of the periodic interferometric receiver.

radiation-detector output will be the harmonics of $f_o = 1/T_p$, but if T_p is very large the components will fall very close together and if $T_p >> 2\tau_p$ the change in amplitude from one component to the next will be so small that the spectrum can be thought of as approaching the continuous spectrum which would occur for T_p equal to infinity.

The velocity of path length change is now given by $s = \gamma_{max}/\tau_p$ and it establishes a relationship between a particular audio frequency in the detector output and the radiation wavenumber, ν:

$$f_\nu = s\nu = (\gamma_{max})\nu/\tau_p \qquad (sec^{-1}) \ . \tag{30}$$

In the case where $T_p = \infty$ the magnitude of the detector output at frequency f_ν corresponds to the magnitude of $E_{m(\nu)}$, where ν is related to f_ν by Eq. (30). It has been assumed here that the path length change begins abruptly at $-\gamma_{max}$ and $-\tau_p$ and ends abruptly at $+\gamma_{max}$ and $+\tau_p$, but that the radiation is present from $t = -\infty$ to $t = +\infty$. If one assumes that $I_{o(\gamma)}$ is a symmetrical function of γ the magnitude of the interferogram from $t = -\infty$ to $t = -\tau_p$ will be constant and equal to the magnitude from τ_p to $t = +\infty$. If this is allowed to exist also from $-\tau_p$ to $+\tau_p$ one has a constant component which exists from $t = -\infty$ to $+\infty$. This component of the interferogram will contribute to the power spectral density only at zero frequency; therefore, for the purposes of this dissertation the contribution of the constant component in the interferogram need not be considered. If T_p is finite but still much greater than $2\tau_p$ these results can be used as an approximation to the actual case. This has been done by at least one group of experimenters[13, 14]. However, this requires that a long dwell period exist between each scan in order for the approximation

to be valid, and during this dwell period no information is being derived from the input signal. This causes a decrease in the S/N ratio of the system. Practical measurements utilizing this type of system can be made with a narrow-band tuned audio amplifier. Long et al. [13, 14] have shown that if the audio bandwidth, B, of the amplifier is great enough relative to $1/\tau_p$ (in the notation of the present paper) then the wavenumber bandwidth of the instrument is dependent upon the bandwidth of the tuned audio amplifier,

$$(31) \qquad (\Delta\nu) = \frac{B}{S} \qquad (cm^{-1}),$$

rather than upon the length of stroke, γ_{max}.

If T_p is only slightly larger than $2\tau_p$ the situation becomes much different, since instead of a continuous or quasi-continuous audio spectrum, one has a spectrum consisting of discrete components of fairly wide frequency separation where the amplitude of one component may vary quite markedly from that of its nearest neighbor. As stated before, these components will be harmonics of $1/T_p$:

$$(32) \qquad f_n = nf_o = n\left(\frac{1}{T_p}\right) \qquad (sec^{-1}).$$

Since the output of the radiation detector is now a periodic function, one determines the Fourier series components rather than the Fourier transform of the interferogram function (see Appendix III).

A convention has been adopted here so that the result has the dimensions of total power at a certain frequency rather than the dimensions of power spectral density. Thus, instead of Eq. (13), one has

$$(33) \qquad P_n = \frac{2\tau_p}{\gamma_{max}\, T_p} \int_o^{\gamma_{max}} I_{o(\gamma)} [\cos 2\pi \nu_n' \gamma] d\gamma \text{ (watts)},$$

where $\nu_n' = n/s\ T_p$ (see Appendix III). From Eq. (33) and the relation that $\nu_n' = n/s\ T_p = n(\tau_p/T_p\ \gamma_{max})$, it is evident that

$$(34) \qquad P_n = \frac{2\tau_p}{\gamma_{max}\, T_p} \int_o^{\gamma_{max}} I_{o(\gamma)} \left[\cos \frac{2\pi n \gamma}{\gamma_{max}} \left(\frac{\tau_p}{T_p}\right)\right] d\gamma \text{ (watts)},$$

which is very close to being $E_{mI(\nu_n)}/8\,\gamma_{max}$ as given by Eq. (13) if the approximation that $T_p \approx 2\tau_p$ is made. Therefore, the periodic mode measured power spectral density is given by

$$(35) \qquad E_{mP(\nu_n')} = 8 P_n \gamma_{max} \doteq E_{mI(\nu_n)} \qquad \text{(watt-cm)},$$

where $\nu_n' \approx \nu_n$, and therefore

$$(36) \qquad E_{mP(\nu_n')} = \int E_{i(\nu)}\, R_{P(\nu_n', \nu)}\, d\nu$$

$$\approx \int E_{i(\nu)}\, R_{I(\nu_n, \nu)}\, d\nu \qquad \text{(watt-cm)},$$

where $R_{P(\nu_n', \nu)} \approx R_{I(\nu_n, \nu)}$.

The periodic process just discussed will yield audio components at a large number of harmonically related frequencies, $f_n = n/T_p$, where the minimum and maximum frequencies which are present are determined by the minimum and maximum wavenumber values of the radiation which reaches, and is detected by, the radiation detector. The magnitude of the component at each frequency will be related to the power spectral density of the radiation in the wavenumber region around $\nu'_n = (n/\gamma_{max})(\tau_p/T_p)$ as given by Eq. (36). Therefore, a rough measurement of the power density spectrum could be obtained by measuring P_n at each frequency f_n. However, since the response of the radiation detector and its associated circuitry varies quite widely at different audio modulation frequencies, it is desirable to perform all of the measurements at one particular audio frequency where n = N. Tuning over the wavenumber region of interest must then be accomplished by changing the relationship between f_N and ν'_N. Since $\nu'_N = N\tau_p/\gamma_{max}T_p$ this can be done by changing γ_{max}. This will also result in a change in the bandwidth, $(\Delta\nu)_p$, of the instrument response function, but since $(\Delta\nu) = 1/\gamma_{max}$ the relative resolution of the instrument remains constant:

$$\text{(37)} \qquad \text{Relative Resolution} = \frac{\nu'_N}{(\Delta\nu)_p} = N\tau_p/T_p \approx N/2 .$$

From a practical standpoint it would be possible to use a good narrow-band amplifier as the means of selecting out the frequency component at f_N, but a better signal-to-noise ratio can be achieved by employing correlation detection, utilizing a reference signal obtained from the mechanism which varies the path-length difference. The mechanics of this method will be considered in the following chapters.

As in the case of the aperiodic interferometric method, improvement of the instrument response function, $R_{P(\nu, \nu'_n)}$, may be achieved by combining several of the basic responses. In the periodic case this involves the adding together of several adjacent audio frequency components. This can be done quite neatly when correlation detection is employed by simply supplying the sum of three properly phased reference signals to the correlator multiplier, but when a sharply tuned amplifier is used as the frequency-selecting mechanism some problems may be encountered due to the relative phase shifts which the amplifier may introduce between the various audio frequency components.

For the case of the periodic interferometric receiver the interferometer output which is modulated at frequency f_N has a power P_N which is approximately equal to $(1/4)E_{i(\nu'_N)}(\Delta\nu)_P$, where $(\Delta\nu)_P$ is the

periodic instrument passband. The noise power of the radiation detector referred to its input will be given by (where τ is the R-C time constant of the correlator)

$$N_D = \frac{(NEP)}{\sqrt{2\tau_D}} \qquad \text{watts}). \tag{38}$$

Thus, the S/N ratio for the periodic case will be

$$(S/N)_P = \frac{P_N}{N_D} \approx \frac{E_{i(\nu_N')}(\Delta\nu)_P\sqrt{2\tau_D}}{4(NEP)} \tag{39}$$

To determine the time for the periodic instrument to scan from ν_1 to ν_2, first remember that the relative resolution, $\nu/(\Delta\nu)_P$, of the periodic instrument remains a constant, which will be called C. Then let the scan from the wavenumber $\nu - \left((\Delta\nu)_P/2\right)$ to $\nu + \left((\Delta\nu)_P/2\right)$ be accomplished in the time period $2\tau_D$. This will give

$$\frac{\partial t}{\partial \nu} = \frac{2\tau_D}{(\Delta\nu)_P} = \frac{2C\tau_D}{\nu} \qquad \text{(second-cm)}, \tag{40}$$

and therefore

$$Q_P = \frac{\displaystyle\int_{\nu_1}^{\nu_2} \frac{E_{i(\nu_N')}(\Delta\nu)_P\sqrt{2\tau_D}}{4(NEP)} \cdot \frac{d\nu}{E_{i(\nu_N')}(\Delta\nu)_P^2}}{2\tau_D \displaystyle\int_{\nu_1}^{\nu_2} \frac{C}{\nu}\, d\nu} \tag{41}$$

$$(41)\ (\text{cont}) \qquad = \frac{\frac{\sqrt{2\tau_D}}{4(\text{NEP})} \int_{\nu_1}^{\nu_2} \frac{1}{\left(\frac{\nu}{C}\right)}\, d\nu}{2\tau_D \int_{\nu_1}^{\nu_2} \frac{C}{\nu}\, d\nu} = \frac{1}{8(\text{NEP})} \sqrt{\frac{2}{\tau_D}} \quad (1/\text{watt-sec}),$$

which except for a factor of two is the same as that for the grating instrument, and still far below the figure of merit for the aperiodic interferometric receiver.

D. The Best Estimate of $E_{i(\nu)}$

The measurement of the power spectral density of the radiation entering a radiometric receiver may have one of two objectives: either to obtain an accurate measurement of the average power received over a given wavenumber region, $(\Delta\nu)$, or to obtain the best possible estimate of $E_{i(\nu)}$ as a function of ν. In the first case $(\Delta\nu)$ is already determined and is probably fairly large, and the main desire is to make the shape of the instrument response function approach a rectangle as nearly as possible. This can be done by the response-function improvement method described in Section B of this chapter.

The second case is somewhat different, since it is desired to have $(\Delta\nu)$ small enough to resolve the narrowest spectral lines appearing in $E_{i(\nu)}$, and yet not so small as to decrease the signal-to-noise

ratio below an acceptable limit.[4] Since $(\Delta\nu)$ is determined by the value of γ_{max}, which is in turn limited by diffraction effects in the instrument,[5] it may not always be possible to make the resolution of the instrument itself sufficiently great to resolve the spectrum of $E_{i(\nu)}$. However, it will be shown that, instrument noise level permitting, it is possible to process the experimental data to obtain any instrument resolution desired.

It has already been shown that $E_{i(\nu)}$ (as modified by the beam-splitter-efficiency and the detector-response curves) and $I_{o(\gamma)}$ form a Fourier transform pair where $E_{i(\nu)}$ is an unknown and $I_{o(\gamma)}$ is known from experiment on the interval $-\gamma_{max} < \gamma < +\gamma_{max}$. If $E_{i(\nu)}$ exists only over a finite interval of the frequency domain the interferogram $I_{o(\gamma)}$ will be an analytic function, and hence if $I_{o(\gamma)}$ and all of its derivatives can be determined exactly at any one point it should theoretically be possible to determine $I_{o(\gamma)}$ for all γ. From a practical point of view, if $I_{o(\gamma)}$ is known with good accuracy over a finite interval of γ it should be possible to obtain a good estimate of $I_{o(\gamma)}$ for values of γ outside of this interval. Slepian and Pollak show[25] how this can be done by expanding $I_{o(\gamma)}$ in terms of the prolate spheroidal wave

---

[4] See Eq. (23) of this chapter.

[5] See Chapter III.

functions, utilizing the special property of these functions which ensures orthogonality both on the finite interval and on the infinite interval of γ. The only restriction is that $E_{i(\nu)}$ must be band-limited. The latter restriction is not severe, since the beam-splitter-efficiency and the detector-response curves cause the effective input power spectral density to become zero below a certain wavenumber ν_{min} and above a certain wavenumber ν_{max}. Thus, converting the theory of Slepian and Pollak to the notation of this dissertation,

$$I_{o(\gamma)} = \sum_{}^{\infty} b_n \psi_n(\gamma) \qquad \text{(watts)}, \tag{42}$$

where $(-\infty < \gamma < +\infty)$ and where the $\psi_n(\gamma)$ are the prolate spheroidal wave functions and the coefficients are given by

$$b_n = \int_{-\infty}^{\infty} I_o(\gamma)\ \psi_n(\gamma) d\gamma = \frac{1}{\lambda_n} \int_{-\gamma_{max}}^{\gamma_{max}} I_o(\gamma)\psi_n(\gamma)\, d\gamma\ , \tag{43}$$

where:

$$\lambda_n = \int_{-\gamma_{max}}^{\gamma_{max}} \psi_n^2(\gamma) d\gamma\ . \tag{44}$$

Both $\psi_n(\gamma)$ and λ_n depend upon γ_{max} and upon the bandwidth of $I_o(\gamma)$ (the range of ν over which the effective input power spectral density exists). A complete discussion of the prolate spheroidal wave

function is given in reference [25]. The important point for the present discussion is that if it can be assumed that $E_{i(\nu)}$ is bandlimited (and if the noise level permits) then $I_{o(\gamma)}$ can theoretically be determined on the interval $-\infty < \gamma < +\infty$, even though it is measured experimentally only on the interval $-\gamma_{max} < \gamma < \gamma_{max}$ (or, since it is an even function, on the interval $0 < \gamma < \gamma_{max}$).

Another method or proving that it is theoretically possible to recover $E_{i(\nu)}$ from $E_{m(\nu)}$ is to show that the integral equation (12) relating $E_{m(\nu)}$ to $E_{i(\nu)}$ may be solved for $E_{i(\nu)}$. Again, if is necessary to assume that $E_{i(\nu)}$ is band-limited. Equation (12) is a Fredholm equation of the first kind and a solution may be obtained by expanding $E_{i(\nu)}$ in a complete orthogonal series. The lower limit over which $E_{i(\nu)}$ is assumed to exist may be set to zero and $E_{i(\nu)}$ and $E_{m(\nu)}$ considered as being double-sided functions, having equal components of magnitudes $E_{i(\nu)}/2$ and $E_{m(\nu)}/2$ respectively at $-\nu$ and $+\nu$. Then

$$(45) \qquad E_{m(\nu)} = \int_{-\nu_{max}}^{\nu_{max}} R_{(\nu, \nu')} E_{i(\nu')} \, d\nu' \quad \text{(watt-cm)},$$

where

$$(46) \qquad R_{(\nu, \nu')} = \frac{\sin 2\pi\gamma_{max}(\nu - \nu')}{\pi(\nu - \nu')} .$$

It is also known[25] that the prolate spheroidal wave functions,[6] which form a complete orthogonal set on the interval $-\nu_{max} < \nu < \nu_{max}$, satisfy the equation

$$(47) \qquad \lambda_k \psi_{k(\nu)} = \int_{-\nu_{max}}^{\nu_{max}} R_{(\nu, \nu')}\, \psi_{k(\nu')}\, d\nu' ,$$

where the eigenfunctions, $\psi_{k(\nu)}$, and their eigenvalues, λ_k, are dependent upon γ_{max} and ν_{max}. $E_{i(\nu)}$ may now be expanded in terms of these eigenfunctions,

$$(48) \qquad E_{i(\nu')} = \sum_k C_k \psi_{k(\nu')} \qquad \text{(watt-cm)}$$

and substituted into Eq. (45) to give

$$(49) \qquad E_{m(\nu)} = \sum_k C_k \int_{-\nu_{max}}^{\nu_{max}} R_{(\nu, \nu')}\, \psi_{k(\nu')}\, d\nu'$$

$$= \sum_k C_k \lambda_k \psi_{k(\nu)} \quad \text{(watt-cm)}.$$

Multiply $E_{m(\nu)}$ by $\psi_{j(\nu)}$ and integrate:

---

[6] The prolate spheroidal wave functions are normalized as follows:

$$\int_{-\infty}^{\infty} \psi_{j(\nu)} \psi_{k(\nu)} d\nu = \begin{cases} 0 & j \neq k \\ 1 & j = k \end{cases}, \text{ and: } \int_{-\nu_{max}}^{\nu_{max}} \psi_{j(\nu)} \psi_{k(\nu)} d\nu = \begin{cases} 0 & j \neq k \\ \lambda_k & j = k \end{cases}.$$

$$(50) \qquad \int_{-\nu_{max}}^{\nu_{max}} E_{m(\nu)}\, \psi_{j(\nu)} d\nu = \sum_{k} C_k \lambda_k \int_{-\nu_{max}}^{\nu_{max}} \psi_{k(\nu)} \psi_{j(\nu)} d\nu$$

$$= C_j [\lambda_j]^2 ,$$

or:

$$(51) \qquad C_k = \frac{1}{(\lambda_k)^2} \int_{-\nu_{max}}^{\nu_{max}} E_{m(\nu)}\, \psi_{k(\nu)}\, d\nu .$$

If one is working with the data in digital form an approximate solution to the integral equation can be obtained by putting the equation into matrix form and solving by means of digital computer techniques. Let $E_{i(\nu)}$ and $E_{m(\nu)}$ be digitized at the wavenumber points designated by ν_k or ν_j, where successive points are separated from one-another by the interval $\delta\nu$. Then the integral equation becomes

$$(52) \qquad E_{m(\nu_k)} = \sum_{j=1}^{N} E_{i(\nu_j)} \frac{\sin 2\pi \gamma_{max} (\nu_k - \nu_j)}{\pi(\nu_k - \nu_j)} \quad (\delta\nu) \text{ (watts-cm).}$$

This is equivalent to the matrix equation

$$(53) \qquad [E_{mk}] = [R_{kj}][E_{ij}]$$

which may be solved for E_{ij}. A better approximation to the integral equation may be obtained by using Simpson's Rule in the writing of the integral equation in digital form:

$$(54) \qquad E_{m(\nu_k)} = \frac{1}{3}\left[E_{i_1}R_{k1} + 4E_{i_2}R_{k2} + 2E_{i_3}R_{k3} + \cdots + 4E_{i(N-1)}R_{k(N-1)} + E_{i_N}R_{kN}\right] \text{ (watt-cm)}.$$

This may also be put in matrix form and solved on the computer.

The preceeding discussion has shown that - given a measured power spectral density, $E_{m(\nu)}$, or its equivalent interferogram function, $I_{o(\gamma)}$, existing only on $-\gamma_{max} < \gamma < \gamma_{max}$ - it is theoretically possible to determine the actual effective input power spectral density or to determine the interferogram function outside of the finite interval on which it is known experimentally. This illusion of being able to obtain additional information for no extra experimental effort exists because of the fact that experimental error or noise was neglected in the preceeding discussion. Even it it can be assumed that $I_{o(\gamma)}$ can be obtained out to a value of γ equal to several times γ_{max} without introducing any additional noise, the total time, T_t, taken to record the data remains unchanged, while the instrument bandwidth, $(\Delta\nu)_I$, is reduced by the same factor as the interval is extended. Thus, Eq. (23) shows that the signal-to-noise ratio is lowered by this same factor.

Since solving the integral equation (45) exactly is tantamount to extending γ_{max} to infinity without increasing T_t, one can surmise

that an attempt to find $E_{i(\nu)}$ exactly by this means would end in failure because of an infinite noise level on the solution. The net result is that one is not able to acquire new information by the preceeding data-processing techniques, but only to trade one type of information for another (i.e., signal-to-noise ratio for spectral resolution).

CHAPTER III
EXPERIMENTAL CONSIDERATIONS

A. Adaptation of the Michelson Interferometer

A submillimeter interferometric receiver may be constructed along lines very similar to the conventional optical Michelson interferometer, except that the half-silvered mirror and the compensating plate must be replaced by a beam splitter suitable for submillimeter-wavelength radiation. Also, the fixed and movable mirrors of the Michelson system must be of the front-surfaced type, and the movable mirror must be driven by an appropriate mechanism for operation in either the aperiodic or the periodic mode of operation. The actual mechanical construction of the Michelson interferometer considered in this paper will be outlined in the next chapter. The present chapter will deal with the characteristics and problems of this general type of instrument.

B. Beam-Splitter Efficiency

It can be shown (Appendix IV) that the beam-splitter efficiency in terms of the ratio of the power delivered to the detector under conditions of zero path length difference to the incident power is

given by $4|\Gamma_R|^2 |\Gamma_T|^2$ where Γ_R and Γ_T are the complex voltage reflection and transmission coefficients of the beam splitter. The maximum efficiency (100 per cent) of the beam splitter occurs when $|\Gamma_R|^2 = |\Gamma_T|^2 = 0.5$. For most practical submillimeter-wavelength beam splitters Γ_R and Γ_T are dependent upon the wavenumber, and the maximum-efficiency condition, it if occurs at all, occurs only at one particular wavenumber. For wire-mesh beam splitters the wavenumber at which the peak efficiency occurs and the width of the peak will depend upon the mesh coarseness, thickness and orientation; and in a dielectric-film type of beam splitter these factors will depend upon the dielectric constant and the thickness of the film. They will also depend upon the angle of incidence and reflection (usually 45 degrees). The losses in the beam splitter will depend primarily upon the beam-splitter material and the method of fabrication. Due to the variation in the beam-splitter efficiency with wavenumber it may be necessary to use several different beam splitters in the instrument to cover the wavenumber region of interest. When the beam-splitter efficiency is considered, the factor $4|\Gamma_R|^2 |\Gamma_T|^2$ must be inserted into most of the results of Chapter II. For example, Equation (29) becomes

$$Q_I = \frac{(\nu_2 - \nu_1)(4|\Gamma_R|^2 |\Gamma_T|^2)}{4\sqrt{2\pi (\Delta\nu)_I \nu_2 \tau_D}\,(\mathrm{NEP})} \quad (1/\text{watt-sec}). \tag{55}$$

C. Grating Efficiency

The diffraction-grating type of receiver also does not deliver all of the incident power in a given wavenumber region to the radiation detector. Most of the losses in this instrument are due to the dispersion of some of the radiation at the desired wavelength into grating orders other than the one desired, which is usually the first order. Even with special precautions the maximum efficiency which can be obtained is on the order of ninety percent[26], and this at only one wavelength. Therefore, comparable to the case of the beam splitters in the interferometric receiver, it may be necessary to use a number of different diffraction gratings to cover the wavenumber region of interest.

D. Fringing Effects in the Michelson Interferometer

The theory of Chapter II considered perfectly collimated radiation entering the Michelson interferometer, which implies a point source of radiation. Since this is, in general, not the case, it is necessary to consider the effects of passing radiation from a source of finite size through the collimating system and the interferometer. For simplicity the collimating optics can be approximated by a thin lens of focal length L as shown in Fig. 5. The radiation from

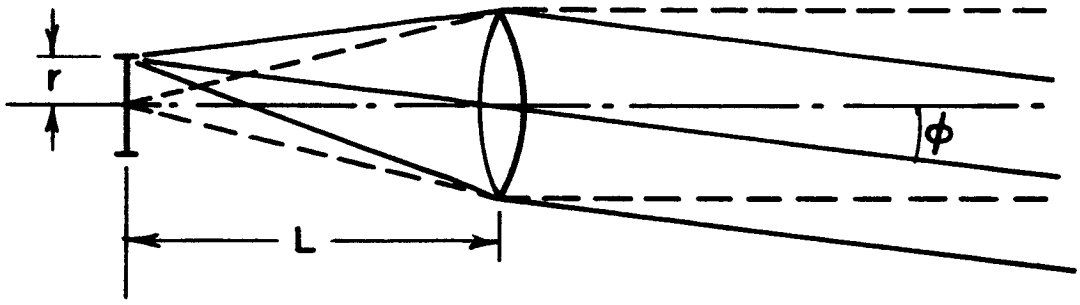

Fig. 5--The collimating system and the radiation source.

a point located on the source (or input aperture) at the center-line focal point of the optical system will produce collimated radiation parallel to the optical system axis, while a point on the source at a distance r from the center will produce collimated radiation at an angle ϕ to the optical system axis, where $\tan \phi = r/L$.

Now consider the general case of a collimated beam of radiation entering the Michelson interferometer at some angle ϕ with respect to the optical system axis as shown in Fig. 6. The dotted lines show the path followed by a single ray when the mirror displacement, G, is zero, while the solid lines indicate the modification made when G is increased to some finite value. The phases of rays A and B are assumed to be equal at the constant phase-front line. From the drawing one can see that

$$q = \left(\frac{G}{\cos \phi}\right) \sin 2\phi \quad \text{(cm)}, \tag{56}$$

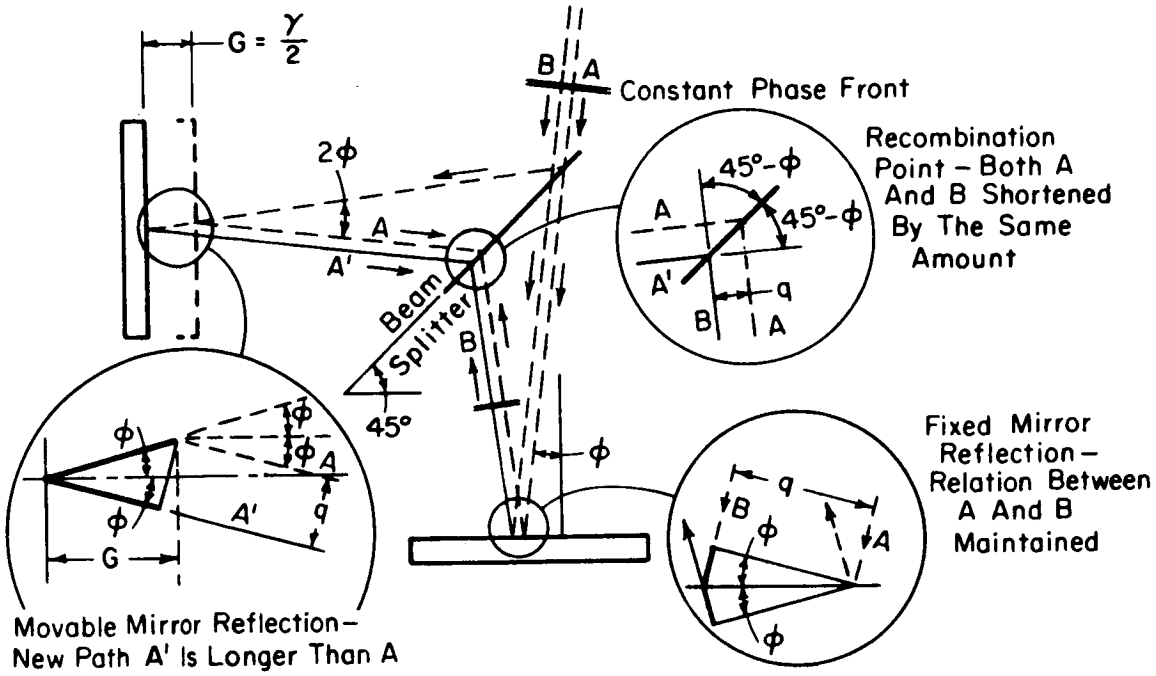

Fig. 6--Effects of off-axis radiation upon the operation of the Michelson interferometer.

which gives for the path-length difference between rays that

$$(57) \qquad \gamma = \frac{G}{\cos\phi} + \left(\frac{G}{\cos\phi}\right)\cos 2\phi$$

$$= \left(\frac{G}{\cos\phi}\right)(1 + \cos 2\phi)$$

$$= \left(\frac{G}{\cos\phi}\right)(2\cos^2\phi) = 2G\cos\phi \quad \text{(cm)}.$$

Therefore, the effective path-length difference is dependent upon the angle of the incoming radiation and hence upon the particular point on the source from which the radiation originated. If a large source were to be used the radiation from different parts of the source would interfere to a substantially non-uniform degree, and if all of the

radiation were refocused onto the detector a good reproduction of the interferogram function could not be obtained at large values of G. This would place a practical limit on the value of G_{max} and hence limit the resolution of the interferometric receiver. For instance, let the source radius, r, be 0.8 cm and the collimating system focal length 28.5 cm: ϕ_{max} would be about 1.6 degrees. If the allowable variation in the path-length-difference phase shift of the radiation at λ = 100 microns (0.01 cm) is taken to be twenty electrical degrees (1/18th of a wavelength) then

$$(58) \qquad [\gamma_{(0°)} - \gamma_{(20°)}] = \frac{0.01}{18} = 0.000556 \quad \text{cm}$$

$$= 2G_{max}[1-\cos 1.6°] = 2G_{max}[0.00039] \quad \text{(cm)},$$

or G_{max} = 0.714 cm or 7,140 microns, thus giving a minimum ($\Delta\nu$) of about 0.7 cm^{-1}. The worst case would occur when the maximum variation in the path-length difference is 180 electrical degrees. This would occur (for λ = 0.01 cm) when $[\gamma_{(0°)} - \gamma_{(180°)}] = 0.005$ cm, G_{max} = 6.41 cm, and the minimum ($\Delta\nu$) equal to 0.078 cm^{-1}.

E. Problems Characteristic of the Aperiodic Mode of Operation

Although the aperiodic mode of operation of the interferometric receiver is probably more simple from a practical standpoint thanis the periodic mode, there are still a number of problems which must be overcome. One of the primary problems is the obtaining of the value of the interferogram function at precisely the desired values of the path-length difference or movable mirror displacement. One way this may be done is by continuously recording the interferogram function on a chart recorder and either manually or automatically making tick marks on the paper at the spots where a reading is desired. However, this necessitates the manual reading of the chart to prepare the interferogram data for computer processing, and this is always time-consuming and a source of possible error. By using digital recording techniques wherein the interferogram function is sampled at the desired values of the mirror displacement the process of preparing the experimental data can be automated to a large degree.

In both of the above cases one is still faced with the problem of accurately determining the value of the mirror displacement. This can be done in a number of ways. One method is to use monochromatic visible light reflected off a corner of the main movable

mirror and a small auxillary mirror to form a visible interference pattern. A photoelectric cell and a counter are used to count the movement of the fringes past a fixed point as the mirror is moved [9, 10]. Properly constructed this would probably be the most accurate method, but also the most complex to build and use. A second method involves the use of a precision mechanical gauge, such as a dial indicator, to measure directly the mirror displacement, and a third method involves the use of a well-constructed ratio-arm assembly, wherein a rather large and easily measured movement at the long end of the ratio arm produces a small movement of the mirror.

It should be obvious that very rugged construction of the instrument is necessary to insure uniform movement of the movable mirror and to eliminate as completely as possible any vibration or wobble in the optical system.[1] All of the mechanical joints of the system, while being tight, should operate easily and smoothly so that no bending or twisting of the structural members results from large frictional loading forces. A small amount of backlash in the system can usually be removed by the proper degree of spring loading.

---

[1] See Appendix V for a discussion of the required accuracy of optical alignment.

If, in the aperiodic mode of operation, the source of radiation has a high equivalent black-body temperature the near infrared and visible radiation entering the instrument may be many orders of magnitude greater than the submillimeter radiation which it is desired to measure. Since all of this radiation is chopped by the radiation chopper it will all contribute to the output of the radiation detector unless it can somehow be rejected or compensated for. If a wire mesh of the proper coarseness for use in the submillimeter region is employed as the beamsplitter, it will be found that much of the near-infrared and visible radiation is scattered, much of it in the general direction of the radiation detector. This scattered radiation does not produce any interference phenomenon as the movable mirror is moved, its net effect being to contribute a "constant" component to the interferogram function which is now produced primarily by the submillimeter-wavelength radiation. The average value of this "constant" component can be balanced out by applying an appropriate d.c. bias voltage to the recorder terminals in series with the output of the synchronous rectifier. However, this does not eliminate any fluctuations in the "constant" component, and these remain as noise contributions to the interferogram function. These fluctuations result primarily from the random fluctuations in the magnitude of the large amount of visible and near-infrared power and from the increase in

the detector NEP due to the greater level of radiation entering it. Thus, it appears that introducing compensation after the radiation detector or destroying the coherence of the near-infrared and visible radiation are not the proper ways to eliminate or reduce this source of noise; but instead one must totally reject the shorter-wavelength radiation at some point before it enters the radiation detector. This also leads to problems, for if a filter which passes only the submillimeter radiation is placed between the source and the radiation chopper the filter will be heated by the near-infrared and visible radiation, and if it has any losses at all in the submillimeter region it will radiate its own submillimeter spectrum into the instrument, thereby confusing the measurement of the desired source of radiation. If a thin filter is placed after the chopper, it will alternately heat and cool as the radiation is interrupted by the chopper and will contribute a confusing signal to the radiation detector. A thicker filter after the chopper will remain at a fairly constant temperature, and its re-radiation of energy will not be important, but its losses in the sub-millimeter region will substantially reduce the desired output signal. Eliminating the ill effects of shorter-wavelength radiation from the instrument will be a difficult problem anytime that it is encountered, such as when solar radiation measurements are being made; and

each case must be considered individually with regard to the desired validity of the spectral measurement and the required signal-to-noise ratio.

Fellgett[5], in his optical instrument, used corner reflectors in his modification of the Michelson interferometer and was able to recover the radiation which in a normal Michelson instrument would be reflected back out the input. He fed this radiation to a second detector and subtracted the resulting signal from the signal derived from the first detector. In this manner he was able to reduce the effects of starlight scintillation upon the recorded interferogram output. From Appendix IV, with unity power input to the Michelson the power into the second detector is given by

$$(59)\quad P_{D_2} = |\Gamma_R|^4 + |\Gamma_T|^4 + 2|\Gamma_R|^2|\Gamma_T|^2 \left[\cos(2(\theta_R-\theta_T))\cos(\theta_1-\theta_2) - \sin(2(\theta_R-\theta_T))\sin(\theta_1-\theta_2)\right] \text{ (watts)},$$

where $\Gamma_R = |\Gamma_R|\epsilon^{j\theta_R}$ and $\Gamma_T = |\Gamma_T|\epsilon^{j\theta_T}$,

and the power into the first detector is

$$(60)\quad P_{D_1} = |\Gamma_R|^2|\Gamma_T|^2 (2 + 2\cos(\theta_1-\theta_2)) \quad \text{(watts)}.$$

For most beam splitters $|\theta_R-\theta_T|$ is approximately ninety electrical degrees within the region where the efficiency factor $4|\Gamma_R|^2|\Gamma_T|^2$

is relatively high. Therefore, one has for the difference in the two detector signals that

$$(61) \quad P_{D1} - P_{D2} = 2|\Gamma_R|^2 |\Gamma_T|^2 (\cos(\theta_1 - \theta_2) + \cos(\theta_1 - \theta_2)) + (2|\Gamma_R|^2 |\Gamma_T|^2 - |\Gamma_R|^4 - |\Gamma_T|^4) \text{ watts},$$

which is to be compared with the original detector signal,

$$(62) \quad P_{D1} = 2|\Gamma_R|^2 |\Gamma_T|^2 (\cos(\theta_1 - \theta_2) + 1) \qquad \text{(watts)}.$$

Two things have happended: the usable signal has been doubled and the d.c. component, which can contribute nothing but noise, has been eliminated or greatly reduced. However, the additional radiation detector will contribute noise to the system, and whether or not the output signal-to-noise ratio will be better or worse will depend upon the relative magnitudes of the scintillation noise and the detector noise. In order not to introduce errors in the measurements and/or additional noise, the detectors must be as nearly identical as possible with respect to both spectral response and time response.

Since scintillation noise can also be expected in the submillimeter region, a system such as Fellgett's could also be valuable at these wavelengths if an ideal beam splitter were available for the

entire region. However, since this is not the case (i.e., $|\Gamma_R| \neq |\Gamma_R|$ and $|\theta_R - \theta_T| \neq 90°$) such a system would probably have little advantage over the conventional Michelson system, although if a beam splitter could be found which would scatter nearly equal amounts of near-infrared radiation into each detector the system might be useful for reducing the ill effects of this shorter wavelength radiation. To the author's knowledge, such an arrangement has not been tried experimentally.

Another method of reducing the effects of near-infrared and visible radiation in the aperiodic mode might be to employ a rotary radiation chopper which would chop the submillimeter radiation but not the near-infrared or visible radiation. Such a chopper might be constructed using blades made of common window glass (which would not chop the radiation at wavelengths shorter than three microns).

F. Problems Characteristic of the Periodic Mode of Operation

The comments made in the previous section on the need for sturdy mechanical construction also apply to the periodic mode of operation, only to a greater degree, for now one must also content with the large accelerations which occur during the turn-around period and with the need for maintaining uniform motion while the mirror is moving in either direction. In order to minimize

vibration, the mass of the moving parts should be kept as small as possible. It may also be necessary to utilize some type of vibration-dampening mountings to reduce the effects of vibration originating in the drive mechanism.

The selection of a radiation detector for use in the periodic mode is more critical than in the aperiodic case, for in the latter the detector need only to respond to the on-off radiation chopping employed there, while in the periodic case the detector must reproduce, with at least some degree of faithfulness, the interferogram time function, or at least the frequency components of this function which are of interest. Therefore, while a resonant detector such as the Golay cell may be adequate in the aperiodic case, a detector with a faster response and less phase shift should be employed for the periodic case.[2] Also, since the signal-to-noise ratio obtained in the periodic case is inherently less than that of the aperiodic case, a more sensitive detector is desirable for periodic-mode operation.

---

[2] Since only one audio frequency (usually in the 10 to 30 cycle-per-second region) is of interest, it may at first seem that a narrow-band (or resonant) detector and/or a narrow band preamplifier would be desirable for the periodic case. This would be true if correlation detection were not used to select the desired audio frequency out of the interferogram time function, in which case the phase shift and the time delay due to the narrow-banding would be of little consequence. However, when correlation methods are employed the phase shift and time delay cannot be tolerated.

The selection of the desired audio frequency components from the interferogram time function can be most easily accomplished by multiplying the detector output with a reference signal (a cosine wave or the sum of several cosine waves at the desired reference frequency or frequencies) and passing the resultant product through an integrator circuit. This is commonly called "correlation detection" and the reference signal which is needed can be obtained from the mirror-drive mechanism. It is necessary to incorporate mechanical adjustments for adjusting the phase of the reference signal generator so as to be able to compensate for phase shifts and time delays in the radiation detector and the electronic circuitry, as well as for minor day-to-day changes in the mirror-drive system. Also, any small amount of residual mechanical backlash present in the mirror-drive system will appear as an effective time lag in the interferogram function and it will be necessary to delay the phase of the reference signal to compensate for this.

Near-infrared and visible radiation also causes some problems in the case of periodic-mode operation. If allowed to enter the radiation detector it will contribute its noise to the detector output and also cause the NEP of the detector to increase. The effects of the noise appearing on the interferogram function are reduced by the correlation detection process before they appear on the measured

power spectral density, but of course the same thing occurs when the interferogram function recorded in the aperiodic case is processed in the digital computer, so the periodic mode has no inherent advantage from this standpoint. However, since only the submillimeter-wavelength radiation is modulated to any appreciable extent in the periodic interferometer it is relatively easy to filter out the shorter-wavelength undesired radiation with a filter placed between the modulator and the detector. Even a very thin filter will remain at nearly constant temperature, and since it comes after the modulator any re-radiation in the submillimeter region will not appear as part of the measured power spectral density.

CHAPTER IV
EXPERIMENTAL EQUIPMENT

A. General Outline

Figure 7 is a top-view schematic drawing of the submillimeter interferometric receiver set up for operation in the aperiodic mode.

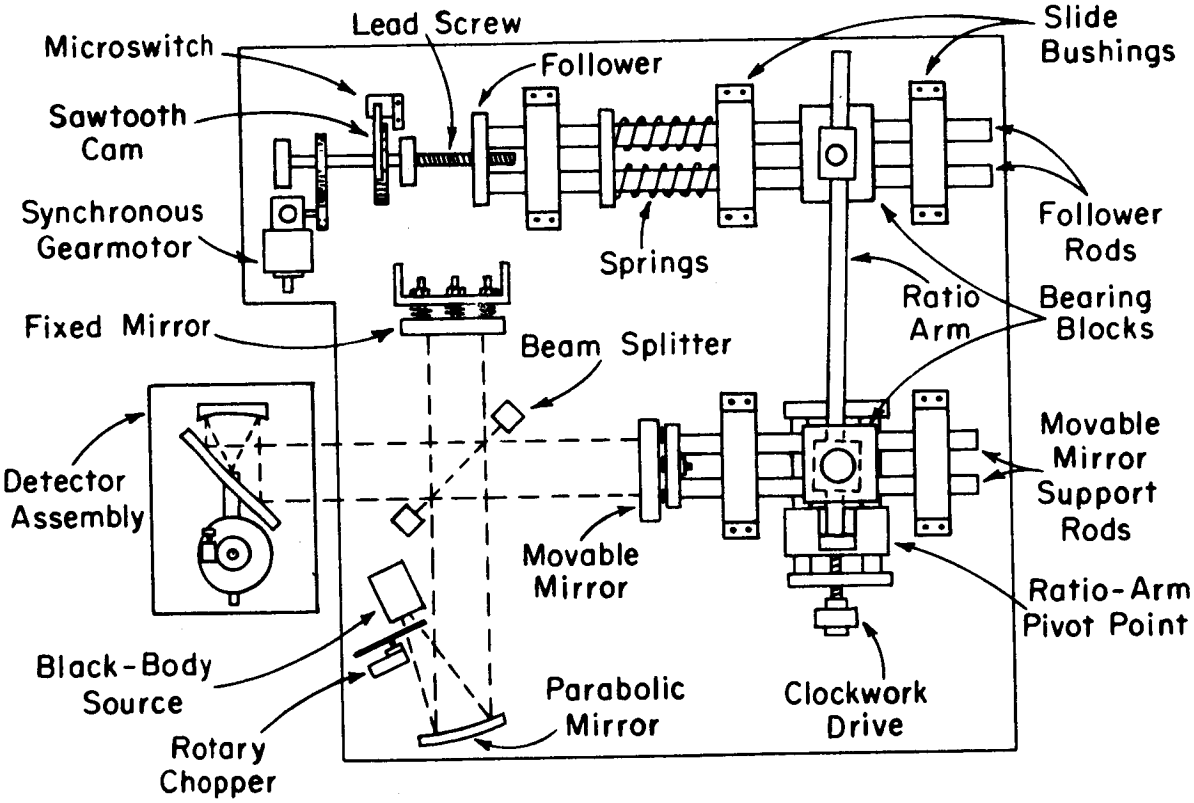

Fig. 7--Top-view schematic of the interferometer as set up for aperiodic-mode operation.

The synchronous gearmotor turns a lead screw which causes the follower block to move in a linear motion and to swing the ratio arm in an arc. This in turn causes a linear motion of the movable-mirror support. The ratio of the mirror-support movement to that of the follower-block movement on the lead screw is dependent upon the position of the ratio-arm pivot point. The latter is adjustable on sliding ways. During an aperiodic test run the pivot point position remains fixed, while during a periodic test it moves slowly. A dial indicator is used to give a direct indication of the position and movement of the movable-mirror support. This dial indicator is calibrated in ten-micron units. A sawtooth cam and a microswitch on the gearmotor lead-screw shaft are used to provide fifteen reference pulses for each turn of the lead-screw shaft (see Fig. 8). These pulses are used to trigger the digital paper-tape recording equipment which converts the analogue output of the radiation-detector system ($I_o(t)$) to digital form and records it on the tape for latter computer processing. Figure 7 also shows the rotary chopper located in the radiation path just before the input optics. A system of front-surfaced optics collimates the input radiation and directs it to the interferometer. The output of the interferometer goes to a detector assembly consisting of a

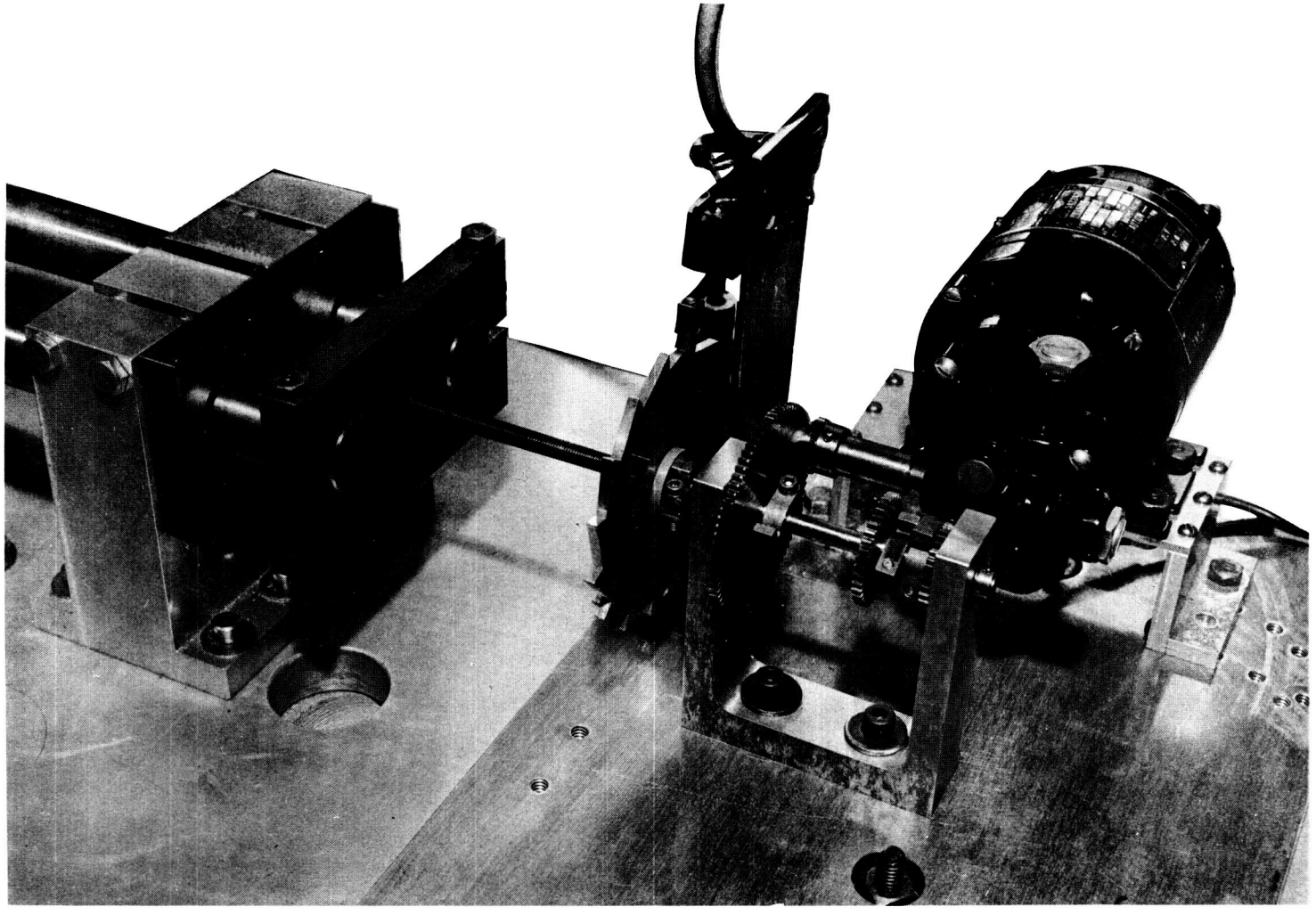

Fig. 8--The aperiodic drive showing the synchronous gearmotor, lead-screw drive, and the sawtooth cam and its microswitch.

Texas Instruments gallium-doped germanium bolometer and an appropriate optical system[27].

For periodic-mode operation the synchronous gearmotor and the lead screw and follower combination are replaced by an Archimedes cam and its follower, the camshaft being coupled into a variable-speed drive located under the radiometer table (see Fig. 10). Also mounted on the cam shaft is a drum to which a photographic negative is attached. The negative bears a graphical representation of the desired reference signal and this is converted into an electrical signal by an exciter lamp and photocell assembly. The stroke of the cam follower is linear over a three-inch range and the movable-mirror stroke (and hence γ_{max} and the tuning of the radiometer) is varied by changing the pivot-point position. This is done in a linear manner by attaching a clockmotor drive to the lead screw which moves the pivot-point bearing block. The clockmotor then varies the position of the ratio-arm pivot point at the proper rate as the test progresses.

All the critical rotary mechanical joints are made by means of two opposed Timken tapered roller bearings which are slightly preloaded to reduce backlash, and all sliding contacts are made by means of Thompson linear ball bushings. The normal mechanical adjustments are made by changing the position of the ratio-arm

bearing block on the cam-follower rods, the position of the similar bearing block on the movable-mirror support rods, and either the rotary position of the reference drum on the cam shaft (periodic operation) or the position of the sawtooth cam on the gearmotor lead screw (aperiodic operation).

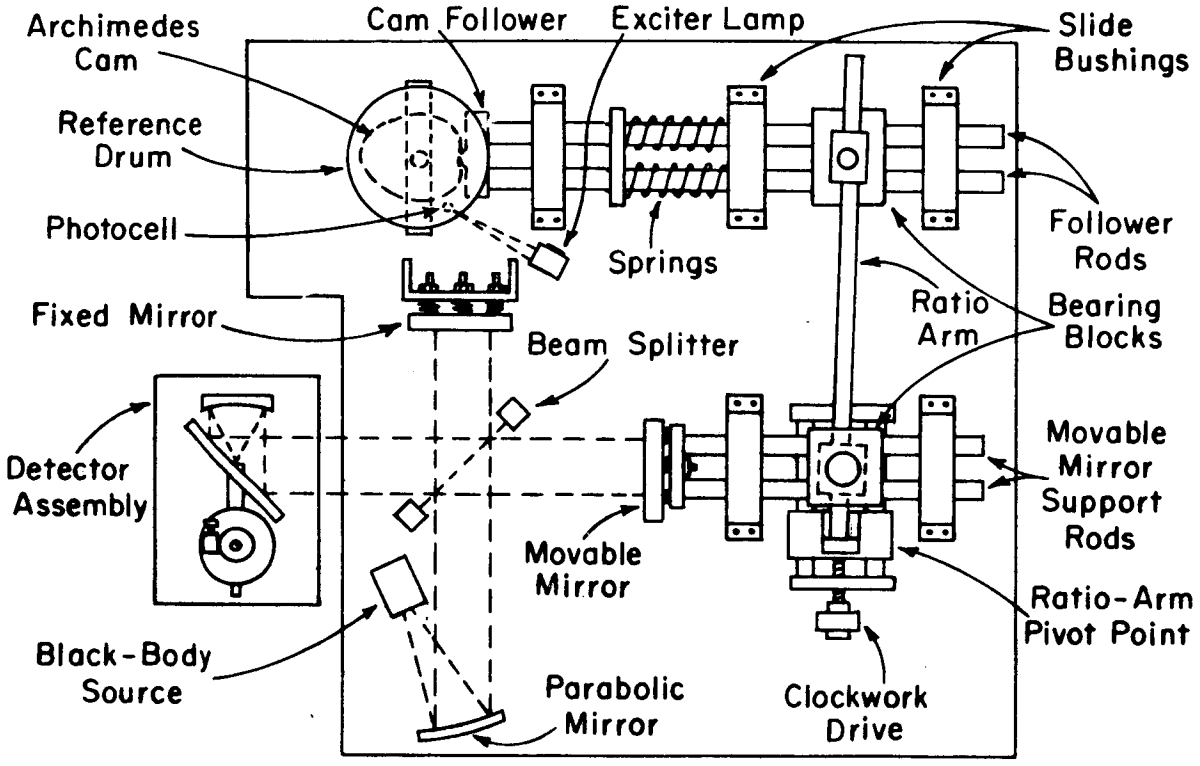

Fig. 9--Top-view schematic of the interferometer as set up for periodic-mode operation.

The optical system of the interferometer consists of a 28.5 cm focal-length off-axis parabolic mirror three inches in diameter which collimates the radiation and sends it to the beam splitter which is an electroformed nickle mesh mounted on a five-inch

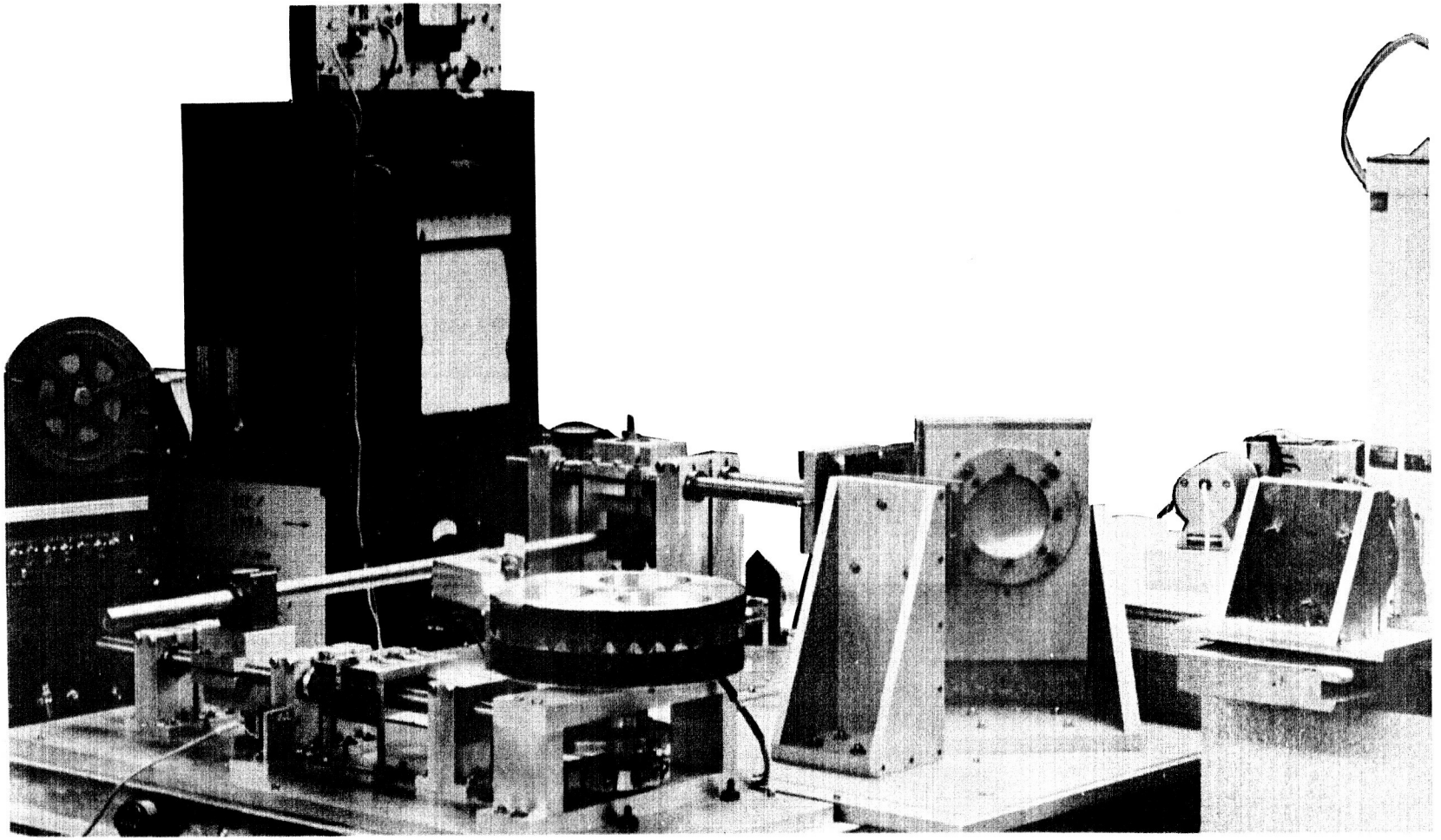

Fig. 10--The instrument as set up for periodic mode operation, with the cam and the reference drum shown in the front center. The ratio arm is to the left of the cam and the movable mirror support to the rear of the cam. The interferometer optics are to the right of the cam and the detector is at the extreme right of the picture.

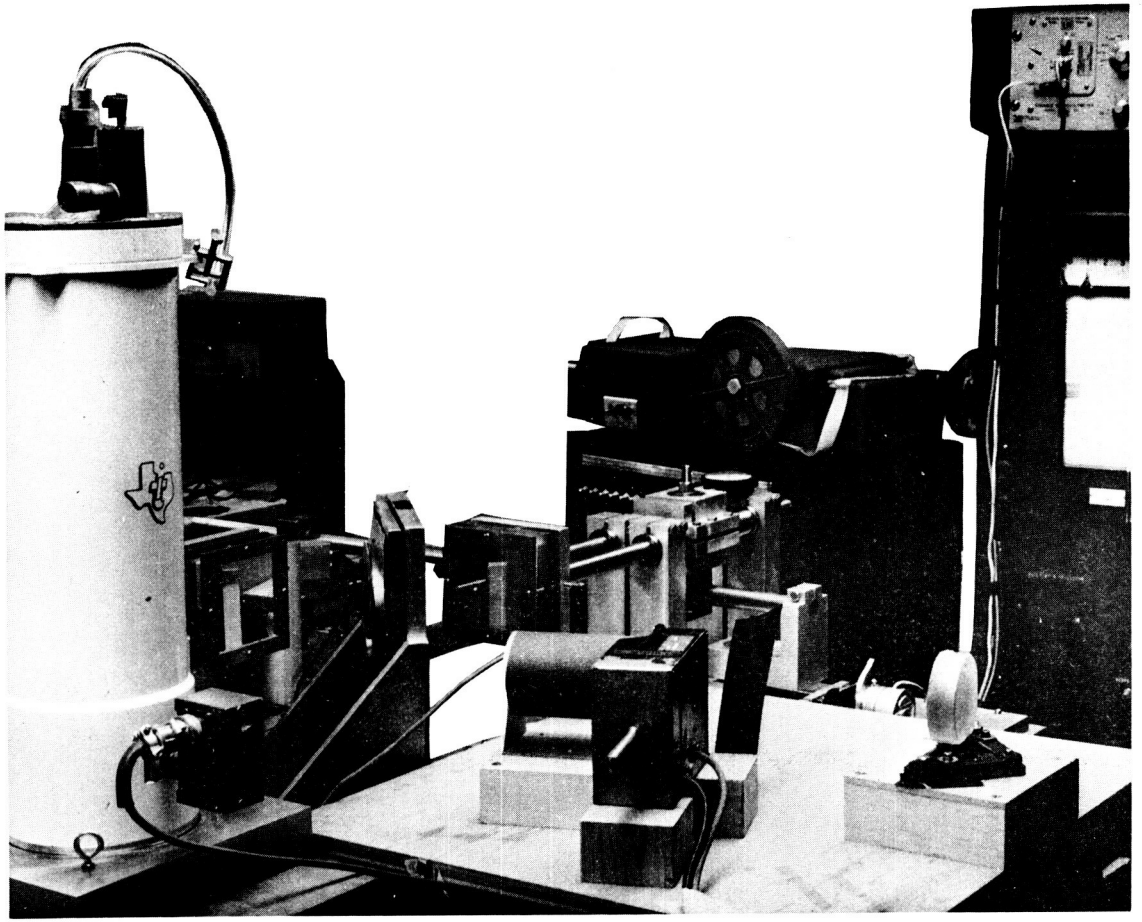

Fig. 11--A view of the optical system showing the detector dewar at the left, the fixed mirror, the beam splitter, and the movable mirror. In the foreground are the black-body source, the rotary chopper (for aperiodic mode operation), and the parabolic mirror. In the rear are the electronic equipment and the paper-tape punch.

outside and four-inch inside diameter metal ring. The mesh surface is pressed against a ground surface in the beam splitter mount by eight screws which bear upon the back side of the metal ring (see Fig. 10). Meshes with a line coarseness of from 500 to 80 lines per inch are used as the beam splitters. Both the fixed and the movable mirror are four-inch square front-surfaced glass mirrors of optical quality. Both the beam splitter and the mirrors are supported on three-point spring-loaded screw adjustments which are used to obtain the proper optical alignment of the interferometer system.

The detector assembly, which is shown in Fig. 12 is built around Texas Instruments' low-temperature bolometer mounted in one of their three-liter liquid-helium dewars. A light pipe three-sixteenths of an inch in inside diameter is used to convey the radiation from the outside of the dewar into the detector element. The outside end of the light pipe is just behind the crystal quartz vacuum window at the end of the tubular extension at the bottom of the dewar. The dewar is mounted so that this tubular extension extends through a plane mirror which is oriented at forty-five degrees to the incoming collimated radiation from the interferometer. The radiation is reflected from the plane mirror to a five-inch diameter,

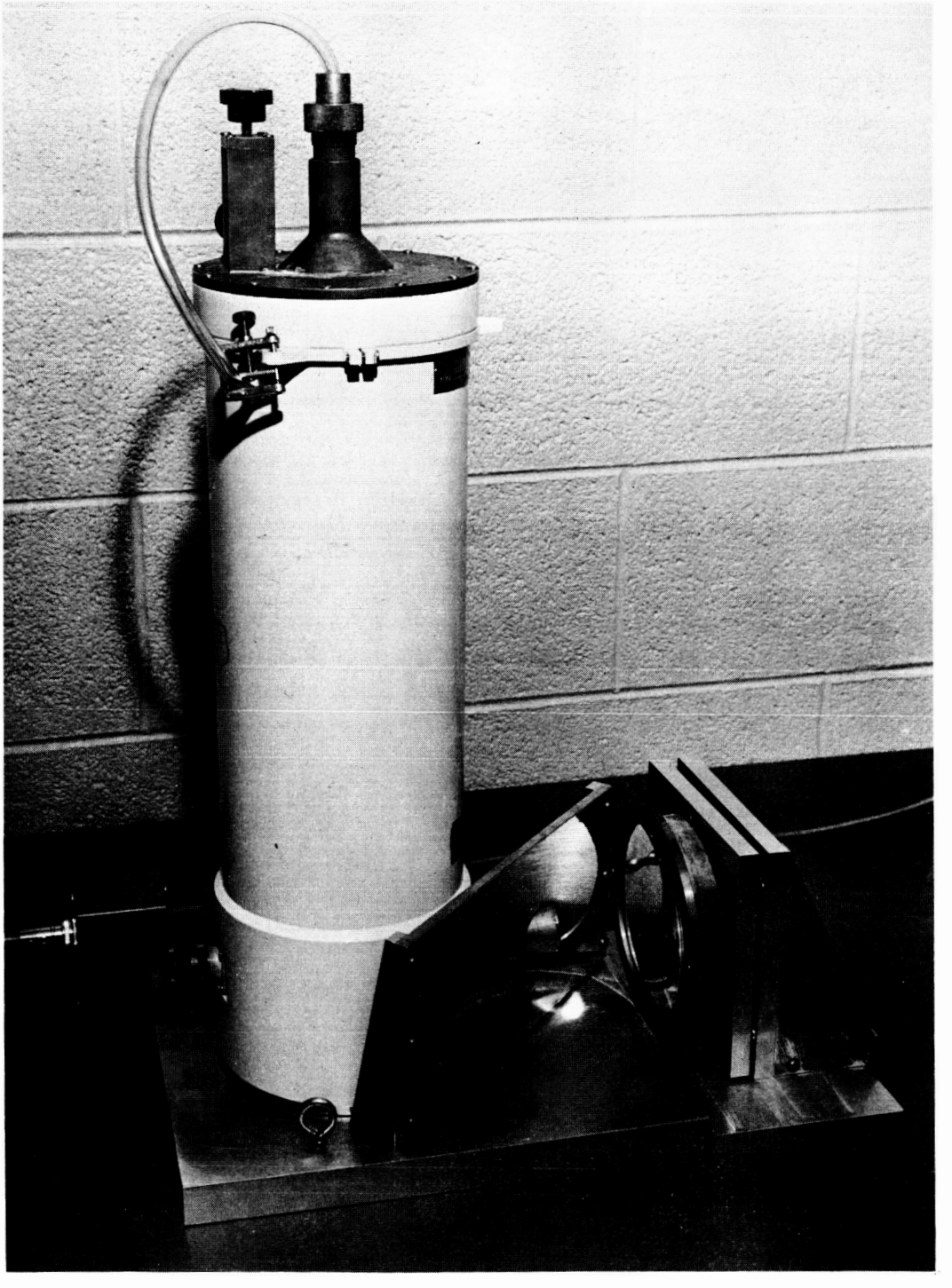

Fig. 12--A view of the detector system. The collimated radiation is reflected from the 45-degree plane mirror onto the spherical mirror at the right, which focuses it upon the end of the tubular dewar extension which extends through the plane mirror.

three-and-one-half-inch-focal-length spherical mirror onto the end of the light pipe.

The electronic system for the aperiodic mode is shown in part (b) of Fig. 13 and the system for the periodic mode is shown in part (a) of Fig. 13. The rotary chopper used to interrupt the radiation in the aperiodic case also provides a square wave reference signal which is used in the synchronous rectification of the radiation detector signal, employing the same multiplier (a transistor-driven Hall-effect device) as is used as the correlator when operating in the periodic mode. The filtered output (in the aperiodic case) is sampled, converted to digital form, and punched into an eight-level paper tape, which can be read directly into an IBM 1620 computer which then prepares the data for input to an IBM 7094 computer which computes the Fourier transform.

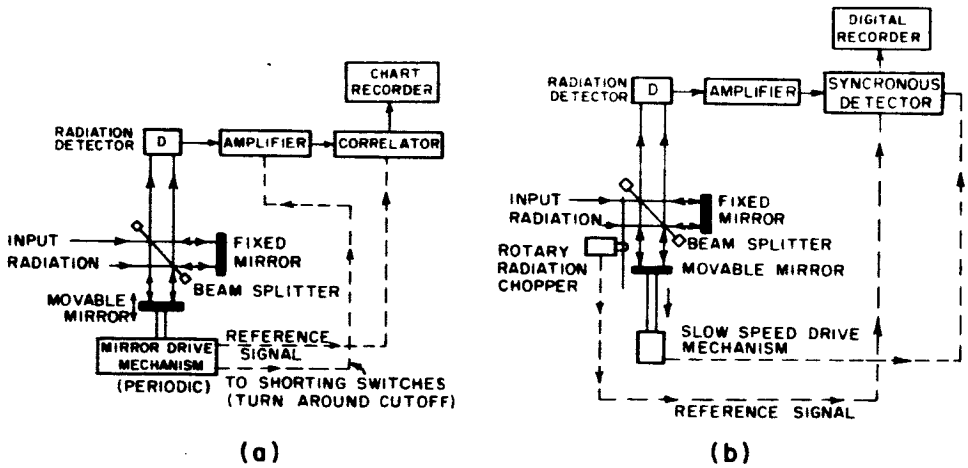

Fig. 13--Block diagrams of the interferometric receiver systems for (a) periodic-mode operation, and (b) aperiodic-mode operation.

In the periodic case the detector output is multiplied with the reference signal derived from the reference drum mounted on the cam shaft of the instrument, and the integrated output is a d.c. voltage which is fed directly to a paper-chart recorder. The deflection of the recorder corresponds to the measured power spectral density in the periodic case.

In both the aperiodic and periodic cases the TI bolometer is supplied with a twenty-microampere bias current from a low-noise precision power supply, and the signal from the bolometer is fed into a tunable 1-1000 cps microvoltmeter which serves as a wideband amplifier during periodic tests and as a sharply tuned amplifier peaked up on the chopping frequency during aperiodic tests. The output of the microvoltmeter is fed into the transistor power amplifiers which drive the Hall-effect multiplier. An integration time of two to six seconds is used following the multiplier, this being satisfactory in most instances unless the signal-to-noise ratio of the detector output is quite low. A longer integration time requires, of course, that the data be taken at a slower rate. With a one-second integration time it was found that the TI detector had a noise power of about $\sqrt{2} \times 10^{-11}$ watt (based upon a measured NEP of about 2×10^{-11} watt per cycle of audio bandwidth). The system is also arranged for use with a Golay-cell radiation detector if this

is so desired, but with a resulting loss of signal-to-noise ratio.

B. Operation of the Interferometric Receiver

1. The aperiodic mode. In the aperiodic mode the pivot point is first positioned to produce the desired maximum displacement of the movable mirror when the gearmotor lead screw is turned the desired number of turns. Then while watching the d.c. output of the detector system on a chart recorder the lead screw is slowly turned until the optical mirror position is reached, at which time the path-length difference is zero and the detector output (the interferogram function) reaches its maximum value since all of the radiation from both beams is in phase. The interferometer's optics are now aligned by adjusting the tilt of the beam splitter and the two mirrors until the maximum output is obtained. Also at this time the sawtooth cam is adjusted to one of the triggering points and the lead screw is backed off few turns and the gearmotor connected and turned on. Just before the mirror position is again reached the digital recording equipment is placed in operation and from this point on the operation of the system is entirely automatic, with the interferogram data being recorded on the punched paper tape. It is best to have the adjustment of the pivot point position such that for each turn of the lead screw (each fifteen data points) the

displacement of the movable mirror is some round number which it is mathematically convenient to work.

2. The periodic mode. Initial adjustments in the periodic mode are best made by operating the instrument as if in the aperiodic mode, only with the cam being used in place of the gearmotor and lead-screw drive. The mirror position is found by turning the cam slowly while observing the interferogram recorded on the chart recorder. The mirror position should be reached with the cam at the half-way point and the movable mirror should then remain at the mirror position while the position of the ratio-arm pivot point is varied. It may be necessary to move the bearing block which connects the ratio arm to the movable-mirror drive rods until this condition is reached. After these adjustments are made the electronic system is connected for operation in the periodic mode and the cam drive started at the normal speed. An oscilloscope is used to observe both the detector signal and the reference signal just before these enter the Hall-effect multiplier, and the two bearing blocks and the position of the reference-signal drum on the cam shaft are adjusted until the detector signal remains in phase with the reference signal for all settings of the ratio-arm pivot point. These three adjustments are all interdependent, but in general it will be found best to adjust the bearing

block on the movable mirror support rods at short strokes of the movable mirror, and to adjust the bearing block on the cam follower rods at long strokes of the movable mirror (i.e., large γ_{max}). One of the new storage-type oscilloscopes will be found to be of great value in carrying out these adjustments. Once the adjustments are completed the ratio-arm pivot point is adjusted to the zero-stroke position and then moved out again to the maximum-stroke position while the number of turns of the lead screw which positions the pivot point are counted. While at the maximum stroke position the length of the linear stroke of the movable mirror (i.e., γ_{max}) is measured and recorded. The clockmotor drive is then engaged to the lead screw and the system output is recorded as the ratio-arm pivot point is slowly moved back towards the zero-stroke position. This recorded output will then be the measured power spectral density as a function of the radiation wavelength. As an aid to calibrating the chart it is helpful to record a tick mark at each completed turn of the lead screw which positions the pivot point.

C. Estimation of $[\Delta T_{s_{min}}]$

The minimum detectable change in the source temperature, $[\Delta T_{s_{min}}]$, will be calculated for an aperiodic interferometric receiver having design parameters approximately equivalent to the one just described.

The first step is the estimation of the minimum change, $[\Delta E_{i_{(\nu)_{min}}}]$, in the input power spectral density which the receiver is capable of detecting. It is assumed that this occurs when the signal-to-noise ratio becomes unity in Eq. (23). Then, considering also the effects of the beam-splitter losses, one has that

$$[\Delta E_{i_{(\nu)_{min}}}] = \frac{4(\mathrm{NEP})}{\sqrt{T_t}(4|\Gamma_R|^2\,|\Gamma_T|^2)(\Delta\nu)_I} \quad \text{(watt-cm)}. \tag{63}$$

Whenever a test source is being used under laboratory conditions quite a long length of time can be taken to make the desired measurements without system stability becoming a problem. For example, assume that T_t = two hours = 7200 seconds, and let the NEP of the detector (including all of the filter losses, etc.) be about 10^{-10} watts. Then at the wavenumber where $4|\Gamma_R|^2\,|\Gamma_T|^2$ is of the order of unity, $[\Delta E_{i_{(\nu)_{min}}}]$ will be

$$(64) \qquad [\Delta E_{i(\nu)_{min}}] = \frac{4(10^{-10})}{\sqrt{7200\,(1)\,(0.65)}}$$

$$\approx 7.26 \times 10^{-12} \quad \text{(watt-cm)},$$

where $(\Delta\nu)_I$ has been taken to be $0.65\ cm^{-1}$. In the case of the periodic instrument the integration time is normally of the order of four to six seconds, which would give an increase in the minimum detectable change in the power spectral density. However, at the same time the wavenumber bandwidth of the periodic instrument is much wider (probably greater than $100/30 \doteq 3.3$ microns at $\lambda = 100$ microns) which would tend to decrease the minimum detectable change in the power spectral density. As a result, $[\Delta E_{i(\nu)_{min}}]$ in the periodic case would probably be less than seven times greater than $[\Delta E_{i(\nu)_{min}}]$ in the aperiodic case.

Once $[\Delta E_{i(\nu)_{min}}]$ has been determined, one needs only to consider the geometry of the instrument optics, the mean source temperature, T_s, and the wavenumber at which the radiation is being measured to arrive at an estimate for $[\Delta T_{s_{min}}]$. Let the interferometer, its detector, and its test source be schematically represented by Fig. 14 where the input and the output mirrors are represented by lenses of diameter D and focal lengths δ_i and δ_o respectively. Let A_s be the area of the source and A_D the area

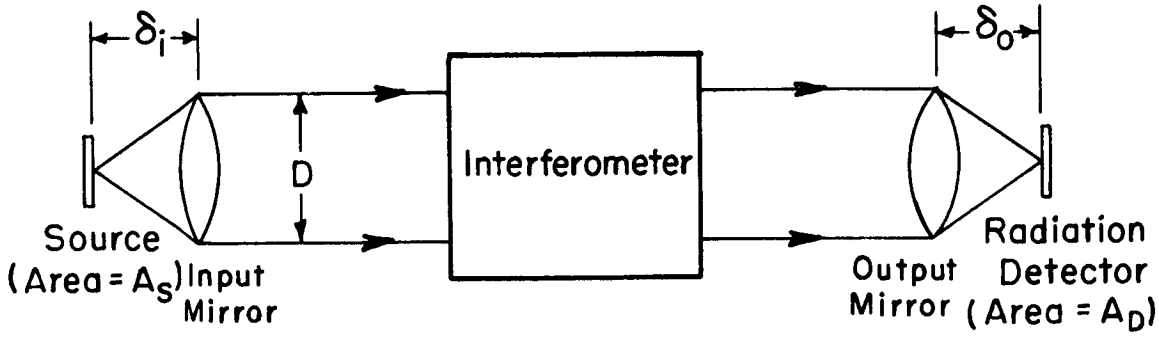

Fig. 14--Schematic representation of the optics of a laboratory test system for determining $[\Delta T_{s_{min}}]$.

of the radiation detector, and let the detector area imaged upon the source be A_D', where

$$A_D' = \left(\frac{\delta_i}{\delta_o}\right)^2 A_D \,. \tag{65}$$

The solid angle into which the source radiates is denoted as $(\Delta\Omega)_I = \pi D^2/4(\delta_i)^2$, and to the first approximation the radiation which the source radiates into this angle reaches the detector in its entirety. It is assumed that $(\Delta\Omega)_I$ is small enough that the cosine factor appearing in the Planck radiation law is approximately unity. One then has, from Eq. (4) in Chapter I,

$$[\Delta T_{s_{min}}] = \frac{\eta\Gamma}{ck} \left[\Delta E_{i_{(\nu)_{min}}}\right] \qquad (°K), \tag{66}$$

where η is given by Eq. (5), where Γ in this case becomes

$$\Gamma = \frac{\lambda^2}{2A_s(\Delta\Omega)_I} \quad , \tag{67}$$

and where A_s may be replaced by A_D' if $A_D' < A_s$.

If the instrument described in the preceding sections of this chapter is now analyzed by the above method, using an operational wavenumber of 100 cm^{-1} (λ = 100μ) one obtains the following parameters:

$$[\Delta E_{i(\nu)_{min}}] \doteq 7.3 \times 10^{-12} \text{ watts}$$

$$\delta_i = 28.5 \text{ cm}$$

$$\delta_o = 8.9 \text{ cm}$$

$$A_D = \frac{\pi}{4}(0.475)^2 = 0.178 \text{ cm}^2$$

$$A_s = \frac{\pi}{4}(1.59)^2 = 1.98 \text{ cm}^2$$

$$A_D' = \left(\frac{28.5}{8.9}\right)^2 (0.178) = 1.827 \text{ cm}^2$$

and

$$\Gamma = \frac{(0.01)^2}{2(1.827)(0.056)} = 4.78 \times 10^{-4} \quad ,$$

where

$$(\Delta\Omega)_I = \frac{\pi}{4}\,\frac{(7.62)^2}{(28.5)^2} = 0.056 \quad .$$

Let T_s = 500°K. Then from Fig. 1 one finds for λ = 100μ that $\eta \approx$ unity, and one has

$$(68)\quad [\Delta T_{s_{min}}] = \frac{(1)(4.78 \times 10^{-4})(2 \times 10^{-11})}{(3 \times 10^{10})(1.38 \times 10^{-23})}$$

$$\doteq 8.6 \times 10^{-3} \qquad (^{\circ}K).$$

Thus, the interferometric instrument is theoretically capable of detecting a smaller temperature change than the normal operating fluctuations in the temperature of the black body test source. Of course, this sensitivity figure does not take into account atmospheric absorption of the radiation and the fluctuations thereof, the possible drift in the electronic equipment over a long period of time (two hours), digitizing errors, etc., all of which would serve to reduce the sensitivity of the instrument. For instance, it was found that the digitizing equipment alone produced about a one percent peak-to-peak error in the recorded interferogram output (based upon the interferogram value at $\gamma = 0$). The effects of such an error, which is proportional to the total power received by the instrument, is discussed in the next paragraph.

The peak value of the interferogram is due to the total power passed by the beam splitter and the radiation filters and which is detected by the radiation detector, or

$$(69)\quad I_{o(\gamma)}\Big|_{max} = \int E_{i_{(\nu)}} d\nu = E_{i_{(\nu)}}\Big|_{av} (\nu_2 - \nu_1)$$

where $E_{i(\nu)}\big|_{av}$ is the average value of $E_{i(\nu)}$ (which now is assumed to include the factors of beam-splitter efficiency, radiation filter attenuation and detector response) and where $(\nu_2 - \nu_1)$ is the effective region over which $E_{i(\nu)}\big|_{av}$ exists. Let the rms noise on the interferogram due to digitizing error, recorder error, etc, be a certain fraction, U, of $I_{o(\gamma)}\big|_{max}$. Then the mean-square noise on the interferogram is equal to $U^2\,[E_{i(\nu)}\big|_{av}(\nu_2 - \nu_1)]^2\,(\text{watts})^2$. Assume now that this has a uniform spectral density from $\nu = 0$ up to the maximum possible ν consistent with the rate of data sampling. If the spacing between data points is $(\Delta\gamma)$ then this value of ν will be $1/2(\Delta\gamma)$. Thus the mean-square noise spectral density will be equal to $U^2\,[E_{i(\nu)}\big|_{av}(\nu_2 - \nu_1)]^2\,(2)\,(\Delta\gamma)\,(\text{watt})^2\text{-cm}$. If this is related to the frequency (in CPS) density of the mean-square voltage noise at the detector output, one has, since $s = d\gamma/dt = \gamma_{max}/T_t = f/\nu$, $U^2\,[E_{i(\nu)}\big|_{av}(\nu_2 - \nu_1)]^2\,(2)\,(\Delta\gamma)(\Omega)(1/s)$. This is the mean-square noise voltage density of the variable $N_{(t)}$ in Eq. (20) of Chapter II. As before, the operation of Eq. (20) is equivalent to passing $4N_{(t)}T_t$ through a bandpass filter of noise bandwidth $1/2T_t$ and maximum gain of $1/2$. Thus, the mean-square noise density on the output signal will be $(1/2)\,[4\Omega T_t U\,E_{i(\nu)}\big|_{av}(\nu_2 - \nu_1)]^2\,(2)(\Delta\gamma)$ $(1/s)(1/2T_t)$, and the rms noise voltage density will be:

$$(70) \qquad N_{(f)} = \frac{4}{\sqrt{2}}\, U^2 E_{i(\nu)}\Big|_{av} \Omega\, (\nu_2 - \nu_1) \sqrt{\frac{T_t(\Delta\gamma)}{s}} \quad .$$

Since from Chapter II the expression for the signal voltage density was $S_{I(f)} = \Omega\ E_{i(\nu)}\big|_{av}/2s$ one has for the noise-to-signal ratio on the output due to any noise which is a constant fraction of the interferogram:

$$(71) \qquad \frac{N_{(f)}}{S_{I(f)}} = \left(2\sqrt{2}\ U E_{i(\nu)}\Big|_{av} \Omega\, (\nu_2 - \nu_1) \sqrt{\frac{T_t(\Delta\gamma)}{s}}\ \right) \times \left(\frac{2s}{\Omega\ E_{i(\nu)}\big|_{av}}\right)$$

$$= 4\sqrt{2}\ U (\nu_2 - \nu_1) \sqrt{(\Delta\gamma)\, \gamma_{max}} \ .$$

Applying Eq. (70) to the instrument just described where $U = \frac{1}{2}(0.707)(0.01) \doteq 0.0035$, where $(\Delta\gamma) = 20 \times 10^{-4}$ cm, where $\gamma_{max} = 1.56$ cm, and where $(\nu_2 - \nu_1)$ is taken to be 70 cm^{-1} one has

$$(72) \qquad \frac{N_{(f)}}{S_{I(f)}} = 4\sqrt{2}\,(3.5)10^{-3}\,(70)\sqrt{20 \cdot 10^{-4} \cdot 156}$$

$$= 775 \times 10^{-4} = 0.0775.$$

Thus, if, for instance, the signal itself was due to a difference of 200°C between the source temperature and the chopper blade temperature, $[\Delta T_{s_{min}}]$ due to the type of noise just discussed would be about 15.5°C. This is much greater than the $[\Delta T_{s_{min}}]$ due to the radiation detector noise or some other fixed-level noise source in the system. It could be reduced by reducing the relative error in the digitizing system, by eliminating all of the radiation except

that of interest (i.e., reducing $(\nu_2 - \nu_1)$), by sampling the interferogram data more often (i.e., by reducing $\Delta\gamma$), or by broadening the instrument response function by decreasing γ_{max}. Another method of reducing this noise would be to reduce the detector signal itself by letting the chopper blade temperature more closely approximate the source temperature until the point is reached where the fixed noises in the system (such as the detector noise) become approximately equal to the noises which are proportional to the input signal.

CHAPTER V
EXPERIMENTAL RESULTS

A. Preliminary Tests

Preliminary tests on the instrument indicated a number of problem areas which had to be cleared up before satisfactory data could be obtained.

For instance, if the path-length difference, γ, is changed very rapidly when γ is close to zero, the value of $I_{o(\gamma)}$ will also change very rapidly, and because of the long time constants in the radiation-detection system and the delay in the data recording system $I_{o(\gamma)}$ will not be recorded accurately. On the other hand, a rate of change of γ which would have given satisfactory results in this region would have let to an excessive time requirement for the test as a whole. A satisfactory compromise was obtained by manually rotating the gearmotor shaft very slowly while γ was in the vicinity of zero and then using two successively higher motor speeds as γ became larger. It was also found that the effects of the error in the digital recording equipment could be reduced by applying a small, stable, direct-current bias just ahead of the digitizing unit, and then increasing

the system gain and adjusting the bias voltage until the interferogram output covered practically the full range of the digitizing unit. Similarly, on the preliminary tests in the periodic mode it was found that the best results could be obtained if the synchronization between the interferogram function and the reference signal was monitored continuously on an oscilloscope and slight adjustments made in the position of the movable mirror so as to accurately maintain the synchronization throughout the entire test.

B. Aperiodic Tests

The aperiodic tests were conducted using four different beam splitters (500, 200, 120, and 80 lines-per-inch respectively), all of which were oriented such that the mesh lines ran at a forty-five degree angle to the horizontal. With the exception of the test using the 120 LPI-mesh beam splitter, all of the tests were conducted using a 0.054-inch thick black polyethelene filter in the radiation path. The purpose of this filter was to reduce the amount of near-infrared radiation reaching the detector. The path from the radiation source to the detector was about two meters long, and the measurements were made under the conditions of 22 to 25 percent relative humidity and 75 to 77 degrees farenheit temperature.

The first two tests were conducted using a γ_{max} of 1.56 centimeters, which gave a $(\Delta\nu)_I$ of about 0.64 cm^{-1}, and the next two tests were conducted using γ_{max} of 1.726 centimeters, which gave a $(\Delta\nu)_I$ of about 0.58 cm^{-1}. The resulting data are presented in Figs. 15 to 18 and in Figs. 19 to 22, respectively. The data thus obtained were further processed for the first two cases (the 500 LPI- and 200 LPI-mesh tests) in the manner described in the section of Chapter II dealing with response-function improvement by means of adding together three basic response functions. These data are presented in Figs. 23 to 26 inclusive, where the passband of the improved instrument response function is 1.28 cm^{-1}. In order to obtain a comparison between an improved and an unimproved instrument response function of the same bandwidth the interferogram data from the 500 LPI- and 200 LPI-mesh tests were processed only out to γ_m = 7800 microns(0.78 cm) and the resulting power spectral densities (now with $(\Delta\nu)_I$ = 1.28 cm^{-1}) plotted as Figs. 27 to 30 inclusive. Finally, an attempt was made at calculating the spectral density at points spaced closer than $[d\nu] = 1/2\,\gamma_{max}$. In this case the calculation was made at wavenumber values separated by $[d\nu] = 1/8\,\gamma_{max}$ after first subtracting the constant component from the interferogram function. These data are presented in Figs. 31 and 32. Figure 31 also shows the results of an attempt to solve the

matrix equation (53) for $E_{i_{(\nu)}}$ (dotted line). Due to the core-storage limitations of the computer, these data could be obtained only over small wavenumber regions on one computer run, and the data presented as the dotted line in Fig. 31 represents a composite of the data from several such computer runs.

A comparison of the data obtained by the aperiodic method with the data obtained by Yoshinaga et al.[28], Oetjen et al.[29], and Yaroslavsky and Stanevich[30] with conventional grating-type monochromators indicates very good agreement with respect to the location and the general shape of the various absorption and transmission bands over the wavenumber regions where the efficiency of the various individual beam splitters was good. About the only major discrepancy was the appearance on the experimental data of two moderately-small absorption lines at about 87 and 88 microns respectively which do not appear in the references, although Reference [29] does indicate a very shallow and broad absorption region in this location. Also, on Figs. 19 to 22 inclusive, which were calculated and plotted on a slightly different scale than the other tests (due to the different γ_{max} used), the spectral curve seems to be shifted very slightly to the left at the higher wavenumber values. This may have been due to a slight error in determining the correct value of γ_{max}.

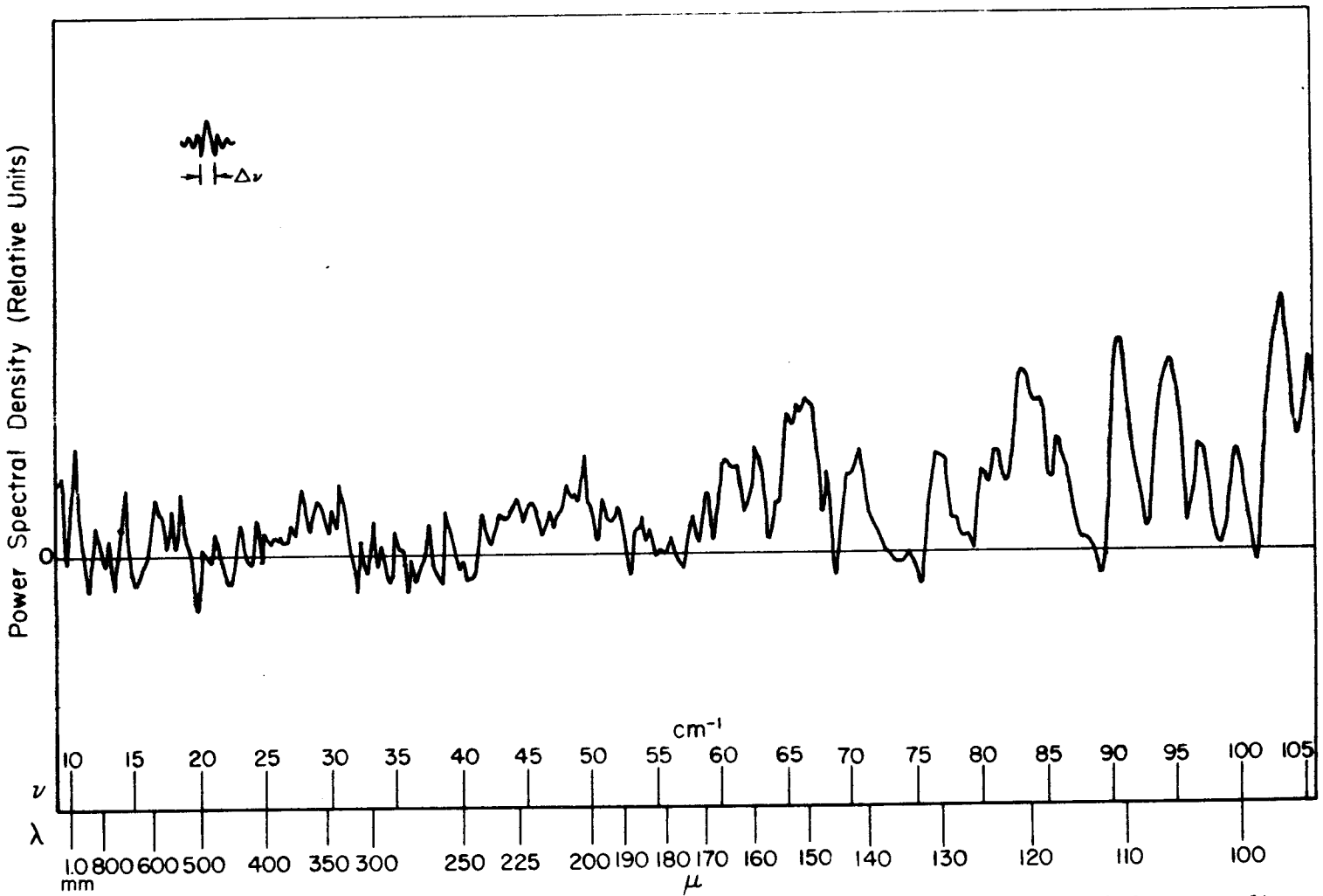

Fig. 15--Basic aperiodic spectral-density data obtained using a 500 LPI-mesh beam splitter; $(\Delta\nu)_I = 0.64\ cm^{-1}$, $Y_{max} = 1.56$ cm, and $\nu = 10$ to $105\ cm^{-1}$. A black-polyethelene radiation filter was used in the optical path.

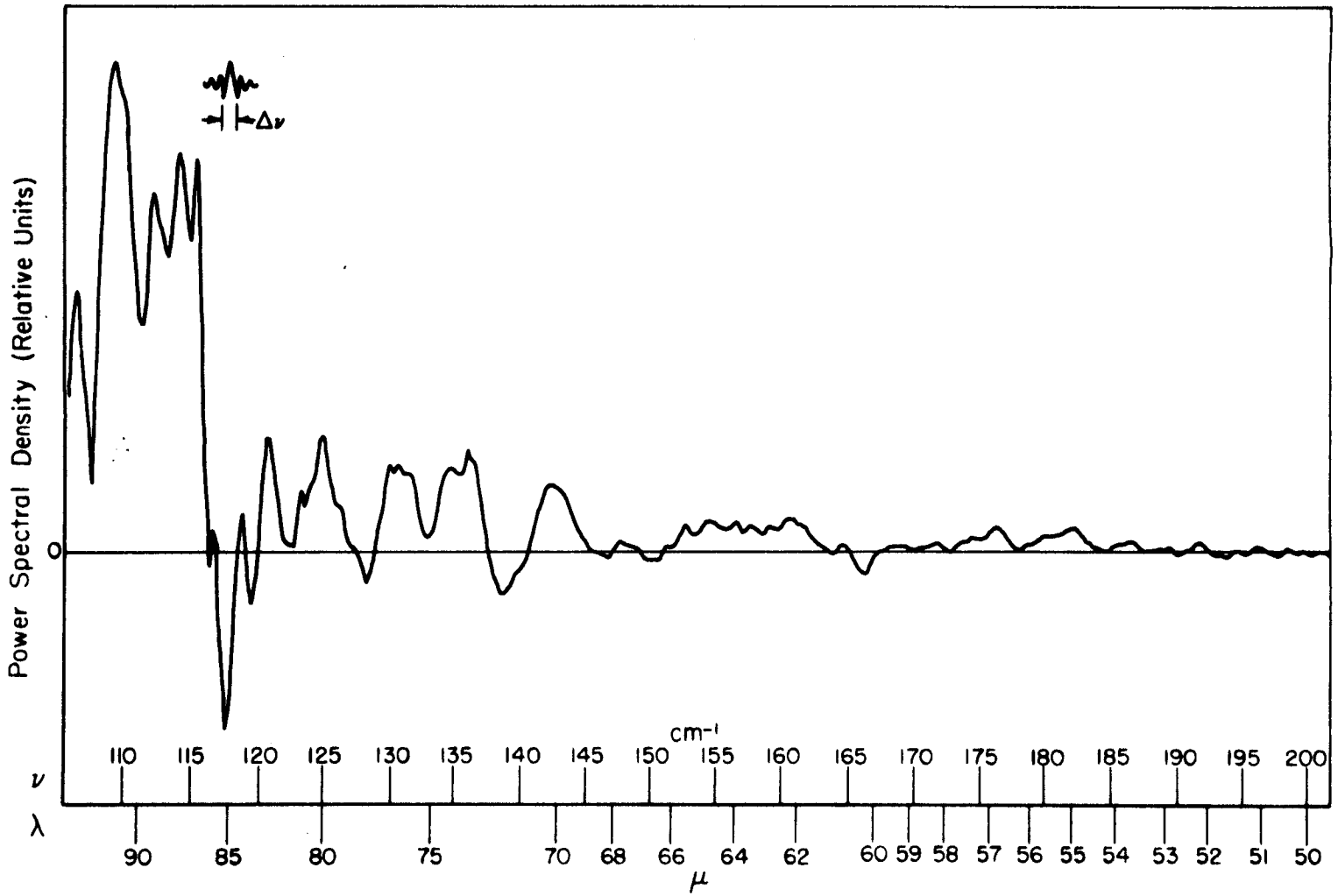

Fig. 16--Basic aperiodic spectral-density data obtained using a 500 LPI-mesh beam splitter; $(\Delta\nu)_I = 0.64\ cm^{-1}$, $\gamma_{max} = 1.56$ cm, and $\nu = 105$ to $200\ cm^{-1}$. A black-polyethelene radiation filter was used in the optical path.

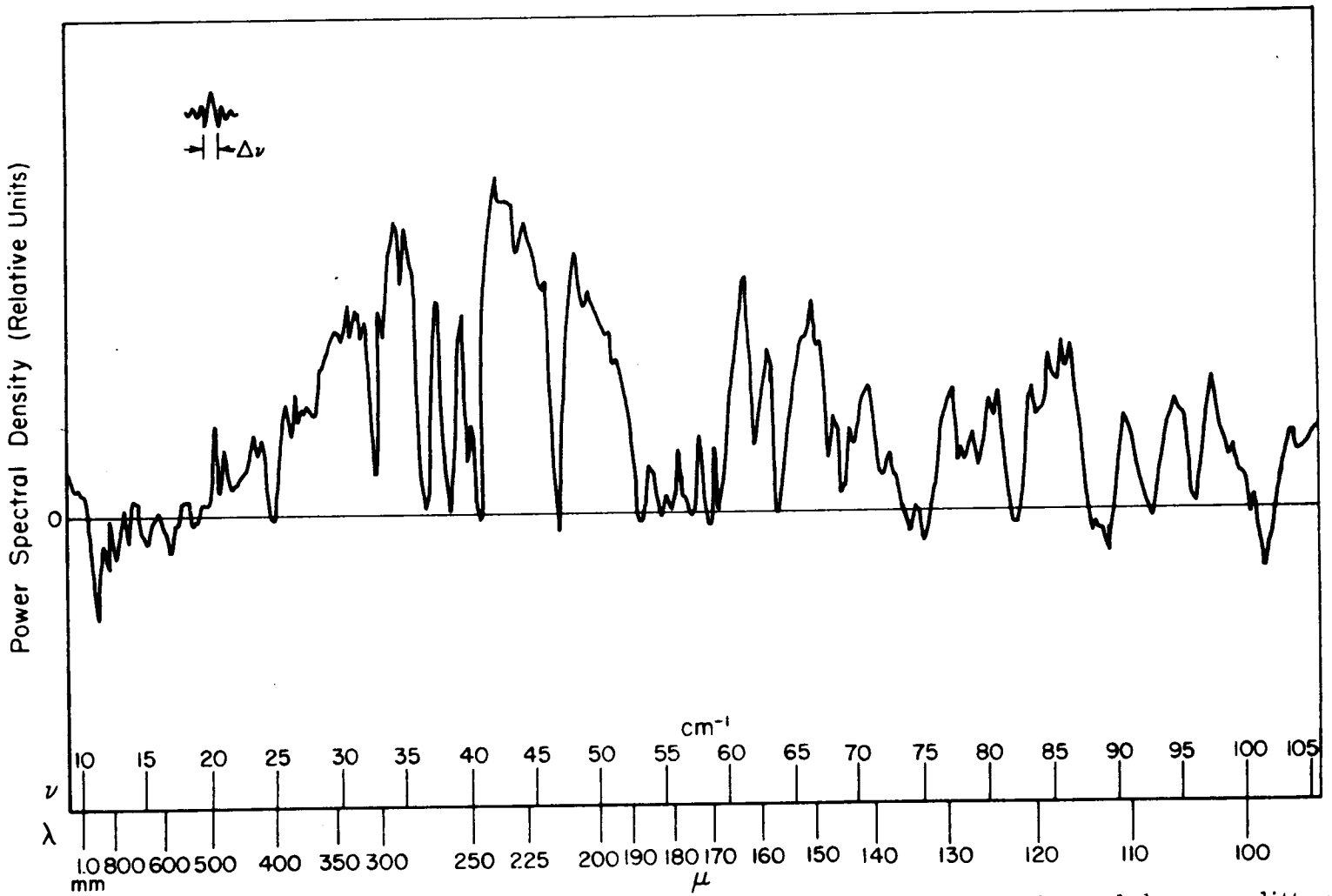

Fig. 17--Basic aperiodic spectral-density data obtained using a 200 LPI-mesh beam splitter; $(\Delta\nu)_I = 0.64\ cm^{-1}$, $\gamma_{max} = 1.56$ cm, and $\nu = 10$ to $105\ cm^{-1}$. A black-polyethelene radiation filter was used in the optical path.

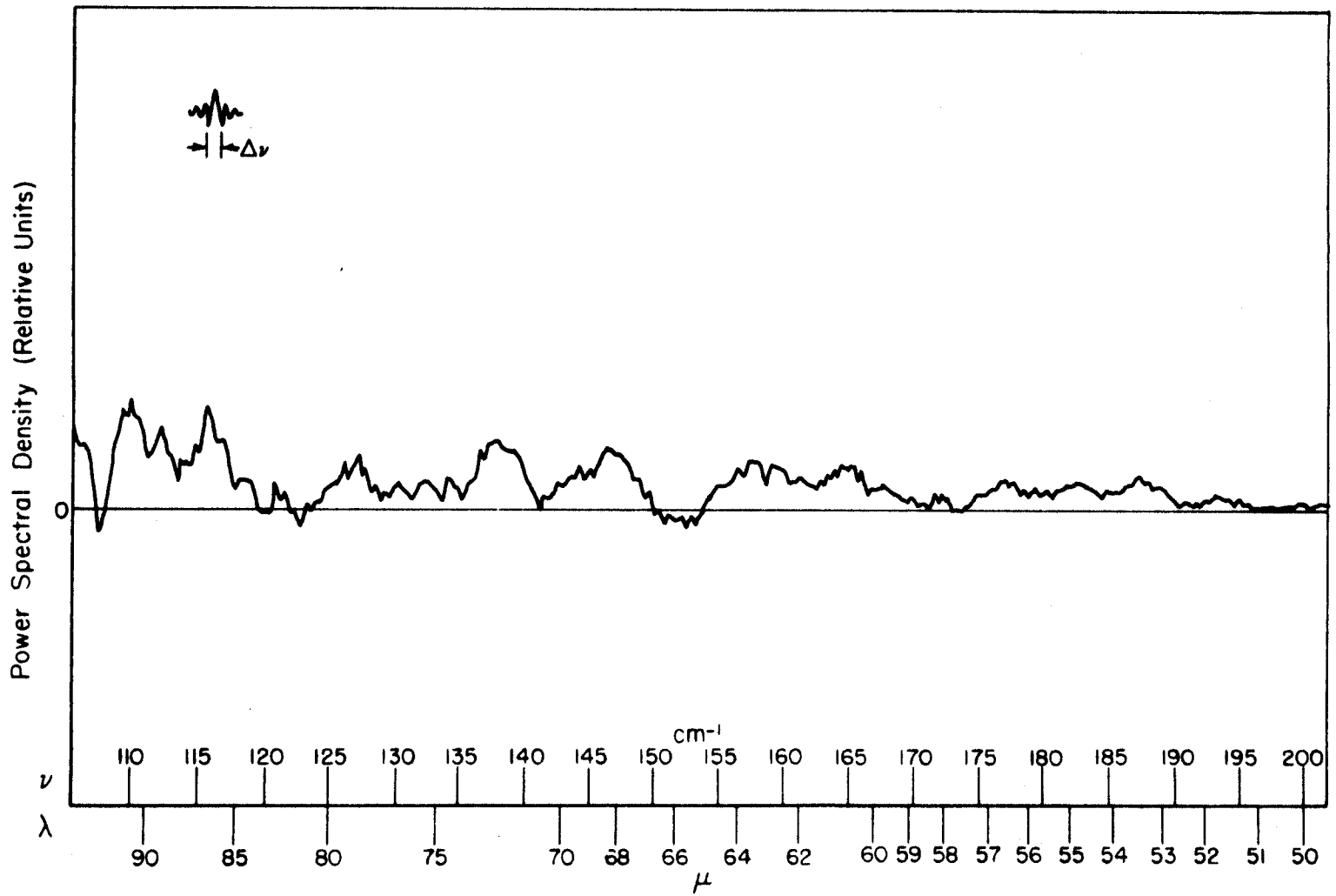

Fig. 18--Basic aperiodic spectral-density data obtained using a 200 LPI-mesh beam splitter; $(\Delta\nu)_I = 0.64\ cm^{-1}$, $\gamma_{max} = 1.56$ cm, and $\nu = 105$ to $200\ cm^{-1}$. A black-polyethelene radiation filter was used in the optical path.

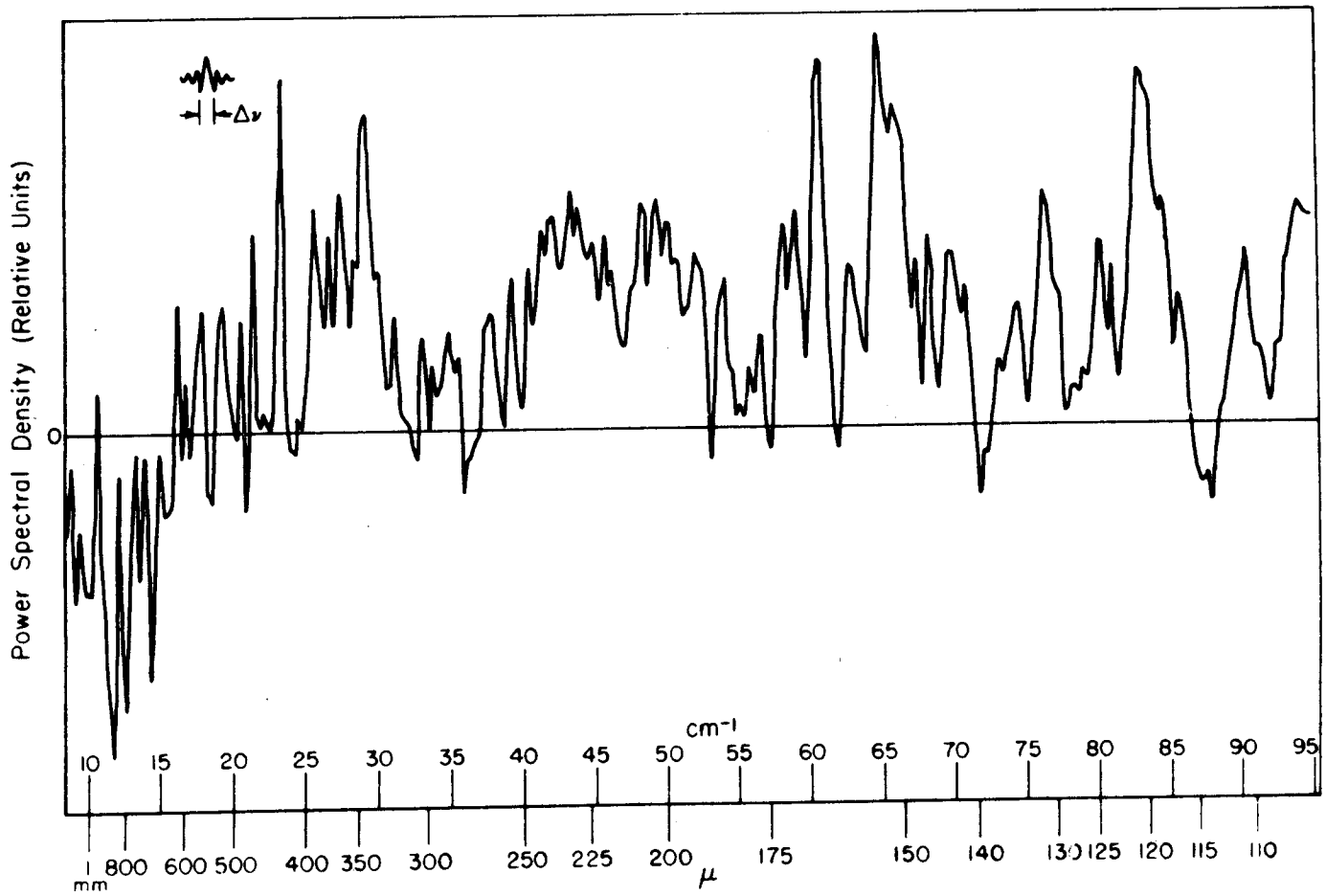

Fig. 19--Basic aperiodic spectral-density data obtained using a 120 LPI-mesh beam splitter; $(\Delta\nu)_I = 0.58$ cm^{-1}, $\gamma_{max} = 1.73$ cm, and $\nu = 10$ to 95 cm^{-1}. No radiation filter was used in the optical path.

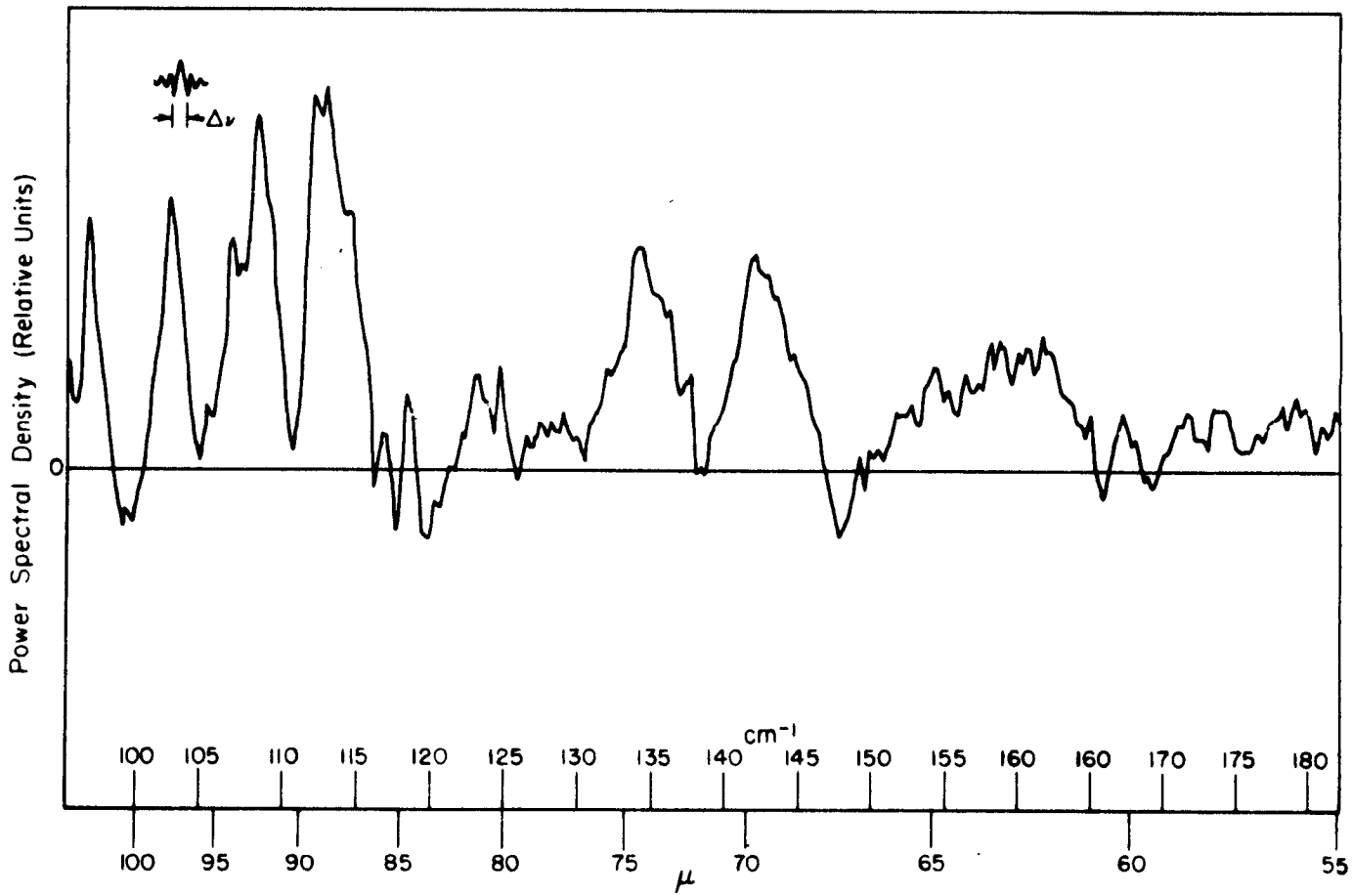

Fig. 20--Basic aperiodic spectral-density data obtained using a 120 LPI-mesh beam splitter; $(\Delta\nu)_I = 0.58\ cm^{-1}$, $Y_{max} = 1.73$ cm, and $\nu = 95$ to $180\ cm^{-1}$. No radiation filter was used in the optical path.

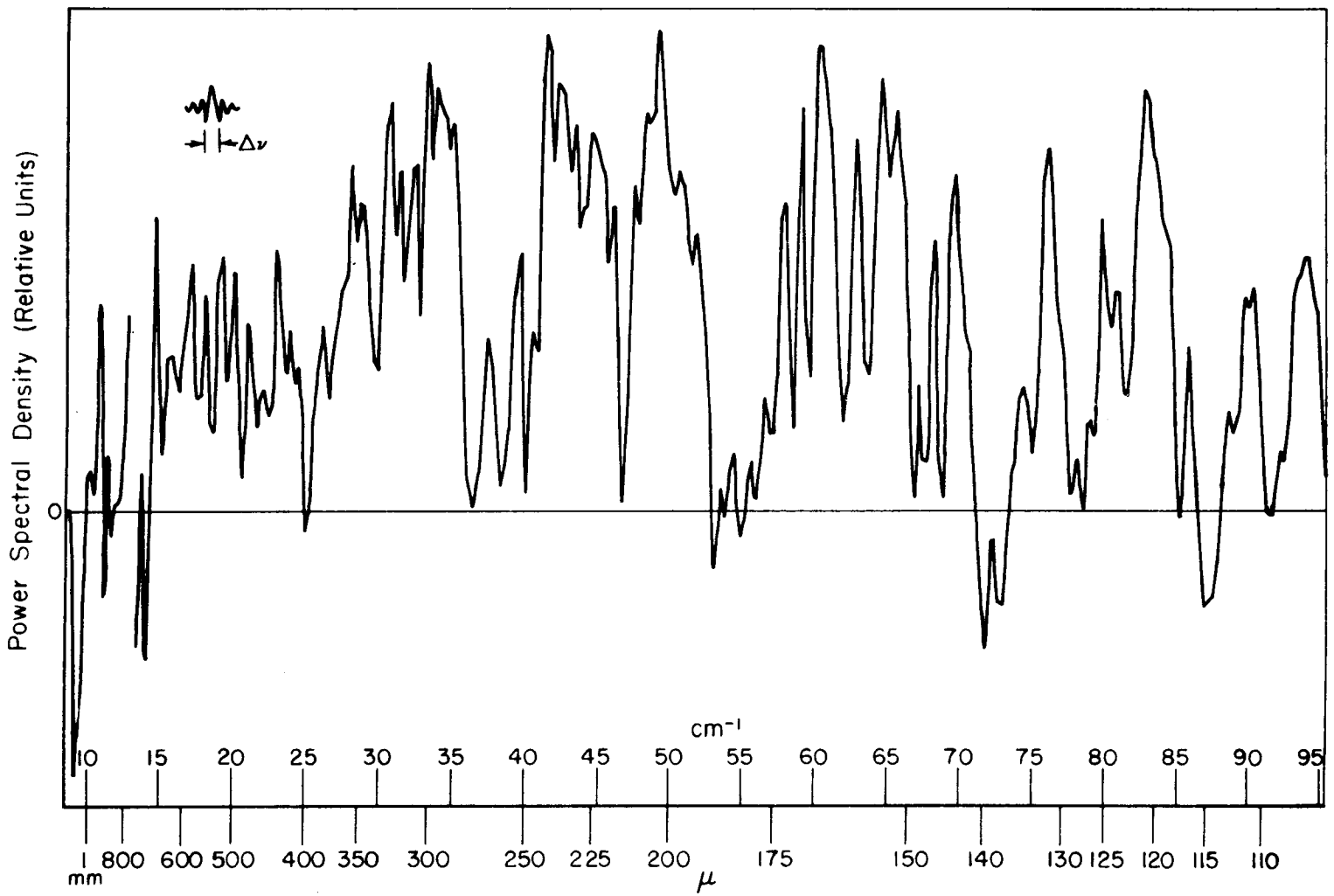

Fig. 21--Basic aperiodic spectral-density data obtained using an 80 LPI-mesh beam splitter; $(\Delta\nu)_I = 0.58\ cm^{-1}$, $\gamma_{max} = 1.73$ cm, and $\nu = 10$ to $95\ cm^{-1}$. A black-polyethelene radiation filter was used in the optical path.

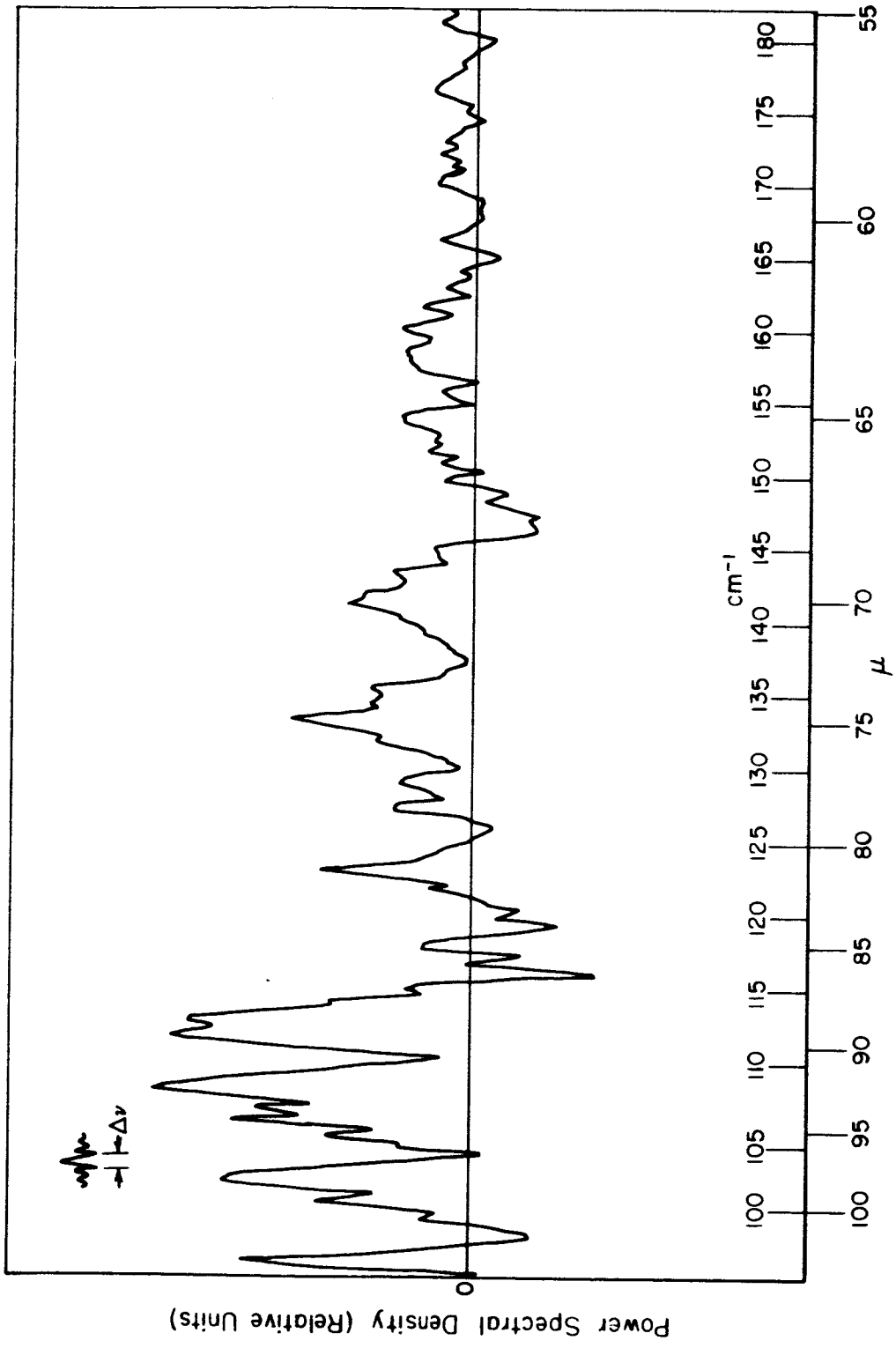

Fig. 22--Basic aperiodic spectral-density data obtained using an 80 LPI-mesh beam splitter; $(\Delta\nu)_I = 0.58\ cm^{-1}$, $Y_{max} = 1.73$ cm, and $\nu = 95$ to $180\ cm^{-1}$. A black-polyethelene radiation filter was used in the optical path.

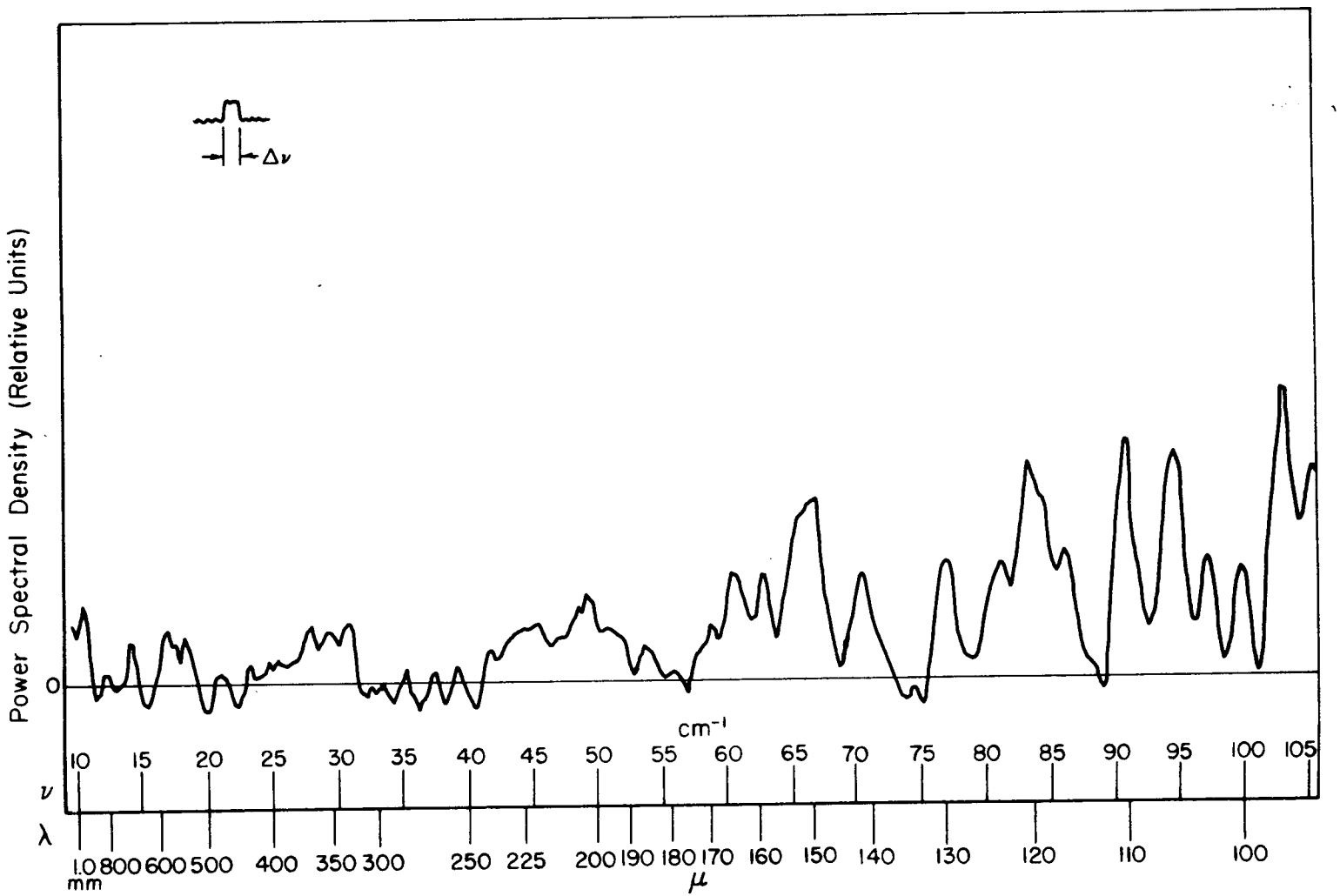

Fig. 23--Aperiodic spectral-density data obtained using the improved instrument response function and a 500 LPI-mesh beam splitter; $(\Delta\nu)_I = 1.28\ cm^{-1}$, $Y_{max} = 1.56$ cm, and $\nu = 10$ to $105\ cm^{-1}$. A black-polyethelene filter was used.

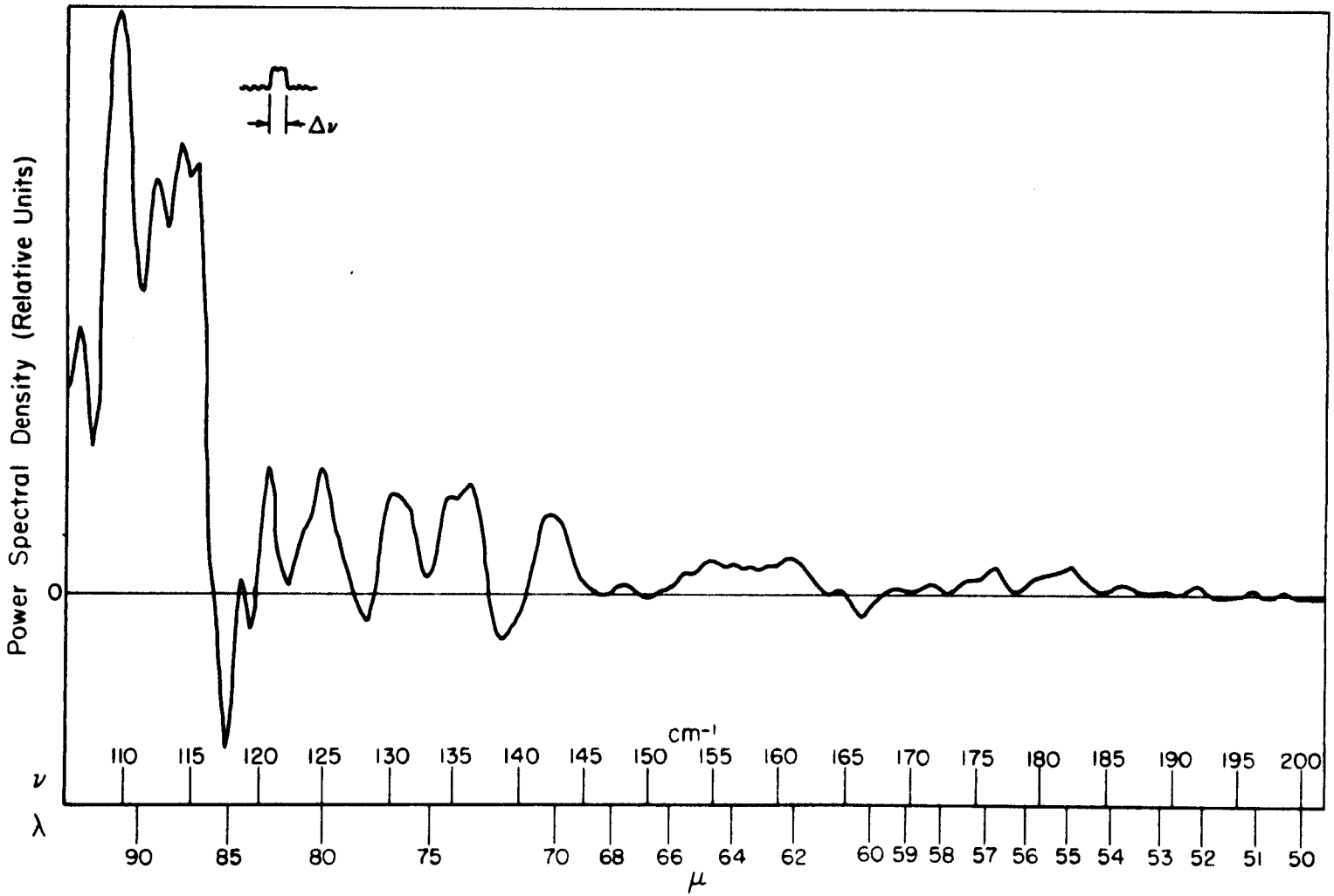

Fig. 24--Aperiodic spectral-density data obtained using the improved instrument response function and a 500 LPI-mesh beam splitter; $(\Delta\nu)_I = 1.28\ cm^{-1}$, $Y_{max} = 1.56$ cm, and $\nu = 105$ to $200\ cm^{-1}$. A black-polyethelene filter was used.

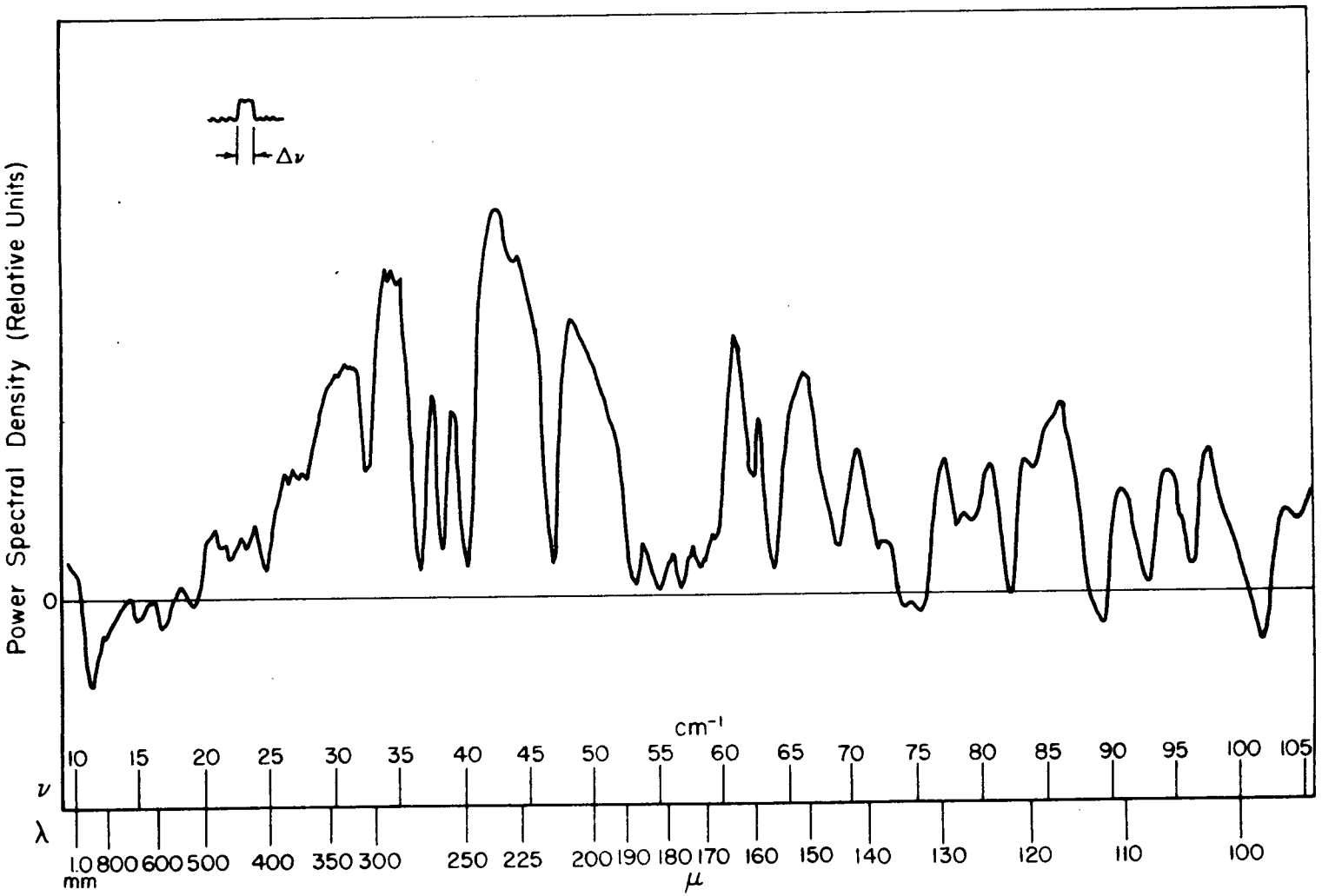

Fig. 25--Aperiodic spectral-density data obtained using the improved instrument response function and a 200 LPI-mesh beam splitter; $(\Delta\nu)_I = 1.28\ cm^{-1}$, $Y_{max} = 1.56$ cm, and $\nu = 10$ to $105\ cm^{-1}$. A black-polyethelene filter was used.

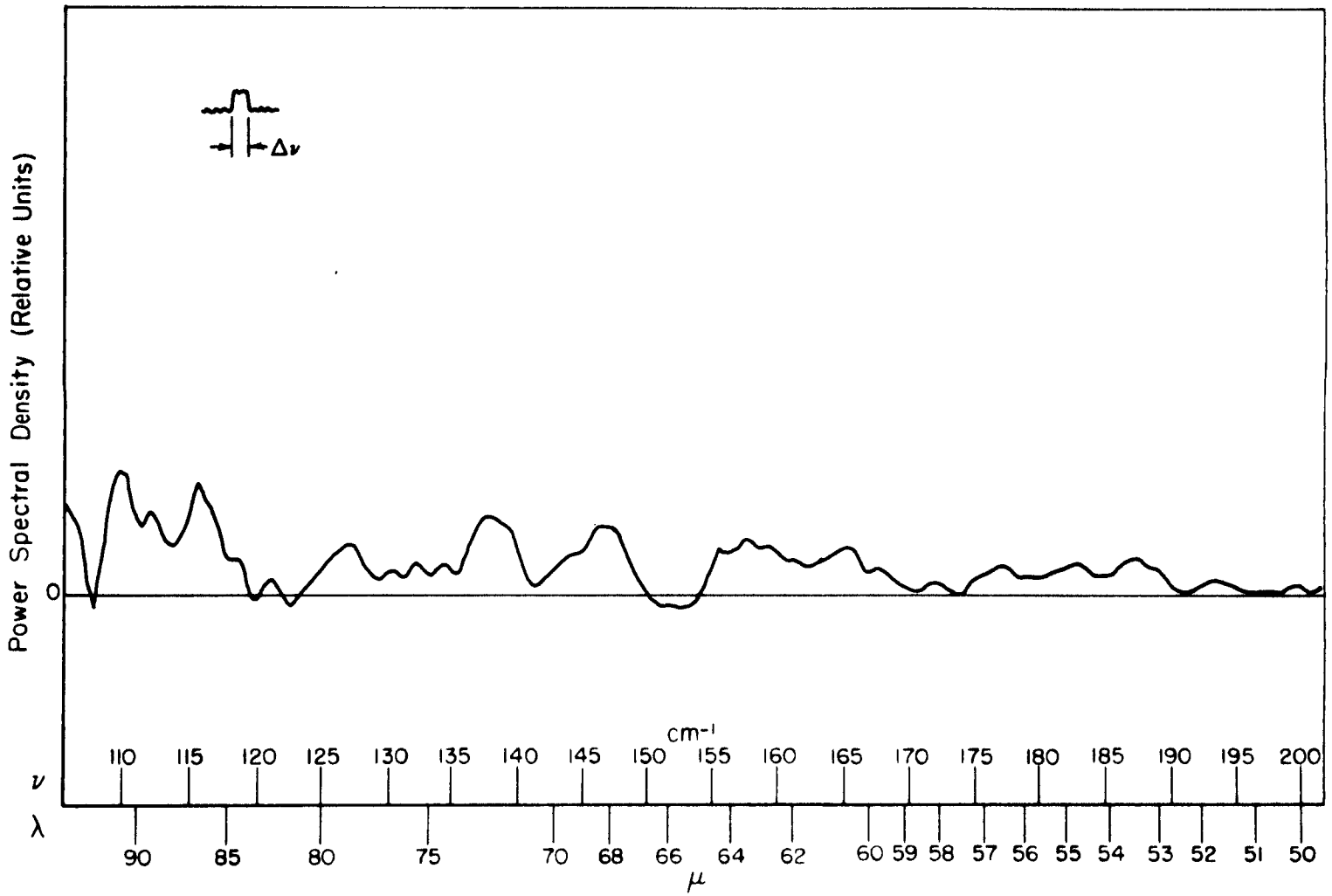

Fig. 26--Aperiodic spectral-density data obtained using the improved instrument response function and a 200 LPI-mesh beam splitter; $(\Delta\nu)_I = 1.28\ cm^{-1}$, $Y_{max}=1.56$ cm, and $\nu = 105$ to $200\ cm^{-1}$. A black-polyethelene filter was used.

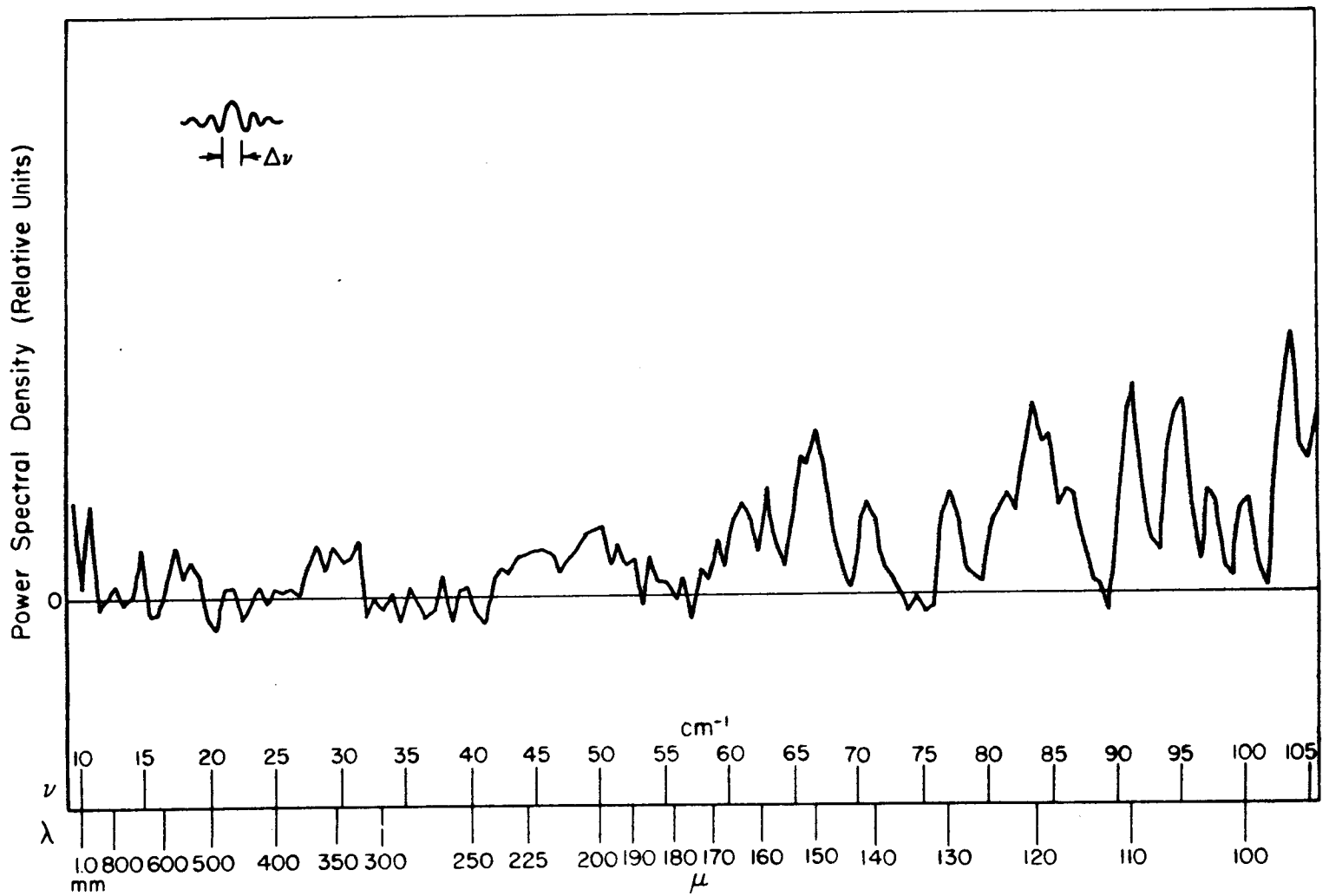

Fig. 27--Basic aperiodic spectral-density data obtained using a 500 LPI-mesh beam splitter; $(\Delta\nu)_I = 1.28\ cm^{-1}$, $Y_{max} = 0.78$ cm, and $\nu = 10$ to $105\ cm^{-1}$. A black-polyethelene filter was used.

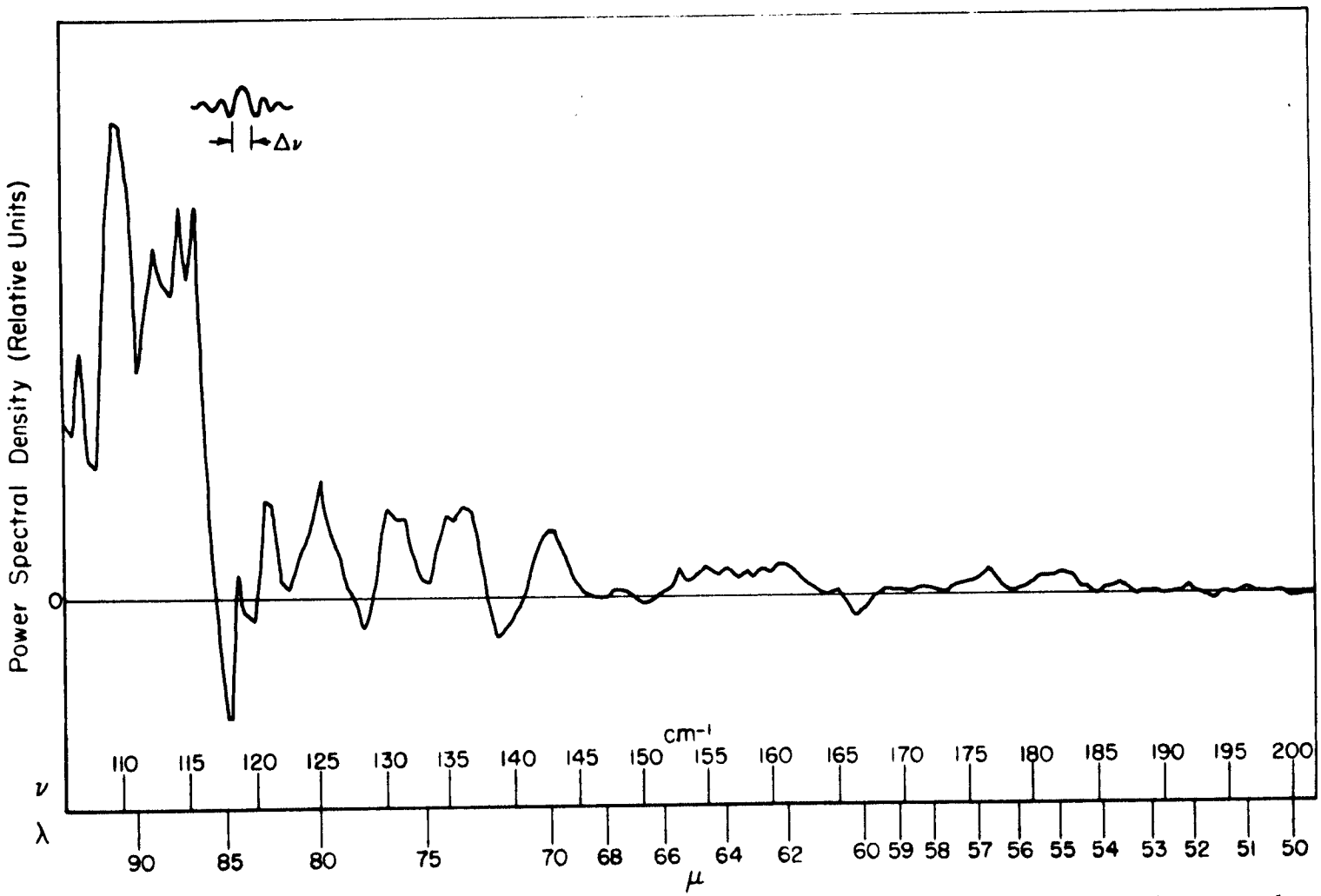

Fig. 28--Basic aperiodic spectral-density data obtained using a 500 LPI-mesh beam splitter; $(\Delta\nu)_I = 1.28\ cm^{-1}$, $Y_{max} = 0.78$ cm, and $\nu = 105$ to $200\ cm^{-1}$. A black-polyethelene filter was used.

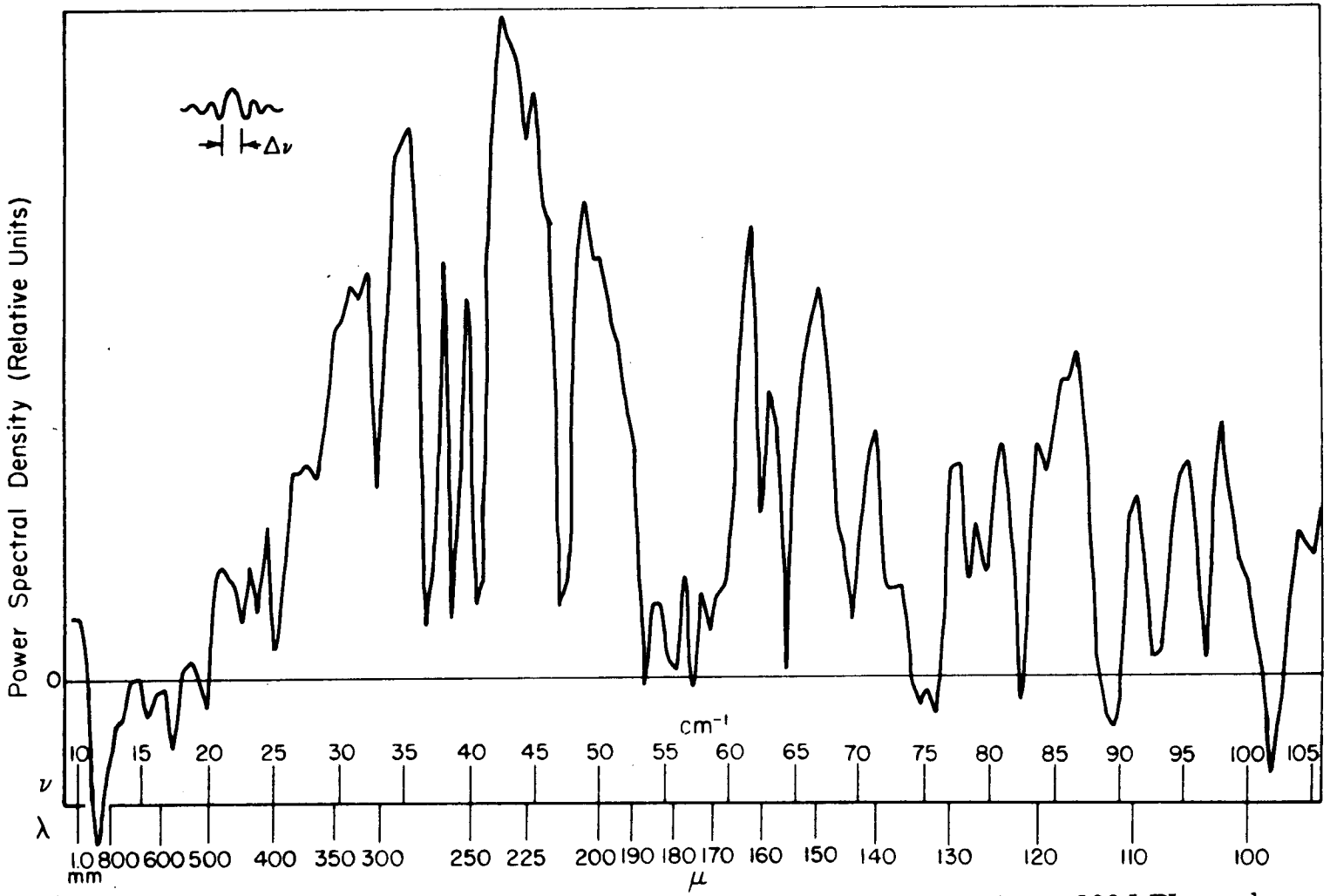

Fig. 29--Basic aperiodic spectral-density data obtained using a 200 LPI-mesh beam splitter; $(\Delta\nu)_I = 1.28\ cm^{-1}$, $Y_{max} = 0.78$ cm, and ν =10 to 105 cm^{-1}. A black-polyethelene filter was used.

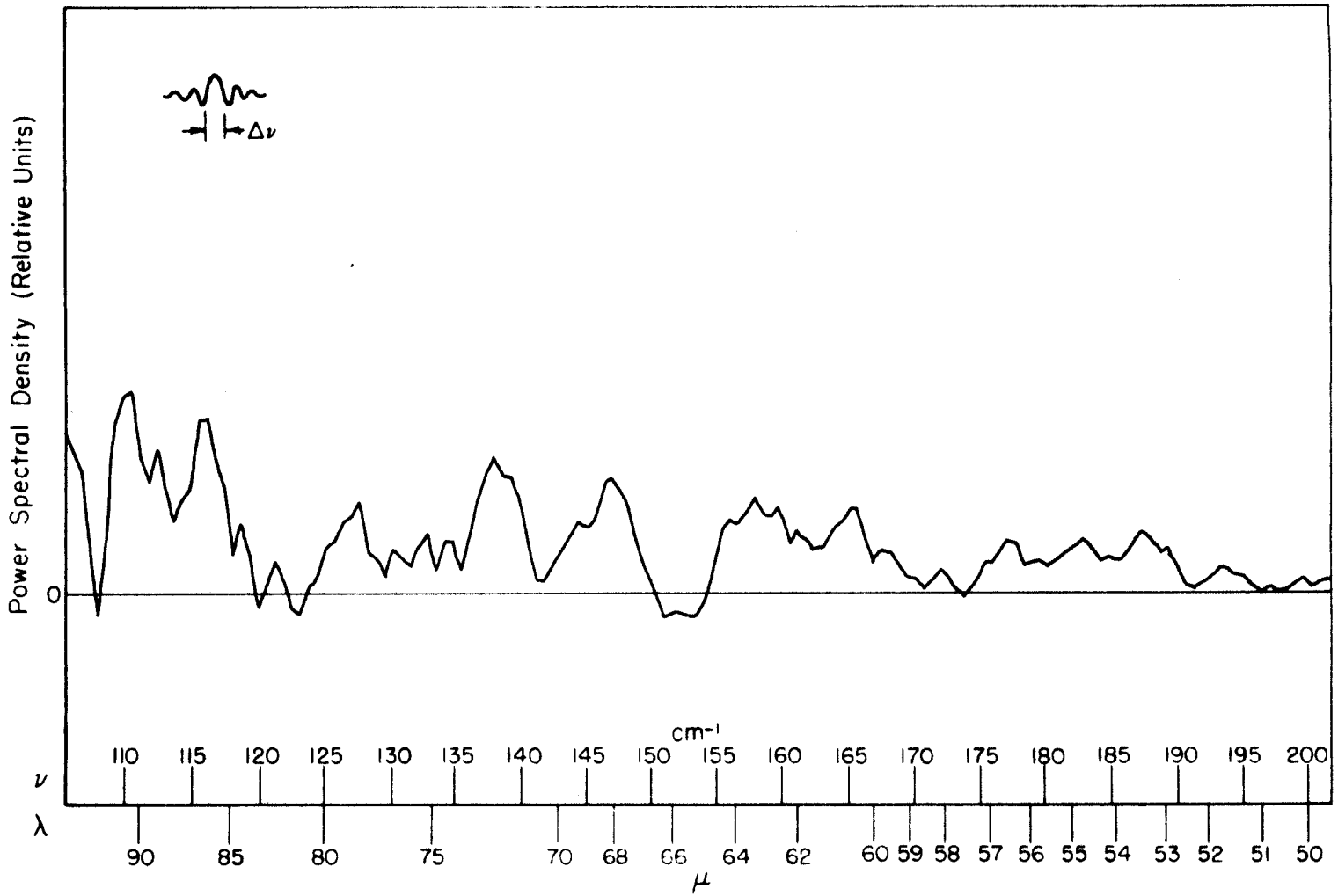

Fig. 30--Basic aperiodic spectral-density data obtained using a 200 LPI-mesh beam splitter; $(\Delta\nu)_I = 1.28\ cm^{-1}$, $\gamma_{max} = 0.78$ cm, and $\nu = 105$ to $200\ cm^{-1}$. A black-polyethelene filter was used.

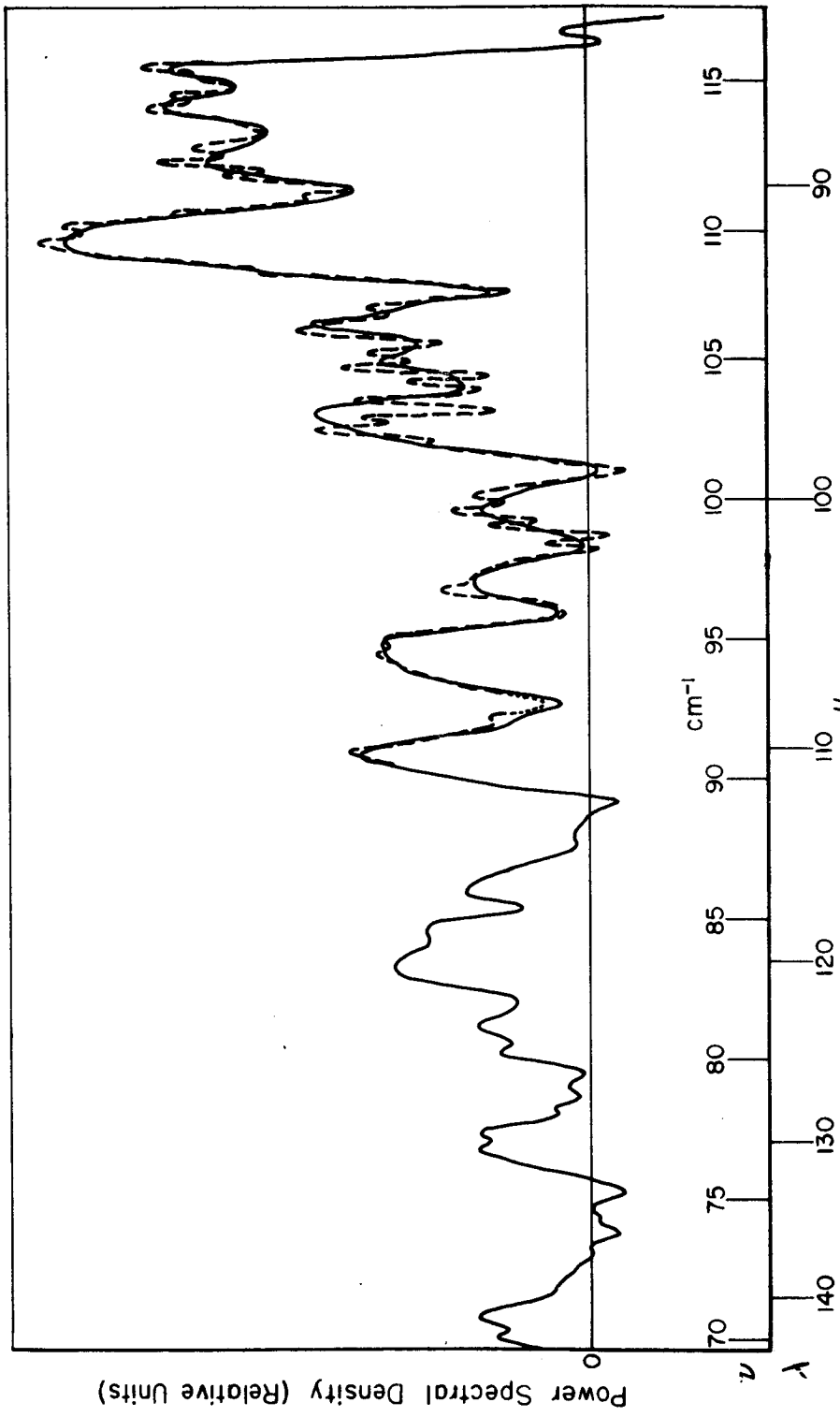

Fig. 31--Aperiodic spectral-density data obtained from the 500 LPI-mesh test after first subtracting out the constant component of the interferogram function; $(\Delta\nu)_I = 0.64\ cm^{-1}$, $\gamma max = 1.56$ cm, and $\nu = 70$ to $117\ cm^{-1}$. A black-polyethelene filter was used. The dotted line shows the results obtained by solving the instrument integral equation in matrix form on the digital computer.

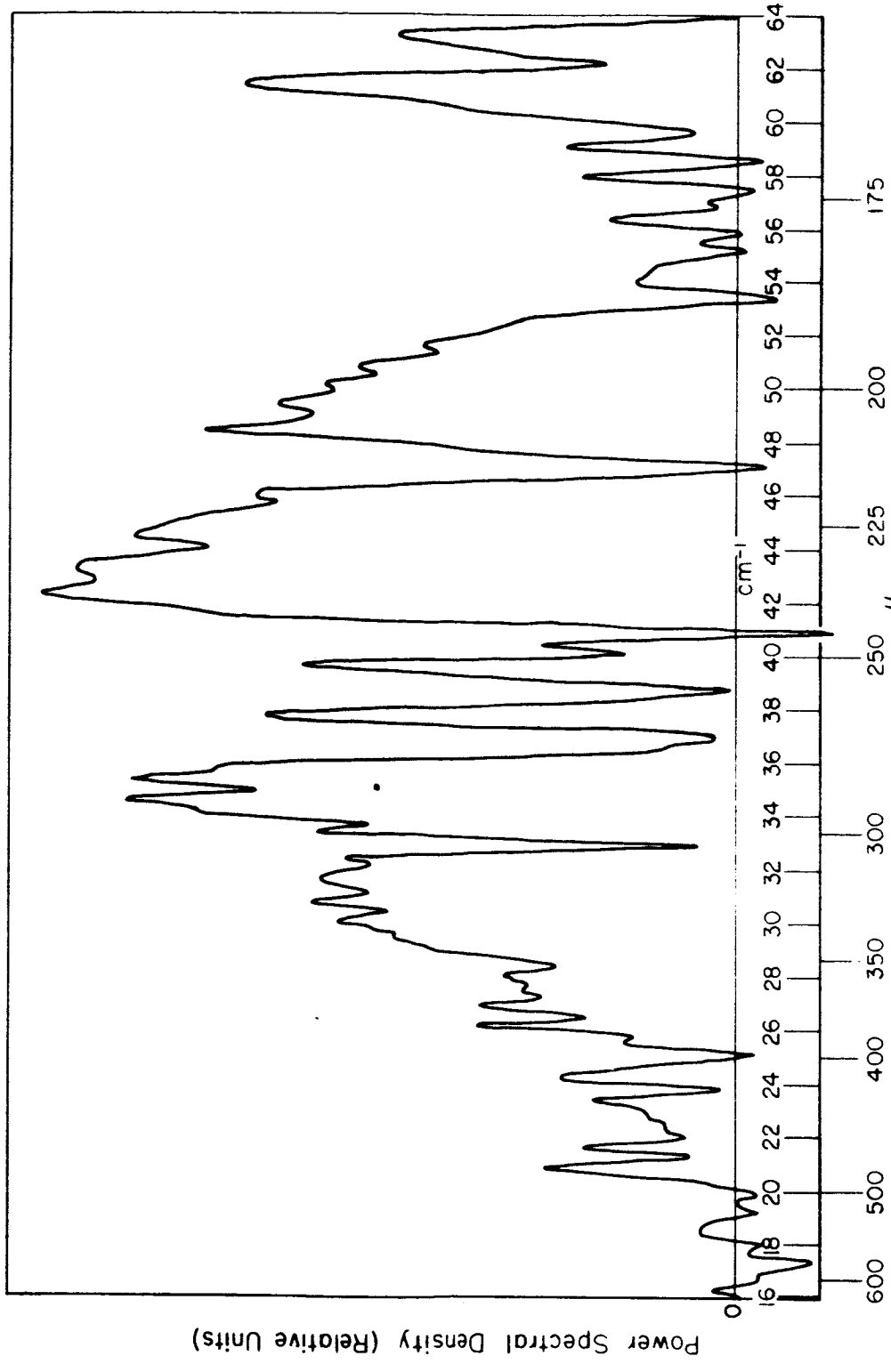

Fig. 32--Aperiodic spectral-density data obtained from the 200 LPI-mesh test after first subtracting out the constant component of the interferogram function; $(\Delta\nu)_I = 0.64\ cm^{-1}$, $Y_{max} = 1.56$ cm, and $\nu = 16$ to 64 cm^{-1}. A black-polyethelene filter was used.

An examination of Figs. 15 to 22 shows that the 500 LPI mesh has a fairly sharp efficiency peak near 90 microns, while the 200 LPI mesh has a much broader peak near 250 microns wavelength. On the other hand, the 120 LPI and the 80 LPI meshes did not appear to have any definite efficiency peaks. Both of the latter tests are more noisy due to the higher system gain which was necessary because of the lower beam-splitter efficiencies. The effect of removing the black polyethelene filter is clearly shown in Fig. 20 by the increased output at wavelengths shorter than 80 microns as compared to the other three tests in which the filter was used.

Some negative output is in evidence on all of the output data charts. This results from two sources - the negative sidelobes of the instrument response function and the imperfect adjustment of the Michelson optical system. The latter reduces the height of the central peak in $I_{o(\gamma)}$ which occurs at $\gamma = 0$ and results in a slight negative shift of all of the output data points. A similar effect will also occur if the path-length difference is changed so rapidly in the vicinity of $\gamma = 0$ that the full magnitude of the central peak is not accurately recorded.

By comparing Figs. 23 to 26 with Figs. 15 to 18 one sees that improving the instrument response function by adding together three of the basic response functions leads to a smoother power spectral density curve, along with a slight decrease in the relative magnitude of the negative portions of the curve as compared to the positive portions. These changes result both from the doubling of the bandwidth and from the squaring up of the main peak and the reduction of the negative side lobes of the instrument response function. However, it should be noted that many of the smaller and narrower absorption bands which were present in the original data have almost disappeared completely in the improved data.

When the improved data (with $(\Delta\nu)_I = 1.28\ cm^{-1}$; Figs. 23 to 26) is compared with the data obtained by processing the interferogram function only out to $\gamma_{max} = 7800$ microns instead of $\gamma_{max} = 15,600$ microns (Figs. 27 to 30) one sees that the former leads to a smoother power-spectral-density curve and again a slight reduction in the relative size of the negative-going portions of the curve. Also, the improved response function de-emphasizes the small narrow absorption bands which the basic response function, because of its large negative side lobes, tends to over-emphasize.

The data obtained by subtracting the constant component of the interferogram function and calculating the measured power spectral

density at wavenumber values separated by $d\nu = 1/8\ \gamma_{max}$ rather than $d\nu = 1/2\ \gamma_{max}$ (Figs. 31 and 32) gives much more uniform-appearing curves than those in Figs. 15 to 17. Also, some of the very slight absorption lines which were only hinted at on Figs. 15 to 17 are more clearly developed on Figs. 31 and 32. As before, almost all of the absorption bands which appear coincide with those observed in references [28, 29, and 30], the major exception again being the two bands on Fig. 31 which appear at 87 and 88 microns. The data obtained as a result of the solution of the matrix equation on the digital computer (dotted line on Fig. 31) at first glance appears to be much noisier than the unprocessed data (solid line). This is to be expected, since the theory predicts that one must trade signal-to-noise ratio for an increase in the resolution (about four times in this case). It is interesting to note, however, that most of the dips which occur on the dotted-line curved correspond with absorption bands either seen by other experimenters or predicted by the theory[28, 29, 30, 31, and 32]. The two large unexplained absorption bands which occur at 77 and 78 microns are broken into three and two separate apparent absorption bands respectively by the process of solving the matrix equation.

C. Periodic Tests

Figures 33 and 34 show the periodic test data obtained using a relative instrument resolution of $\nu/(\Delta\nu)_p = 7.5$. The curves on Fig. 33 marked "fast scan" show the results of tests made using a reference frequency of about 13 cycles per second while the curves marked "slow scan" represent data taken when the instrument operating speed was slowed to where the reference frequency was just over 8 cycles per second. On Fig. 34 the 120 LPI-mesh test was run with a 13 cycle-per-second reference signal and the 80 LPI-mesh test was run with a 9 cycle-per-second reference signal. Although the resolution of the instrument was quite low when obtaining the data presented in Figs. 33 and 34, the general location of the peaks and dips corresponds to the major regions of transmittance and absorption in the data of other experimenters. Figure 33 indicates that the 500 LPI mesh has a beam-splitter-efficiency peak near 85 microns, while the 200 LPI mesh has its efficiency peak near 230 microns wavelength as in the aperiodic case, but Fig. 34 (the results of the 120 and 80 LPI-mesh tests) indicates a tendency for the output to peak up at less than 100 microns. This is a result somewhat similar to the absence of an expected large efficiency peak at longer wavelength (approximately

370 microns for the 120 LPI mesh or 550 microns for the 80 LPI mesh), and may be due to some extent to a dropoff in the source intensity and/or greater atmospheric absorption at the longer wavelengths. Also, neither of these two tests were conducted with a black polyethelene filter in the radiation path, while the 200 LPI-mesh periodic test (the only one which did not peak up at wavelengths greater than 100 microns) was conducted using such a filter.

Figures 35 and 36 show the results obtained with a relative resolution of $\nu/(\Delta\nu)_P = 30$. The 500, 200, and 120 LPI-mesh tests were conducted using a 14 cycle-per-second reference signal. No radiation filter was placed in the optical path for any of the tests. As a result of the latter condition, all four of the tests resulted in the measured power spectral density having an output which peaked up at wavelength shorter than 100 microns. Some difficulties were experienced with the 80 LPI-mesh test which invalidated the data for wavelengths longer than about 100 microns; consequently these data were not plotted. A comparison of the data obtained on these periodic tests with that of other experimenters showed very good agreement in the location of the transmission and absorption bands, particularly when compared with the results

published by Yaroslavsky and Stanevich [30] who apparently used an instrument having about the same resolution.

The last group of periodic data (Figs. 37 and 38) was taken using an improved response function obtained by combining three reference frequencies. The resulting relative resolution of the improved response function was $\nu/(\Delta\nu)_p = 15.5$, and the tests were run with a center reference frequency of about 15 cycles per second with no radiation filters in the optical path. Again, all of the tests resulted in a measured power spectral density which peaked up near 85 microns, although the 200 LPI-mesh test did have a somewhat smaller peak in the 210-235 micron region. Good agreement was again obtained with the results published in the literature, although the resolution of the instrument seemed to be somewhat better than the predicted value of 15.5. There seemed to be little real difference between the data shown in Figs. 35 and 36 and that shown in Figs. 37 and 38 except that the results in the latter case appear to be more "solid" (i.e., the absorption bands did not plunge as near the zero axis as in the former case) and some of the curves (the 120 LPI-mesh results in particular) seemed smoother and less noisy.

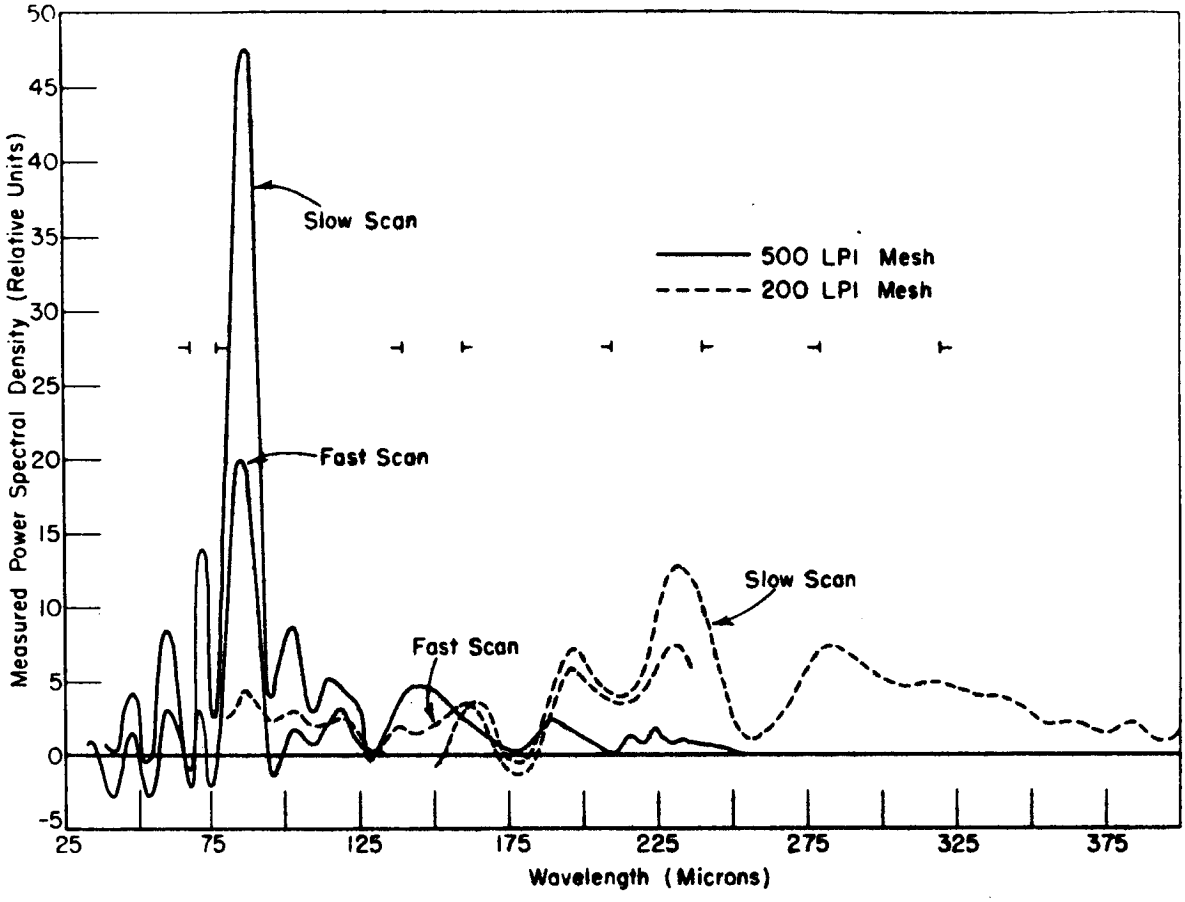

Fig. 33--Spectral density data obtained on periodic tests using 500 LPI-mesh (solid line) and 200 LPI-mesh (dotted line) beam splitters; $\nu/(\Delta\nu)_p$ - 7.5. A black-polyethelene filter was used on the 200 LPI-mesh test, but none on the 500 LPI-mesh test.

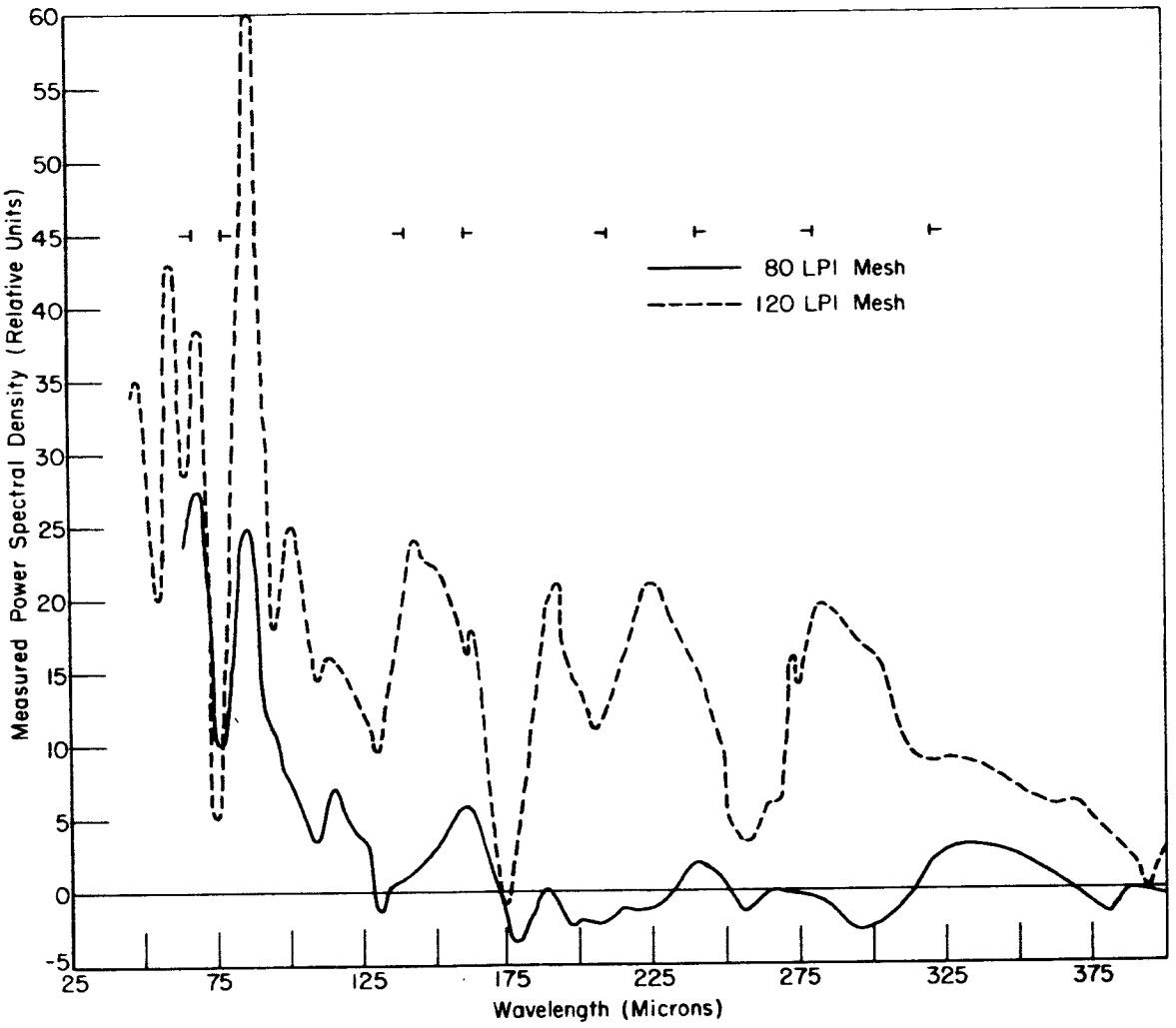

Fig. 34--Spectral-density data obtained on periodic tests using 120 LPI-mesh (solid line) and 80 LPI-mesh (dotted line) beam splitters; $\nu/(\Delta\nu)_P = 7.5$. No radiation filters were used.

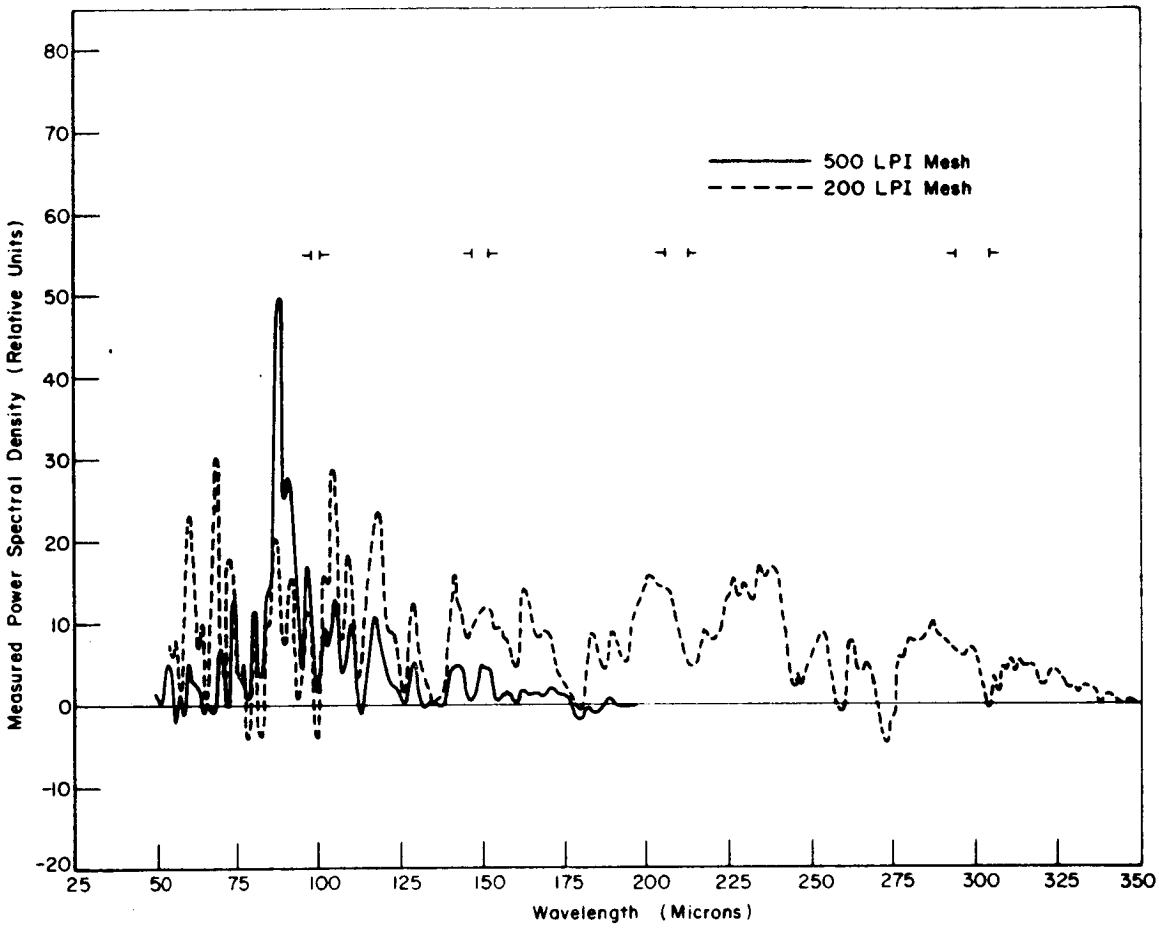

Fig. 35--Spectral-density data obtained on periodic tests using 500 LPI-mesh (solid line) and 200 LPI-mesh (dotted line) beam splitters; $\nu/(\Delta\nu)_P = 30$. No radiation filters used.

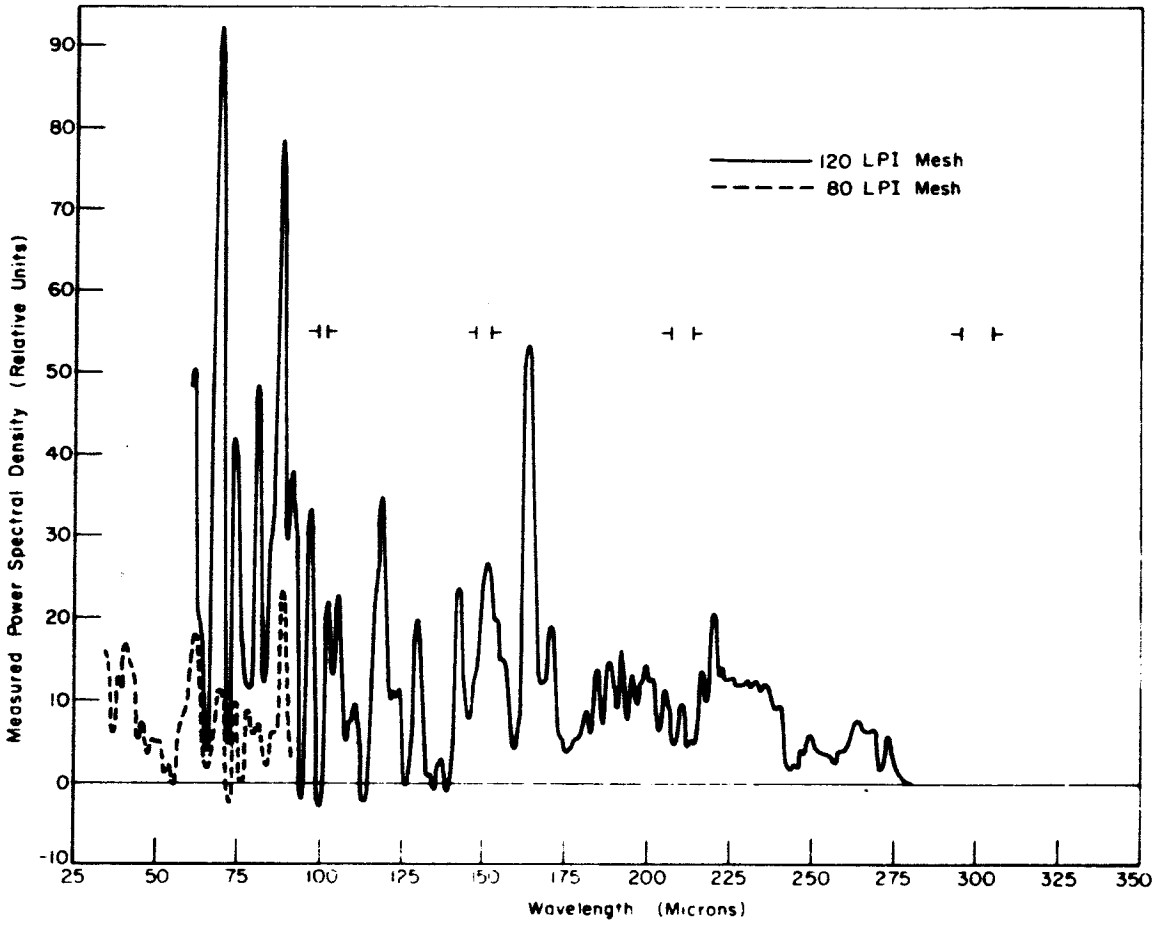

Fig. 36--Spectral-density data obtained on periodic tests using 120 LPI-mesh (solid line) and 80 LPI-mesh (dotted line) beam splitters; $\nu/(\Delta\nu)_p = 30$. No radiation filters used.

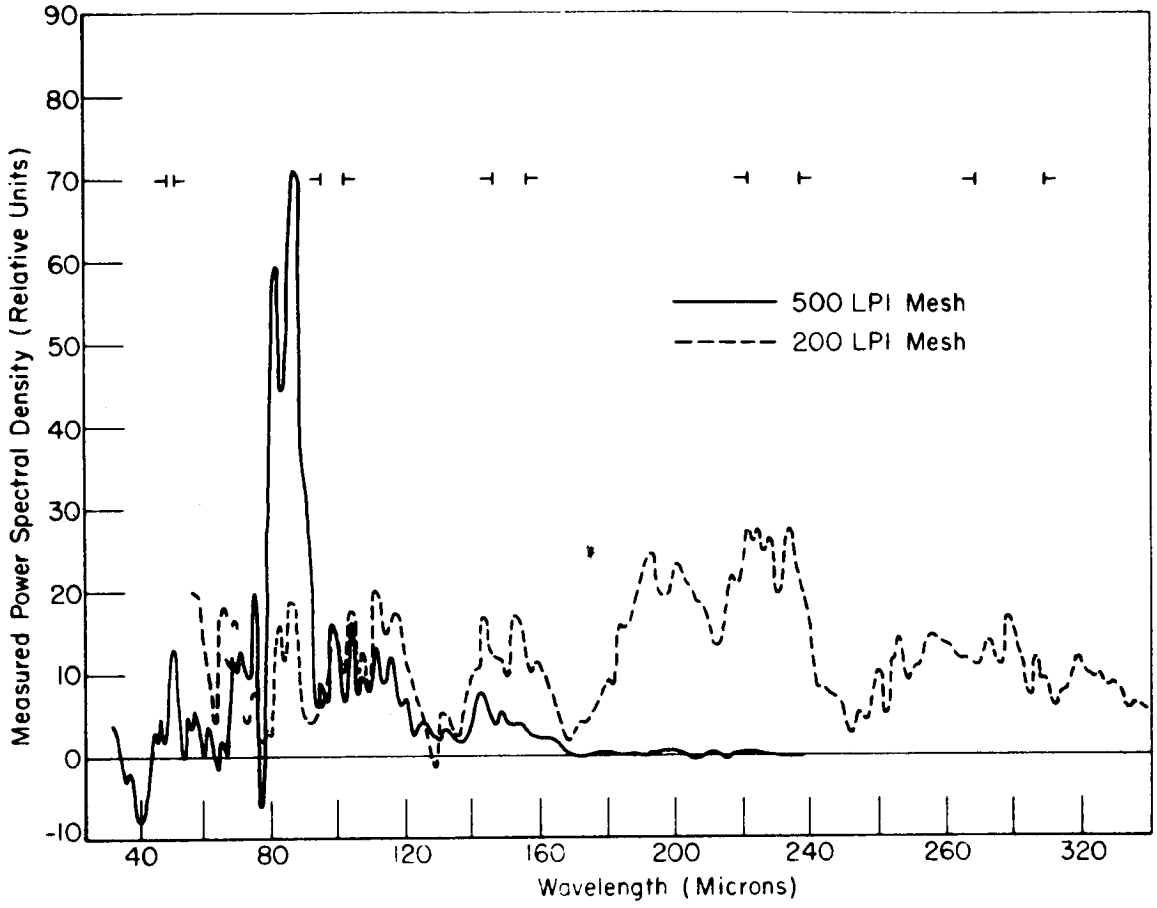

Fig. 37--Spectral-density data obtained on periodic tests using 500 LPI-mesh (solid line) and 200 LPI-mesh (dotted line) beam splitters); $\nu/(\Delta\nu)_P = 15.5$ using an improved instrument response function and no radiation filters.

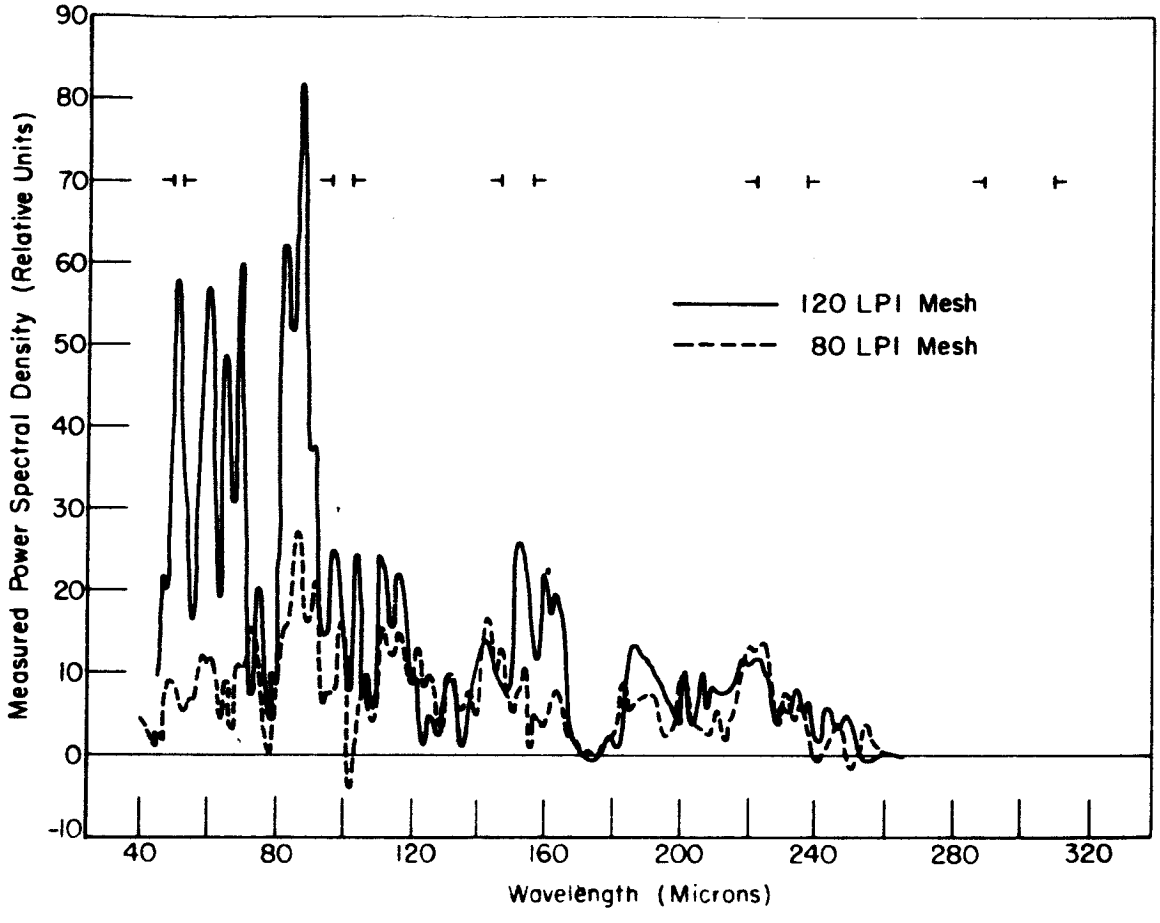

Fig. 38-- Spectral-density data obtained on periodic tests using 120 LPI-mesh (solid line) and 80 LPI-mesh (dotted line) beam splitters; $\nu/(\Delta\nu)_p = 15.5$ using an improved instrument response function and no radiation filters.

D. Minimum Detectable Temperature Change

The basic data (Figs. 15 to 22) were examined to obtain an estimate of the signal-to-noise ratio and $[\Delta T_{s_{min}}]$. The maximum spectral density in each test was assumed to be due to a change of 200°C between the chopper blade temperature and the source temperature. The 500 LPI-mesh data had an apparent noise-to-signal ratio of about 1.2 percent over all of the spectral region. This was estimated in two ways. First, since black polyethelene and crystal quartz filters were used it was assumed that there was little radiation near 50 microns wavelength and consequently all of the variations in the measured power spectral density in the vicinity of 50 microns were considered to be noise. Secondly, in the portion of the spectrum where $E_{m_{I(\nu)}}$ was large any small dips not corresponding to known absorption lines were assumed to be noise. Based upon these methods $[\Delta T_{s_{min}}]$ was estimated to be less than 2.5°C. This is considerably smaller than the 15.5°C estimated at the end of Chapter IV due to digitizing errors. The discrepancy may be due to the digitizing error not being as large as originally believed, or may be due to it not having a uniform spectral density as was assumed in the analysis of Chapter IV (i.e., the noise may be concentrated at some frequency not corresponding to the wave-number region considered here).

The noise-to-signal ratio in the 200 LPI case was about 1.7 percent giving a $[\Delta T_{s_{min}}]$ of about 3.5°C, while for the 120 LPI and 80 LPI cases $[\Delta T_{s_{min}}]$ was estimated at 5°C and 5.5°C respectively. The data obtained by calculating the power spectral density using the improved instrument response function (Figs. 23 to 26) led to an estimated $[\Delta T_{s_{min}}]$ of about 2°C.

CHAPTER VI
CONCLUSIONS

In this dissertation it has been shown that the interferometric receiver is a suitable means of determining the spectral characteristics of a radiation source. In general the aperiodic mode of operation is the most efficient and gives the best results when the information which is desired is a high-resolution measurement of the power spectral density over a wide range of wavenumbers. The periodic mode of operation is best applied to making broadband measurements centered upon from one to several values of wavenumber, but is not as good as is the conventional grating monochromator.

In the aperiodic mode of operation a resolution comparable to that of a grating-type instrument can be obtained and the operation in this mode using a relatively weak black-body radiation source has yielded results which compare quite well with those obtained by other experimenters using grating-type instruments and platinum-strip or mercury-arc radiation sources. A relative resolution of more than 100 has been obtained with the present instrument, but this could easily be increased by another order of magnitude through

the use of a smaller and more intense radiation source and/or longer focal length optics, or by relaxing the very stringent limitations which were placed upon the permissible diffraction effects. Operation in the aperiodic mode is quite simple to achieve, and an instrument designed to operate only in this mode could be quite ruggedly and simply built, would be lightweight, and have low electrical power consumption. Completely automatic or remote-control operation would be easily obtainable, and the output could be quite easily adapted to telemetry methods. By careful selection of the mesh used for the beam splitter the instrument could be made to cover a wide wavenumber region without the necessity of changing to another beam splitter.

The periodic mode of operation is much more difficult to achieve and requires more attention during the recording of test data (at least if one is scanning through a wavelength region) than does the aperiodic method. The construction must inherently be heavier and the power consumption higher because of the large mechanical accelerations involved. Probably the most useful application of the periodic method would be in the continuous monitoring of some radiation source or path at one particular wavelength where the magnitude of the received radiation was desired to be known as a function of some other parameter which

varies with time. It was also found that some of the mechanical problems which are inherent in the periodic mode of operation can be compensated for by providing both phasing and time-delay adjustments between the moving interferometer mirror and the reference signal generator, and by providing signal blocking during the mirror-motion turn-around period[21].

Both modes of operation are amenable to attempts to improve the quality of the resulting experimental data by means of improving the instrument response function. In the aperiodic case this is done in a digital computer at any convenient time after the experiment is run and the interferogram data is taken. Since the same interferogram data may be processed using several different instrument response functions it is possible to compare several sets of output data made with different signal-to-noise ratios and resolutions which have all originated from the same input data, and to adjust the instrument parameters ex post facto to obtain the most valuable output data for a specific purpose.

This dissertation project has shown that both the aperiodic and the periodic modes of operation of the interferometric receiver may be obtained in practice, and that from the theoretical and practical standpoints each mode has its own assets and problems. The method of response-function improvement which was proposed

in the theory was shown to be experimentally achievable with good results in the aperiodic mode but with only fair results in the periodic mode. Some of the problems of periodic-mode operation have also been solved. In conclusion, one can say that the interferometric receiver, in one or the other of its two basic forms, should make a useful radiometer receiver for a number of various applications in the submillimeter wavelength region.

APPENDIX I
RELATION OF $[\Delta T_{s_{min}}]$ TO $[\Delta P_{min}]$

The radiant power emitted per unit of black-body surface per unit of solid angle is

$$(I\text{-}1) \qquad p_\lambda \Delta\lambda = \frac{c}{4\pi} \Psi_\lambda \Delta\lambda \left(\frac{\text{watts}}{\text{cm}^2 \text{ sterad.}} \right)$$

where Ψ_λ is Planck's radiation density factor. If the radiation being measured is in the centimeter-wavelength region where $ch/\lambda k \ll T_s$ for most sources being observed (i.e., for $T_s > 10°K$ at $\lambda = 1.25$ cm), $p_\lambda \Delta\lambda$ becomes

$$(I\text{-}2) \qquad p_\lambda \Delta\lambda = \frac{2kcT_s}{\lambda^4} \Delta\lambda \left(\frac{\text{watts}}{\text{m}^2 \text{ sterad.}} \right) .$$

However, this formula is not necessarily true for the submillimeter region where the quantity $ch/\lambda k$ may be several hundred degrees Kelvin. In this case (i.e., where $T_s < 50°K$ and $\lambda < 3$ mm) the exact equation becomes

$$(I\text{-}3) \qquad p_\lambda \Delta\lambda = \frac{2c^2h}{\lambda^5} \frac{\Delta\lambda}{(\epsilon^{ch/\lambda kT_s} - 1)} \left(\frac{\text{watts}}{\text{m}^2 \text{ sterad.}} \right) .$$

The total power in a wavelength increment $\Delta\lambda$ incident upon an effective antenna area $A_{e(\theta,\phi)}$ located a distance L_s from a source of incremental area $d\sigma$ located at the angles θ and ϕ is given by

$$(I\text{-}4) \qquad dP = p_\lambda A_{e(\theta,\phi)} \frac{d\sigma}{L_s^2} \Delta\lambda = p_\lambda A_{e(\theta,\phi)} d\Omega \Delta\lambda \quad \text{(watts)},$$

where $d\Omega$ is the solid angle subtended by the source $d\sigma$ when viewed from the receiving area. An extensive black-body source can be considered as the sum of the small incremental areas denoted by $d\sigma$. Therefore, integrating the above equation gives the total power received from an extensive black-body source over a range of wavelengths λ to $(\lambda + \Delta\lambda)$:

$$(I\text{-}5) \qquad P = \frac{2c^2 h(\Delta\lambda)}{\lambda^5} \int_{\Delta\Omega} \frac{A_{e(\theta,\phi)}}{(\epsilon^{ch/\lambda k T_s} - 1)} d\Omega \text{ (watts)},$$

where p_λ is assumed constant over $\Delta\lambda$ and where $T_s = T_{s(\theta,\phi)}$ is, in general, a function of θ and ϕ, the direction angles. Compare this to a similar approximate equation for the centimeter-wavelength region where $ch/\lambda k \ll T_s$:

$$(I\text{-}6) \qquad P = \int_{\Delta\Omega} \frac{c\, A_{e(\theta,\phi)}\ 2k\ T_{s(\theta,\phi)}\ (\Delta\lambda)}{\lambda^4}\ d\Omega$$

$$= \int_{\Delta\Omega} \frac{c\, A_{e(\theta,\phi)}\ 2k\ T_{s(\theta,\phi)}\ (\Delta\nu)}{\lambda^2}\ d\Omega \text{ (watts)},$$

where $|\Delta\lambda| = \lambda^2\ |\Delta\nu|$.

From antenna theory, the gain function (referred to an isotropic source) of an antenna in a particular direction is given by

$$(I\text{-}7) \qquad G_{(\theta,\phi)} = \frac{4\pi}{\lambda^2}\ A_{e(\theta,\phi)} \quad ,$$

where $A_{e(\theta,\phi)}$ is the apparent area of the dish antenna when viewed from the direction given by θ and ϕ. Thus, one may substitute for $A_{e(\theta,\phi)}$ in (I-5). This leads to

$$(I\text{-}8) \qquad \int_{\Delta\Omega} A_{e(\theta,\phi)}\, d\Omega = \frac{\lambda^2}{4\pi} \int_{\Delta\Omega} G_{(\theta,\phi)}\, d\Omega \quad (\text{cm})^2 ,$$

and

$$(I\text{-}9) \qquad P = \frac{c^2 h(\Delta\lambda)}{2\pi\lambda^3} \int_{\Delta\Omega} \frac{G_{(\theta,\phi)}}{(\epsilon^{ch/\lambda k\, T_{s(\theta,\phi)}} - 1)}\ d\Omega \text{ (watts)},$$

where $d\Omega = d\theta\, d\phi$. In the centimeter region this becomes

$$(I\text{-}10) \qquad P = \frac{ck(\Delta\nu)}{2\pi} \int_{\Delta\Omega} T_{s(\theta,\phi)}\ G_{(\theta,\phi)}\ d\Omega \quad (\text{watts}).$$

Now, if the angular beamwidth of the antenna is less than the angle subtended by the source, $T_{s(\theta,\phi)}$ will be approximately

constant over the range of integration. If $G_{(\theta,\phi)}$ is integrated over the entire beamwidth, letting

$$\int_{\Delta\Omega} G_{(\theta,\phi)}\, d\Omega = 4\pi,$$

the equation which relates the input power to the receiver over a range ($\Delta\lambda$) to the equivalent black-body temperature of a source which is larger than the antenna beamwidth will become

$$P = \frac{2c^2 h(\Delta\lambda)}{\lambda^3(\epsilon^{ch/\lambda kT_s} - 1)} \quad \text{(watts)}. \tag{I-11}$$

For the centimeter region this reduces to

$$P = 2kcT_s(\Delta\nu) \quad \text{(watts)}. \tag{I-12}$$

In the preceding derivation it has assumed that radiation of all polarizations is being received and detected. If the antenna-receiver input combination is such as to accept only one polarization, and if the received signal (noise) has random polarization, then (I-11) and (I-12) must both be divided by two. This gives

$$P = \frac{hc^2(\Delta\lambda)}{\lambda^3(\epsilon^{ch/\lambda kT_s} - 1)} \quad \text{(watts)}, \tag{I-13}$$

or

$$P = ckT_s(\Delta\nu) \quad \text{(watts)}. \tag{I-14}$$

Comparing the general equations which must be applied in the submillimeter region with the approximate equations for the centimeter region it is seen that for a centimeter receiver of given bandwidth the power input to the receiver may be related to the black-body temperature of the source by a constant which is independent of the wavelength of the radiation being received, but that for the submillimeter case this relationship is a complex one involving the wavelength as a parameter. This is especially evident if the minimum observable change in the black-body temperature is expressed in terms of the minimum detectable change in the receiver input power. For the centimeter case, from Eq. (I-14),

$$[\Delta T_{s_{min}}] = \frac{(\Delta P_{min})}{ck(\Delta \nu)} \quad (^\circ K), \tag{I-15}$$

where $[\Delta P_{min}]$ is the minimum detectable power in the wavenumber region $(\Delta \nu)$, while for the submillimeter case, from Eq. (I-13),

$$[\Delta T_{s_{min}}] = \frac{\lambda^2 k T^2}{c^3 h^2 (\Delta \nu)} \frac{(\epsilon^{hc/\lambda kT} - 1)^2}{(\epsilon^{hc/\lambda kT})} [\Delta P_{min}] \ (^\circ K). \tag{I-16}$$

While (I-15) for the centimeter region is a simple proportionality relation, the general equation (I-16), which must often be applied in the submillimeter region for small values of T_s, is a complex expression which depends upon both the wavelength, λ,

being measured and the equivalent black-body temperature, T_s, of the source. It is easily seen that (I-16) reduces to (I-15) when $hc/\lambda kT \ll 1$. Actually, if $\epsilon^{hc/\lambda kT}$ can be approximated by

$$1 + \frac{hc}{\lambda kT} + \frac{h^2c^2}{2\lambda^2k^2T^2} + \frac{h^3c^3}{6\lambda^3k^3T^3} \quad ,$$

then (I-15) is a good approximation. This occurs for wavelengths greater than approximately 0.2 millimeter if the temperature being measured is over 100°K.

A submillimeter radiometer receiver having the same $[\Delta P_{min}]$ as a microwave radiometer reciever would not be able to detect as small of a change in the black-body source temperature as would the microwave receiver. The ability of the submillimeter receiver to detect a change in T_s is related to its ability to detect a change in the input power by the factor $\eta = ck(\Delta T_s)(\Delta\nu)/(\Delta P)$. This is plotted in Fig. 1 in Chapter I.

In the foregoing it has been assumed that the gain and the beamwidth of the antenna are determined primarily through diffraction effects by the antenna size and the wavelength of operation. If a coherent receiver (or a point receiver) is available, such a description is valid both in the submillimeter and in the centimeter wavelength regions. Unfortunately, there are no point detectors (or coherent receivers) available in the submillimeter region at

the present time. Instead, one must depend upon incoherent receivers with extensive receiving areas. For these receivers the beamwidth of the antenna pattern may not be diffraction limited. Consider, for example, a receiver (or detector) which has an input area of a square centimeter placed at the focal point of the antenna (i.e., a circular collecting mirror of focal length δ_1). One can show from geometrical optics that any incident radiation striking the reflector at an angle within the solid angle $[\Delta\Omega]_s$ given by a/δ_1^2, where a is the receiver input area, would at least partially reach the receiver input (if diffraction and aberration effects are neglected, all of the radiation within this angle would reach the receiver input). Here δ_1 is the focal length of the mirror. In other words, the resolution of this optical system is given by d/δ_1 (d = diameter of the receiver input) and the maxi-gain of the antenna would be approximately $4\pi\,\delta_1^2/a$.[1] For the mirror diameter, D_m, and the receiver input area both of reasonable size, $(D_m/\lambda)^2 >> \delta_1^2/a$ and the gain of the antenna is

---

[1] Notice that the solid angle $\Delta\Omega$ is the geometric optical resolution limit. It is slightly different from the definition of the beamwidth of an antenna. In order to calculate the actual beamwidth of the antenna we must first find the gain function $G(\theta,\phi)$ by means of geometrical optics, using aberration theory, and then find the beamwidth according to the conventional definition. Such a derivation is beyond the scope of the present paper.

limited by geometrical considerations due to the extensive area of the receiver input rather than by diffraction effects due to the size of the collecting mirror. Assuming that the beamwidth is much less than the solid angle subtended by the source one can write from (I-4) that

$$(I\text{-}17) \qquad P = \frac{2c^2 h(\Delta\lambda)}{\lambda^5 \left(\epsilon^{ch/\lambda k T_s} - 1\right)} \cdot \frac{a A_m}{\delta_1^2} \quad \text{(watts)},$$

where A_m is the geometrical area of the collecting mirror.

Expressing the minimum-detectable temperature change of an equivalent black body in terms of the minimum detectable input power change at the radiometer receiver input gives

$$(I\text{-}18) \qquad [\Delta T_{s_{min}}] = \frac{\lambda^6 \delta_1^2 (\epsilon^{ch/\lambda k T_s} - 1)^2 k T^2 [\Delta P_{min}]}{2 c^3 h^2 a A_m (\Delta\lambda)(\epsilon^{ch/\lambda k T_s})} \ (^\circ K).$$

This differs from Eq. (I-16) by the factor

$$(I\text{-}19) \qquad \Gamma = \frac{\lambda^2}{2a} \frac{\delta_1^2}{A_m} = \frac{\lambda^2}{a} (F_o)^2 \frac{2}{\pi},$$

which for very small wavelengths and large mirror apertures is much less than 1.0. (Here F_o expresses the effective aperture (f-stop) of the antenna.) This would give the submillimeter radiometer an advantage over the microwave radiometer insofar as the

ratio $[\Delta P_{min}]/[\Delta T_{s_{min}}]$ is concerned,[2] providing the η factor is not >> 1.0. This helps to offset somewhat the inherent lack of sensitivity in submillimeter receivers, and the effects of the η factor.

Consider a typical far-infrared spectrograph which could be used as a radiometer receiver in the submillimeter-wavelength region, where $F_o = \sqrt{\pi \delta_1^2/4A_m}$ = the effective aperture of the antenna, $F_r = \sqrt{\pi \delta_2^2/4A_r}$ = the effective aperture of the receiver, a = the receiver input area, and A_r is the area of the receiver optics if different from A_m. As long as $F_o \leq F_r$ all of the received power except that lost by absorption and scattering in the optical system will be delivered to the radiation detector. However, if the effective aperture of the receiver is less than that of the antenna the Γ factor (Eq. (I-19)) must now be written as

$$\Gamma = \frac{\lambda^2 \delta_1^2}{2a A_r \left(\frac{\delta_1^2}{\delta_2^2}\right)} = \frac{\lambda^2}{2a} \left(\frac{\delta_2^2}{A_r}\right) = \frac{2\lambda^2}{\pi a} (F_r)^2 , \tag{I-20}$$

or the f-stop number of the antenna optical system is replaced by the f-stop number of the receiver optical system.

---

[2] This occurs because $\Gamma << 1.0$ in the submillimeter case where an extensive-area detector is used. The increase in sensitivity thus obtained results from this extensive detector (or receiver input) area, and is accompanied by a decrease in the spatial resolution as compared to what could be obtained with a coherent point detector where the beamwidth is determined by diffraction effects.

Summarizing, the power delivered to the detector is

$$(I\text{-}21) \qquad P = (\Gamma)^{-1} \frac{c^2 h(\Delta\lambda)}{\lambda^3 (\epsilon^{ch/\lambda k T_s} - 1)} \quad \text{(watts)},$$

where Γ is calculated in terms of the limiting (either the receiver or the antenna) aperture.

If the minimum power change which the detector can detect in the wavenumber region $(\Delta\nu)$ is $[\Delta P_{min}]$ then the minimum detectable change in the black body temperature is

$$(I\text{-}22) \qquad [\Delta T_{s_{min}}] = \frac{\Gamma\eta[\Delta P_{min}]}{ck(\Delta\nu)} = \frac{\lambda^2 \Gamma[\Delta P_{\nu_{min}}]\eta}{ck(\Delta\lambda)} \quad (^\circ K),$$

which is Eq. (4) of Chapter I.

APPENDIX II
GRATING MONOCHROMATOR RELATIONSHIPS

The angular dispersion of a diffraction grating (assuming a Paschen-type mounting) is given by [26]

$$\frac{\partial \lambda}{\partial \psi} = \frac{d \cos \psi}{m} \qquad \text{(cm)},$$

where ψ is the angle of diffraction, m is the order number, and d is the grating-line spacing. If the exit-slit width as viewed from the grating position subtends a constant angle $\Delta\psi$, then the wavelength bandwidth is approximately given by

$$\Delta\lambda = \frac{\partial \lambda}{\partial \psi} \Delta\psi = \frac{d \cos \psi}{m} \Delta\psi \qquad \text{(cm)},$$

and since $\left| \frac{\partial \nu}{\partial \lambda} \right| = \nu^2$, one has for the wavenumber passband

$$|\Delta\nu| = \left| \frac{\partial \nu}{\partial \lambda} \right| |\Delta\lambda| = \frac{\nu^2 d \cos \psi}{m} |\Delta\psi| \quad (\text{cm}^{-1}),$$

which is used in deriving Eq. (26) in the text. In a similar manner, if the slit position is varied through the grating's diffraction pattern at a constant rate, $\frac{d\psi}{dt}$ (the maximum value of which can be $\left|\frac{d\psi}{dt}\right| = \frac{|\Delta\psi|}{2\tau_D}$ if variations in the spectral density are to be recorded satisfactorily), then

$$\left| \frac{\partial \nu}{\partial t} \right| = \frac{\nu^2 d \cos \psi}{2m \tau_D} \left| \Delta \psi \right| \qquad (\mathrm{cm}^{-1}\ \mathrm{sec}^{-1}),$$

which is the scanning rate which is used in Eq. (26) in the text.

APPENDIX III
FOURIER TRANSFORM RELATIONSHIPS

In complex form the Fourier-transform pair is

$$g_{(t)} = \int_{-\infty}^{\infty} h_{(f)} \, \epsilon^{-i2\pi ft} \, df$$

$$h_{(f)} = \int_{-\infty}^{\infty} g_{(t)} \, \epsilon^{+i2\pi ft} \, dt.$$

Let the general function $g_{(t)}$ be set equal to (using the variables defined in Chapter II)

$$g_{(t)} = I_{o(t)} \text{ for } -\frac{T_p}{2} < t < +\frac{T_p}{2}$$

$$= 0 \text{ otherwise,}$$

and let $h_{(f)}$ now be the transform of this particular $g_{(t)}$. Then if another general time function is defined as

$$g'_{(t)} = I_{o(t)} \text{ for } \frac{T_p}{2} < t < \frac{3T_p}{2}$$

$$= 0 \text{ otherwise,}$$

$g'_{(t)}$ will be the same as $g_{(t)}$ except that it will be shifted along the time axis:

$$g'_{(t)} = g_{(t-T_p)}$$

$$= \int_{-\infty}^{\infty} h_{(f)} \epsilon^{-i2\pi f(t-T_p)} df$$

$$= \int_{-\infty}^{\infty} [h_{(f)} \epsilon^{i2\pi f T_p}] \epsilon^{-i2\pi ft} df .$$

Therefore,

$$h'_{(f)} = h_{(f)} \epsilon^{i2\pi f T_p} .$$

Similarly, if

$$g''_{(t)} = \begin{cases} g(t + T_p) & \text{for } -\frac{3T_p}{2} < t < -\frac{T_p}{2} \\ 0 \text{ otherwise,} \end{cases}$$

then

$$h''_{(f)} = h_{(f)} \epsilon^{-i2\pi f T_p} .$$

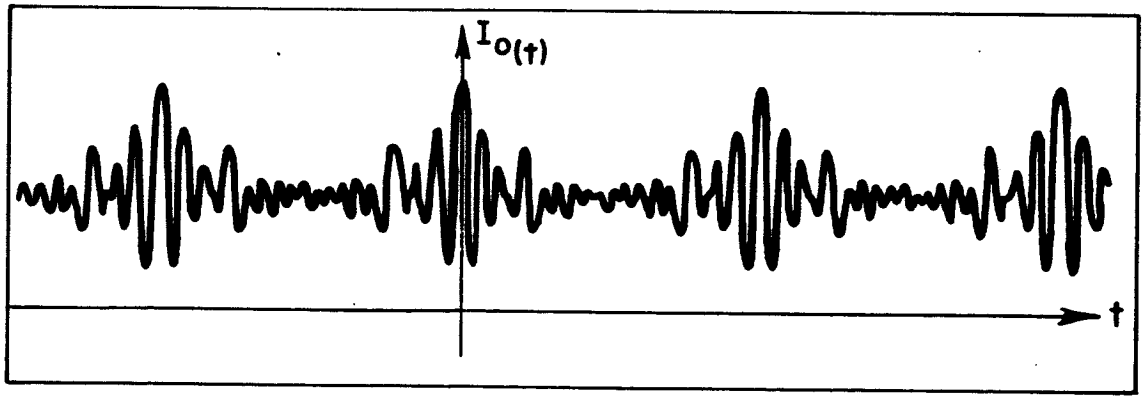

Fig. III-1--$I_{o(t)}$ as a series of individual functions of length T_p.

If this is carried out for an infinite series such as is shown in Fig. III-1, where the total function is the periodic function, $I_{o(t)}$, then

$$H_{(f)} = h_{(f)} + h'_{(f)} + h''_{(f)} + \cdots$$

$$= h_{(f)} \left[1 + \epsilon^{i2\pi f T_p} + \epsilon^{-i2\pi f T_p} + \cdots\right]$$

$$= h_{(f)} \left[1 + 2 \cos 2\pi f T_p + 2 \cos 4\pi f T_p + \cdots\right].$$

It can now be shown (see the end of this Appendix) that the part in the brackets is equivalent to a series of unit impulse functions multiplied by $1/T_p$ appearing at the frequencies $f = n/T_p$ where $n = 0, \pm 1, \pm 2, \ldots$. Therefore, $H_{(f)}$ consists of a series of impulses of magnitude (not height) $\frac{h(f)}{T_p}$ appearing at $f_n = n/T_p$. The integrated area of any particular impulse is given by

$$P_n = \int_{\Delta f \to 0} H_{(f_n)}\, df = \frac{1}{T_p} \int_{-\infty}^{\infty} g_{(t)}\, \epsilon^{i2\pi f_n t}\, dt,$$

which in terms of the symbols used in Chapter II gives

$$P_n = \frac{1}{T_p} \int_{-\frac{T_p}{2}}^{\frac{T_p}{2}} I_{o(t)} \cos 2\pi f_n t \; dt.$$

Using the relation $t = \gamma/s$ and $f_n = s\nu'_n$ this gives

$$P_n = \frac{2}{T_p} \int_{o}^{\frac{T_p}{2}} I_{o(\gamma)} \cos 2\pi \nu'_n \gamma \; d\,\frac{\gamma}{s} \quad .$$

However, since the variable part of $I_{o(\gamma)} = 0$ between τ_p (which occurs at $\gamma = \gamma_{max}$) and $T_p/2$, this can be written as

$$P_n = \frac{2\tau_p}{\gamma_{max} T_p} \int_o^{\gamma_{max}} I_{o(\gamma)} \cos 2\pi \nu_n' \gamma \, d\gamma ,$$

which is Eq. (33) in the text.

Proof that $H_{(f)}$ is a series of unit impulses:

$$\text{The Fourier series} \quad F_{(x)} = \frac{a_o}{2} + \sum_{k=1}^{\infty} a_k \cos kx,$$

where

$$a_k = \frac{1}{\pi} \int_{-\pi}^{\pi} F_{(x)} \cos kx \, dx,$$

can be put into the form

$$F_{(f)} = \frac{a_o}{2} + \sum_{k=1}^{\infty} a_k \cos 2\pi T_p(kf),$$

where

$$a_k = 2T \int_{-1/2T_p}^{1/2T_p} F_{(f)} \cos k(2\pi T_p)f \, df.$$

If $F_{(f)}$ consists of unit impulse functions occuring at $f = n/T_p$ where $n = 0, \pm 1, \pm 2, \ldots$, then $a_k = 2T_p$ for all values of k and the Fourier series of $F_{(f)}$ will be

$$F_{(f)} = [T_p + 2T_p \cos 2\pi f T_p + 2T_p \cos 4\pi f T_p + \ldots].$$

APPENDIX IV
BEAM SPLITTER EFFICIENCY[1]

Consider a beam splitter which is much thinner that the wavelength of the radiation being measured. Define the complex electric field components as shown in Fig. IV-1, and define the

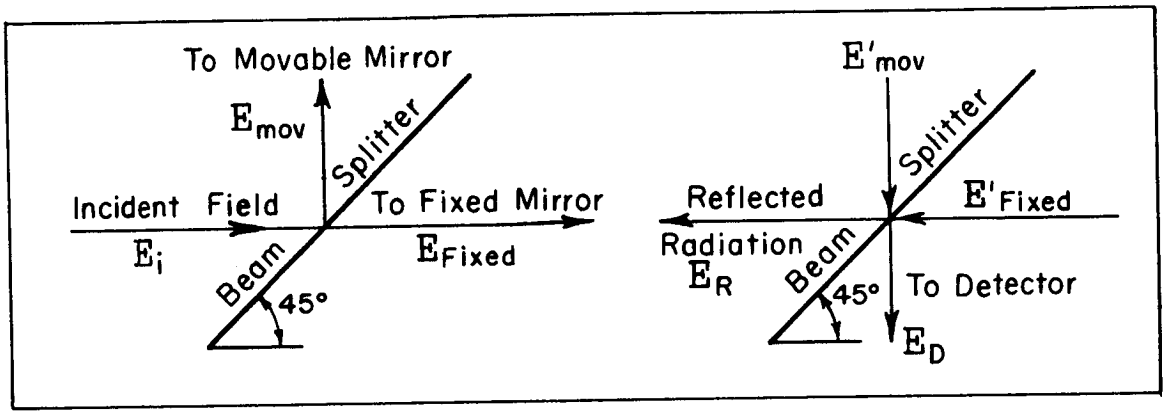

Fig. IV-1--The electric fields associated with radiation in the Michelson interferometer.

complex reflection coefficient of the beam splitter as Γ_R and the complex transmission coefficient as Γ_T. Then

$$E_{mov} = \Gamma_R E_i \quad \text{and} \quad E_{fixed} = \Gamma_T E_i ,$$

---

[1] Experimental studies of the efficiency of various wire-mesh beam splitters have been made at The Ohio State University[22] and at the University of Freiburg (Germany)[33].

$$E'_{mov} = E_{mov}\,\epsilon^{j\theta_{mov}} \quad \text{and} \quad E'_{fixed} = E_{fixed}\,\epsilon^{j\theta_{fixed}},$$

$$E_D = \Gamma_T E'_{mov} + \Gamma_R E'_{fixed}$$

$$= \Gamma_T \Gamma_R E_i\,\epsilon^{j\theta_1} + \Gamma_R \Gamma_T E_i\,\epsilon^{j\theta_2},$$

and

$$E_R = \Gamma_R E'_{mov} + \Gamma_T E'_{fixed}$$

$$= \Gamma_R \Gamma_R E_i\,\epsilon^{j\theta_1} + \Gamma_T \Gamma_T E_i\,\epsilon^{j\theta_2}.$$

For the case where the path-length difference is equal to zero, $\theta_1 = \theta_2 = \theta$, which gives

$$E_D = 2E_i\,\epsilon^{j\theta}(\Gamma_T \Gamma_R)$$

and

$$E_R = E_i\,\epsilon^{j\theta}(\Gamma_R^2 + \Gamma_T^2).$$

The efficiency of the beam splitter can be defined as $\left|\frac{E_D}{E_i}\right|^2 = 4\,|\Gamma_R|^2\,|\Gamma_T|^2$. When the value of $|\Gamma_R|^2 = |\Gamma_T|^2 = 0.5$ the efficiency factor is unity and $E_R = 0$ due to the fact that for a lossless beam splitter $(\Gamma_R + \Gamma_T)$ must equal unity, and Γ_R and Γ_T must differ in phase by ninety degrees. Thus, Γ_R^2 and Γ_T^2 must differ by 180 degrees, or $(\Gamma_R^2 + \Gamma_T^2) = 0$ under the peak-efficiency condition.

Furthermore, it can be shown that if $\Gamma_R = |\Gamma_R| \epsilon^{j\theta_R}$ and $\Gamma_T = |\Gamma_T| \epsilon^{j\theta_T}$

$$\frac{|E_D|^2}{|E_i|^2} = |\Gamma_R|^2 \, |\Gamma_T|^2 \, (2 + 2 \cos(\theta_1 - \theta_2))$$

and

$$\frac{|E_R|^2}{|E_i|^2} = |\Gamma_R|^4 + |\Gamma_T|^4 + 2|\Gamma_R|^2 \, |\Gamma_T|^2 \, (\cos 2(\theta_R - \theta_T)\cos(\theta_1 - \theta_2) - \sin 2(\theta_R - \theta_T) \sin(\theta_1 - \theta_2)).$$

These then are the relations which, assuming unity incident power, give P_{D_1} and P_{D_2} respectively as used in Eqs. (60) and (59) of the text.

APPENDIX V
REQUIRED ACCURACY OF OPTICAL ALIGNMENT

There are two major sources of optical misalignment which may contribute to errors in determining the interferogram function in the aperiodic case. The first of these is an angular error in the adjustment of the beam splitter and/or the mirrors of the interferometer, and the second is the non-uniformity of motion of the movable mirror with respect to the angular position of the sawtooth cam which triggers the digital recorder system. A less serious source of error is the relative error in determining the value of the maximum path-length difference, γ_{max}. It is not as important as the first two sources because it will lead only to the same relative error in determining the wavelength of a particular spectral characteristic as was present in determining γ_{max}.

From Chapter III it was found that a phase difference of 20 electrical degrees at λ = 100 microns corresponds to a displacement error of about 0.0006 centimeters. Thus, considering a ray of radiation divided by the beam splitter into two equal-magnitude rays which are sent to the fixed and movable mirrors respectively,

one sees that the adjustment of the mirrors must be such that the two beams reflected from the mirrors back to the beam splitter must strike the beam splitter within about 0.0006 centimeters of each other. Since the change in the position of the point at which the beam strikes the beam splitter is (for very small angles) proportional to the product of the distance from the beam splitter to the mirror times twice the angular change made in the mirror orientation, one finds that for the instrument described in Chapter IV the mirrors must be adjusted to and maintained within approximately 0.0009 degree. Since the three adjusting screws which support each of the mirrors are about two inches apart, this corresponds to a tolerance of adjustment on each of the screws of about 0.00003 inch, which certainly requires careful mechanical design and adjustment, but is by no means unachievable.

Applying the tolerance criterion of one-half of 0.0006 centimeters (since γ is twice the displacement of the movable mirror) to the uniformity of motion of the movable mirror (which also implies the ability to maintain the mirror position within 0.0003 centimeters), and the ratio of 1.7 inches to 0.78 centimeter which exists between the lead-screw-follower motion and the movable-mirror motion, it is found that the uniformity tolerance limit of the lead screw which is driven by the gearmotor must be about

0.00065 inch, which should not be difficult to obtain. The tolerances on the sawtooth cam may be quite wide, since the distance between points corresponds to only 0.001 centimeter motion of the movable mirror. The looseness of the ratio-arm-pivot-point bearings, the pivot-mounting-block slide bushings and the bushings through which the ratio arm slides must not total more than 0.0003 centimeter or about 0.0001 inch, at least for motion of the movable mirror in one direction. This latter criterion need not hold for motion in both directions, since in the periodic case where motion reversal occurs at the end of each linear stroke, any backlash occurring during the reversal may be compensated for by the proper adjustment of the reference signal. Also, although it would be desirable to have the pivot point shift by no more than 0.0001 inch in a direction parallel to the movable-mirror motion as the pivot-point mounting block moves along its ways, this is not an absolutely necessary requirement if, while during operation in the periodic mode where it is desired to scan in terms of the wave-number to which the instrument is tuned, the synchronization of the radiation-detector output with the reference signal is constantly monitored and corrected as the test progresses.

REFERENCES

1. Williams, R.A. and Chang, W.S.C., "An Analysis of the Interferometric Submillimeter Radiometer," Report 1093-9, 23 July 1962, Antenna Laboratory, The Ohio State University Research Foundation; prepared under Grant Number NsG-74-60 for National Aeronautics and Space Administration.
2. Williams, R.A. and Chang, W.S.C., "Radiometry in the Submillimeter Region using the Interferometric Modulator," IEEE Trans. on MTT, vMTT-11, 513 (1963).
3. Michelson, A.A., "On the Application of Interference Methods to Spectroscopic Measurements," Phil. Mag., v31, 338, and v34, 280 and 407, (1892).
4. Fellget, P., Doctorial thesis, Cambridge University (England), (1951).
5. Fellgett, P., "Spectrome'tre interfe'rentiel multiplex pour measures infra-rouges sur les e'toiles," J. Phys. et Rad., v19, 237 (1958).
6. Fellgett, P., "A propos de la the'orie du spectrome'tre interfe'rentiel multiplex," J. Phys. et Rad., v19, 187 (1958).

7. "Colloque International sur les Progre's Re'cents en Spectroscopie Interfe'rentielle," J. Phys. et Rad., v19, No. 3, (1958).

8. Connes, J., "Domaine d' utilisation de la me'thode par transforme'e de Fourier," J. Phys. et Rad., v19, 197 (1958).

9. Gebbie, H.A., Roland, G., and Delbouille, L., "Molecular Emission Spectroscopy from 2μ to 12μ by a Michelson Interferometer," Nature, v191, 264 (1961).

10. Gebbie, H.A., and Stone, N.W.B., "A Michelson Interferometer for Far Infrared Spectroscopy of Gases," Infrared Phys., v4, 85, (1964).

11. Strong, J.D. and Vanasse, G.A., "Lamellar Grating Far-infrared Interferometer," J. Opt. Soc. Am., v50, 113 (1960).

12. Vance, M., "An Interferometric-modulator Order-separator for a Far-infrared Spectrograph," Doctorial dissertation, The Ohio State University Department of Physics, (Disseration Abstracts, v23, No. 10, (1963).

13. Long, M.W. and Butterworth, J.C., "New Technique for Microwave Radiometry," IEEE Trans. on MTT, v MTT-11, 389 (1963).

14. Long, M.W., "A Frequency Selective Power Meter for Millimeter Waves," Engr. Exp. Sta., Georgia Inst. of Tech., Proj. A-701 Final Rpt. (1964).

15. Culshaw, W., "The Michelson Interferometer at Millimetre Wavelengths," Proc. Phys. Soc. London, v63B, 939 (1950).

16. Strong, J.D., "Interferometric Modulator (paper abstract), J. Opt. Soc. Am., v44, 352 (1954).

17. Strong, J.D., "Interferometry for the Far Infrared," J. Opt. Soc. Am., v47, 354 (1957).

18. Strong, J.D. and Vanasse, G.A., "Modulation interfe'rentielle et calculateur analogique pour un spectrome'tre interfe'rentiel," J. Phys. et Rad., v19, 192 (1958).

19. Genzel, L., "Aperiodic and Periodic Interference Modulation for Spectrographic Purposes," J. Molec. Spectr., v4, 241 (1960).

20. Williams, R.A., "A Proposed Method for Improving the Pass-band Characteristics of the Periodic Interferometric Modulator," Report 1093-15, 1 June 1963, Antenna Laboratory, The Ohio State University Research Foundation; prepared under Grant NsG-74-60 for National Aeronautics and Space Administration.

21. Williams, R.A. and Chang, W.S.C., "Interferometric Wavelength Selection for Submillimeter Radiometry," Polytechnic Inst. Brooklyn, Proc. of Symp. on Quasi-Optics, v14, 607 (1964).

22. Bell, E.E., Oetjen, R.A., Rowntree, R.F., and Vance, M.E., 'The Ohio State University Research Foundation Final Report on Spectroscopy in the Far Infrared Region," Contract AF-19(604)-4119, September 1963.

23. Blackman, R.B. and Tukey, J.W., The Measurement of Power Spectra, Dover, New York City, 1959.

24. Harrison, G.R., Lord, R.C., and Loofbourow, J.R., Practical Spectroscopy, Prentice-Hall, New York, 1948, Chapters 4, 5, 6, and 17.

25. Slepian, D. and Pollak, H.O., "Prolate Spheroidal Wave Functions, Fourier Analysis and Uncertainty - I," Bell Sys. Tech. J., v40, 43 (1961).

26. Jenkins, F.A. and White, H.E., Fundamentals of Optics, McGraw-Hill, New York City, 1957, p. 328.

27. Low. F.J., "Low-temperature Germanium Bolometer," J. Opt. Soc. Am., v51, 1300 (1961).

28. Yoshinga, H., Fujita, S., Minami, S., Mitsuishi, A., Oetjen, R.A., and Yamada, Y.,"Far Infrared Spectrograph for use from the Prism Spectral Region to about 1 Millimeter Wavelength," J. Opt. Soc. Am., v48, 315 (1958).

29. Oetjen, R.A., Haynie, W.H., Ward, W.M., Hansler, R.L., Schauwecker, H.E., and Bell, E.E., "An Infrared Spectrograph for use in the 40-150 Micron Spectral Region," J. Opt. Soc. Am., v42, 559 (1952).

30. Yaroslavsky, N.G. and Stanevich, A.E., "The Long Wavelength Infrared Spectrum of H_2O Vapor and the Absorption Spectrum of Atmospheric Air in the Region 20-2500 Microns (500-4 cm^{-1})," Optics and Spectroscopy (English translation), v7, 380 (1959).

31. Palik, E., The Ohio State University Research Foundation Report 659-4 on Infrared Techniques and Measurements (OSU Physics Department research for Wright Air Development Center Contract AF-33(616)-3312, 25 January 1957).

32. Lin, B.J., The Ohio State University Research Foundation Report 1093-22 (Antenna Laboratory research for National Aeronautics and Space Administration Grant NsG-74-60, Annual Report, August 1964).

33. Vogel, P. and Genzel, L., "Transmission and Reflection of Metallic Mesh in the Far Infrared," Infrared Physics, v4, 257 (1964).

BIBLIOGRAPHY

Connes, P, "Spectrome'tre Interfe'rentiel a Se'lection par l' amplitude de Modulation," J. Phys. et Rad., v19, 215, (1958).

Crocker, A., Gebbie, H.A., Kimmitt, M.F., and Mathias, L.E.S., "Stimulated Emission in the Far Infra-red," Nature, v201, 250 (1964).

Dicke, R.H., "The Measurement of Thermal Radiation at Microwave Frequencies," Rev. Sci. Instr., v17, 268 (1946).

Gebbie, H.A., "Spectres d' Absorption Atmosphe'rique dans l' infra-rouge lointain per interfe'rome'trie a deux ondes," v19, 230 (1958).

Gebbie, H.A., Stone, N.W.B., and Findlay, F.D., "A Stimulated Emission Source at 0.34 Millimeter Wavelength," Nature, v202, 685 (1964).

Gebbie, H.A., Stone, N.W.B., Findlay, F.D., and Robb, J.A., "Interferometric Observations on Far-infrared Stimulated Emission Sources," Nature, v202, 169 (1964).

Gebbie, H.A., Vanasse, G.A., "Interferometric Spectroscopy in the Far Infrared," Nature, v178, 432 (1956).

Golay, M.J.E., "Bridges Across the Infrared Radio Gap," Proc. IRE, v40, 1161, (1952).

Harris, D.B., "Microwave Radiometry," Microwave J., v3, p41, April 1960 and p47 May 1960.

Jacquinot, P, "Quelques recherches sur les raies faibles dan les spectres optiques," Proc. Phys. Soc. London, v63B, 969 (1950).

Kaufman, I, "The Band between Microwave and Infrared Regions," Proc. IRE, v47, 381 (1959).

Mertz, L., "Optical Fourier Synthesizer," J. Opt. Soc. Am., v46, 548 (1956).

Parshin, P.F., "Signal-to-noise Ratio in Spectra Obtained by the Method of Fourier-spectroscopy," Optics and Spectr. (English Transl.), 16, 275 (1964).

Putley, E.H., "The Detection of Sub-millimeter Radiation," Proc. IEEE, v51, 1412 (1963).

Strong, J.A. and Vanasse, G.A., "Interferometric Spectroscopy in the Far Infrared," J. Opt. Soc. Am., v49, 844 (1959).

Vanassee, G.A., Strong, J.A., and Loewenstein, E., "Far Infrared Spectra of H_2O and H_2S taken with an Interferometric Spectrograph," J. Opt. Soc. Am., v49, 309 (1959).

GLOSSARY OF SYMBOLS

Chapter I

λ	Wavelength (in centimeters unless otherwise stated)
T_s	Source temperature (degrees Kelvin)
ν	Wavenumber (centimeters^{-1})
$E_{(\nu)}$	Power spectral density (watt-cm)
k	Boltzman's constant, 1.38×10^{-23} (watt-sec/degree Kelvin)
c	Speed of light, 3×10^{10} (centimeters/second)
h	Planck's constant, 6.625×10^{-34} (watt-seconds^2)
$[\Delta P_{min}]$	Minimum change in the input power which a radiation receiver can detect (watts)
$[\Delta T_{smin}]$	Minimum change in the source temperature which can be detected (degrees Kelvin)
η	A factor depending upon λ and T_s which expresses the correction due to the use of the exact form of the radiation law (see Fig. 1)
Γ	A factor expressing the dependence of $[\Delta T_{smin}]$ upon the source size, observation wavelength, and the parameters of the radiometer optical system
$(\Delta\nu)$ or $[\Delta\nu]$	Radiometer receiver passband (centimeters^{-1})
δ_1	Focal length of the submillimeter radiometer collecting optics (centimeters)

a	Input aperture area of the submillimeter receiver, or the image size of the radiation detector at the receiver input, whichever is smaller (centimeters^2)
A_m	Aperture area (geometrical) of the collecting optics of the submillimeter radiometer (centimeters^2)
F_o	f-stop number of the collecting optics (or of the submillimeter receiver if its f-stop number is numerically greater than that of the collecting optics)
π	3.1416
$[\Delta\Omega]_s$	Solid angle subtended by the source when viewed from the radiometer (square radians - dimensionless)
A_e	Effective antenna aperture of a linearly-polarized centimeter - wavelength antenna (centimeters^2)
$[\Delta E_{(\nu)_{min}}]$	Minimum detectable power spectral density (watt-cm)

Chapter II

$E_{i(\nu)}$	Power spectral density of the input radiation (watt-cm)
γ	Path length difference (centimeters unless otherwise stated)
$E_{o(\nu,\gamma)}$	Power spectral density at the output of the interferometer (the detector input) as a function of the path length difference (watt-cm)
$I_{o(\gamma)}$	Total power at the interferometer output (detector input) (watts)
γ_{max}	Maximum path length difference (centimeters unless otherwise stated)
$I'_{o(\gamma)}$	$I_{o(\gamma)}$ truncated at $\pm\ \gamma_{max}$ (watts)
$W_{(\gamma)}$	Window function which truncates $I_{o(\gamma)}$

$E_{mI(\nu)}$	Measured power spectral density obtained by the aperiodic interferometric process (watt-cm)
$R_{I(\nu, \nu')}$	Instrument response function in the aperiodic case (centimeters)
ν'	Same as ν, but used as a dummy variable (centimeters^{-1})
ν_n	Values of ν at which $E_{mI(\nu)}$ may be computed with validity (centimeters^{-1})
n	Index number (integer)
$\Delta\nu$	Width of the main peak of the instrument response function (centimeters^{-1})
$\Delta\gamma$	Spacing between data points taken in the aperiodic case (centimeters unless otherwise stated)
$E'_{mI(\nu)}$	$E_{mI(\nu)}$ obtained with the improved form of the instrument response function (watt-cm)
γ'_{max}	γ_{max} value corresponding to the improved instrument response function (centimeters)
ℓ	Number of basic instrument response functions combined to give the improved response function
$(\Delta\nu)_G$	Bandwidth of the grating monochromator (centimeters^{-1})
K	Fraction of the input radiation diffracted into the first grating order in the grating instrument
P_D	Power delivered to the radiation detector in the grating receiver (watts)
(NEP)	Noise-equivalent power of the radiation detector as determined by an audio correlator of one cycle-per-second effective bandwidth (watt-sec$^{1/2}$)
τ_D	Time constant of the correlator circuit or synchronous rectifier used in the radiometer receiver (seconds)

$(S/N)_G$	Signal-to-noise ratio of the grating receiver
$N_{(f)}$	The mean-square noise voltage spectral density of the noise appearing on the interferogram function expressed as a voltage time function (volts^2 /second)
$I_{o(t)}$	$I_{o(\gamma)}$ expressed as a time function (watts)
Ω	Radiation detection system response factor (volts/watt)
f	Audio frequency (cps or seconds^{-1})
s	Velocity of change of the path length difference (centimeters/second)
$S_{I(f)}$	Voltage output spectrum of the aperiodic receiver correlator due to the radiation power at the wave-number ν = fs (volt-seconds)
$N_{(t)}$	The noise voltage on the interferogram time voltage function (volts)
T_t	The total length of time spent in measuring the entire spectral region of interest (seconds)
$(S/N)_I$	Signal-to-noise ratio of the interferometric receiver
$(\triangle \nu)_I$	Bandwidth of the interferometric receiver (centimeters^{-1})
ν_2 , ν_1	Limits (upper and lower) of the spectral region it is desired to measure (centimeters^{-1})
Q	Radiometer receiver figure of merit (1/watt-sec)
t	Time (seconds)
Q_G	Grating instrument figure of merit (1/watt-seconds)
Q_I	Aperiodic interferometer receiver figure of merit (1/watt-seconds)

M	Number of spectral elements to be determined between the limits ν_1 and ν_2
m	Grating order number
d	Grating line spacing (centimeters)
ψ	Angle at which radiation is diffracted from the grating
$\lvert\Delta\psi\rvert$	Slit width expressed in terms of the angle subtended by the slit when viewed at the grating
τ_P	Time required to scan from $\gamma = 0$ to $\gamma = \gamma_{max}$ or the equivalent in the periodic case (seconds)
T_p	Period of operation of the periodic interferometric receiver (seconds)
f_o	Frequency of operation of the periodic receiver (seconds^{-1})
f	Audio frequency associated with the radiation wavenumber ν in the case of the periodic receiver (seconds^{-1})
f_n	The n^{th} audio harmonic of the frequency f_o (seconds^{-1})
P_n	Power of the radiation modulated at the audio frequency f_n in the periodic case (watts)
ν_n'	Value of ν corresponding to the periodic instrument's n^{th} audio harmonic frequency, f_n (centimeters^{-1})
$E_{mP}(\nu_n')$	Measured power spectral density in the periodic case (watt-cm)
$R_{P}(\nu_n', \nu)$	Instrument response function of the periodic instrument (centimeters)
N	A particular value of the integer index number, n
$(\Delta\nu)_P$	Resolution of the periodic instrument (centimeters^{-1})

N_D	Noise power level at the output of the periodic instrument (watts)
$(S/N)_P$	Signal-to-noise ratio of the periodic instrument
C	Relative resolution of the periodic instrument
Q_P	Q for the periodic case (1/watt-seconds)
ν_{max}	The maximum wavenumber at which $E_{i(\nu)}$ is assumed to be non-zero (centimeters^{-1})
b_n	Coefficients of the expansion of $I_{o(\gamma)}$ in terms of the eigenfunctions $\psi_{n(\gamma)}$
$\psi_{n(\gamma)}$	The prolate spheroidal wave functions
λ_n	Eigenvalues of $\psi_{n(\gamma)}$
	(λ_j, λ_k, $\psi_{j(\nu)}$, $\psi_{k(\nu)}$, C_j, and C_k are the eigenvalues, prolate spheroidal wave functions and expansion coefficients corresponding to the expansion of $E_{i(\nu)}$ on the ν axis)
$E_{m(\nu_k)}$	Measured power spectral density at the incremental wavenumber value ν_k (watt-centimeter)
$E_{i(\nu_j)}$	The input power spectral density at the incremental wavenumber value ν_j (watt-centimeters)
$(\delta\nu)$	The minimum increment between ν_j and ν_{j+1} (centimeters^{-1})
$[E_{m_k}]$	The measured power spectral density expressed as a matrix (watt-centimeters)
$[R_{kj}]$	The instrument response function expressed as a square matrix
$[E_{i_j}]$	The input power spectral density expressed as a matrix (watt-cm)

Chapter III

Γ_R	Voltage reflection coefficient of the beam splitter
Γ_T	Voltage transmission of the beam splitter
L	Focal length of the input collimating system (centimeters)
ϕ	Angle of the collimated radiation in the interferometer (degrees or radians)
r	Distance from the center of the source of a particular point of radiation being considered (centimeters)
G	Displacement of the movable mirror in the Michelson system (centimeters unless otherwise stated)
q	Length of the ray path shown in Fig. 6 (centimeters)
G_{max}	Maximum value of the movable mirror displacement (centimeters)
ϕmax	ϕ corresponding to the radiation from the outer rim of the source
P_{D_2}	Power delivered to the second radiation detector in Fellgett's system (watts)
θ_R	Phase angle of Γ_R
θ_T	Phase angle of Γ_T
θ_1	Phase shift to and from the fixed mirror
θ_2	Phase shift to and from the movable mirror
P_{D_1}	Power delivered to the first (normally the only) radiation detector (watts)

Chapter IV

$[\Delta E_{i(\nu)}\text{min}]$	The minimum detectable power spectral density in the case of the aperiodic interferometric receiver (watt-centimeters)
δ_i	Focal length of the interferometer input optics (centimeters)
δ_o	Focal length of the detector optics (centimeters)
D	Diameter of the interferometric receiver optics (centimeters)
A_s	Area of the radiation test source (centimeters^2)
A_D	Area of the radiation detector (centimeters^2)
A'_D	Detector area imaged upon the plane of the source area (centimeters^2)
$(\Delta\Omega)_I$	Solid angle into which the test source radiates
U	Fraction that digitizing noise is of the maximum $I_{o(\gamma)}$

Chapter V

$[d\nu]$	Spacing between points (in wavenumber) at which $E_{m(\nu)}$ is calculated in the aperiodic mode

Appendix I

$\Delta\lambda$	Bandwidth of the grating instrument expressed in terms of the wavelength rather than the wavenumber (centimeters)
Ψ_λ	Planck's radiation density factor (watts/cm^4)
P_λ	Black-body radiation power per solid angle per surface area per wavelength increment (watts/cm^3-sterad)
$A_{e(\theta,\phi)}$	Effective antenna area as viewed from direction of θ and ϕ (cm^2)

P	Power incident upon the radiometer antenna (watts)
L_s	Distance from the radiometer to the source (cm)
$d\sigma$	Increment of radiation source area (cm^2)
$d\Omega$	Solid angle of $d\sigma$ as viewed from the radiometer
$\Delta\Omega$	Total solid angle of the source
$T_{s(\theta, \phi)}$	T_s in the direction given by θ and ϕ (^oK)
$G_{(\theta, \phi)}$	Antenna gain function (referred to an isotropic source)
d	Diameter of the receiver input (cm)
D_m	Diameter of the antenna mirror (cm)
A_r	Area of receiver optics (cm^2)
F_r	f-number of the receiver optics

Appendix IV

$g_{(t)}$	Generalized time function
$h_{(f)}$	Generalized frequency function
x	Generalized coordinate
$H_{(f)}$	Fourier transform of $I_{o(t)}$
$F_{(x)}$	Generalized function of x
a_k	Coefficients of the Fourier series of a generalized function
$F_{(f)}$	Generalized function of frequency
E_i	Electric field of the incident radiation (volts/centimeter)

E_{mov}	Electric field of the radiation reflected towards the movable mirror by the beam splitter (volts/centimeter)
E'_{mov}	Electric field of the radiation returning from the movable mirror (volts/centimeter)
E_{fixed}	Electric field of the radiation reflected towards the fixed mirror by the beam splitter (volts/centimeter)
E'_{fixed}	Electric field of the radiation returning from the fixed mirror (volts/centimeter)
E_D	Electric field of the radiation transmitted to the detector (volts/centimeter)
E_R	Electric field of the radiation reflected back out the input of the receiver (volts/centimeter)